

Towards brain-on-a-chip: Microfluidic and microelectrode array platforms for morphological and electrophysiological observations on the propagation of Alzheimer's disease

THÈSE N° 6854 (2016)

PRÉSENTÉE LE 22 AVRIL 2016

À LA FACULTÉ DES SCIENCES ET TECHNIQUES DE L'INGÉNIEUR

LABORATOIRE DE MICROSYSTÈMES 4

PROGRAMME DOCTORAL EN BIOTECHNOLOGIE ET GÉNIE BIOLOGIQUE

ÉCOLE POLYTECHNIQUE FÉDÉRALE DE LAUSANNE

POUR L'OBTENTION DU GRADE DE DOCTEUR ÈS SCIENCES

PAR

Yufei REN

acceptée sur proposition du jury:

Prof. Y. Barrandon, président du jury

Prof. Ph. Renaud, directeur de thèse

Dr J. West, rapporteur

Dr D. Lowe, rapporteur

Dr B. Schneider, rapporteur



ÉCOLE POLYTECHNIQUE
FÉDÉRALE DE LAUSANNE

Suisse
2016

To my parents and all my teachers

Acknowledgements

First, I would like to give my deepest gratitude to my supervisor, Prof. Philippe Renaud, for offering me this PhD position. He guided me during this journey of exploring science and backed me up when I was facing difficulties. He not only supported my work as a brilliant researcher, but also gave me the encouragement to chase for a colourful life in Switzerland as a kind mentor. Philippe, I can never forget that sentence you said during our discussion we had when Shun-Ho Huang (Manson) just arrived in Switzerland in March 2012. At the end of our meeting, you told Manson, “Enjoy your life in Switzerland. That is the most important.” This made me feel your warmth for students and wisdom for life.

I would like to express my sincerest appreciation to the jury members for my private defense: Prof. Yann Barrandon from EPFL, Dr. Bernard Schneider from EPFL, Dr. Jonathan West from University of Southampton, Dr. David Lowe from AC Immune SA and my supervisor Prof. Philippe Renaud. Thank you again for participating my private defense and for your constructive feedback on my work and their valuable advices for the continuous work on this project. I would like to thank Dr. Sophie Pautot as well, one of our collaborators from Dresden, who played an important role in our beads-based 3D cell culture. Thanks to Dr. Mark Olivier Heuschkel from Qwane SA for sharing his knowledge and technology of microelectrode arrays (MEAs). Special thanks go to Prof. Patrick Fraering and his PhD student Sébastien Mosser, you have provided me neural cells unconditionally during the four years of my PhD study. Sébastien, you are not only my No. 1 “Cell Provider”, but also a true friend for life.

At the beginning of my PhD life, I was a beginner in the neuroscience domain and was so confused about where to go for my future research. It was Dr. Anja Kunze who gave me a hand when I was struggling. She is so knowledgeable and well organised for her work. During my third year of my PhD, Anja invited me to contribute for a book chapter together. This was such a great opportunity for me to precipitate of what I have learnt during my study and I appreciate it a lot. I would like to thank Dr. Bilge Eker Bartsch who was a postdoc in the lab. It was shew who led me on this PhD road and I really enjoyed the time we were working together. Manson is another very important person during my PhD life. We did several projects together and had a happy time together in research. Manson is not only a good partner for research, but also for travelling. He always encourages me to do sport and brought me to cycle around the Léman Lake. We had so many good memories during his stay in Switzerland. I would like to thank all my colleagues for their support. I learnt a lot from you including the scientific side from the group meetings and the active attitude for daily life. Especially, I would like to thank Arnaud, for correcting my papers patiently and especially for his influence on my way of doing research and sharing life experiences with me. I will treasure all these happy moments we had during these four years. At the same time of my PhD, I also assisted several master students’

projects and participated the teaching assignment for the master course “Microsystèmes et Capteurs”. From these experiences, I learnt how to teach and communicate with students. I would like to thank the master students, Francesca Sorba and Sébastien Hissette, for your contribution to this work.

One of the reasons that I did not feel lonely at the beginning of my life in Switzerland where is far away from my home country is because of my friendship with Chen Yu, you are really like a sister to me. You took such good care of me. I will treasure all our memories together. All my friends in Switzerland, I wish all the best for all of you and may all your dreams come true.

In the end, I would like to say a big “thank you” to my family, especially to my mother. I cannot image how many difficulties you have had to go through to raise me since my father passed away and how difficult it was for you to make the decision to send me to Switzerland, 11,054.8 km away from you. Whenever I thought about this, I could not control my tears. I had been through so many sorrowful nights missing you.

Thankfully, I found my other half, Gabriel, in the cleanroom during my studies at EPFL. You are such a kind-hearted person with a pair of liquid eyes that can tell beautiful stories. Also your parents, Raymond and Marina, they are taking care of me like their own child. Your family brought me the warm home feeling that I am and I will always appreciate. Gaby, I cannot put our love into words because it is beyond words. Without you, my life could not be so colourful. I love you.

Lausanne, 10th October 2015

Abstract

Since the first compartmentalized neuronal culture described by Robert B. Campenot in 1977, compartmentalized microfluidic devices have been widely used to engineer the cellular environment for cell culture. In previous research by Dr. Anja Kunze, a microfluidic device was able to build a “co-pathological” model with neuronal culture for neurodegenerative disease studies. In this model, two neuronal populations were cultured in independent compartments, while the axons of both populations were able to grow away from their own population and arrived in the same compartment, which was between the two compartments for the neuronal populations. When one neuronal population was exposed to a drug and expressed a specific disease state, different disease states were observed in the axon compartment towards the other unexposed cell population. This co-pathological pattern was achieved and early stage of disease propagation was observed in this compartmentalized microfluidic device. An example of this propagation pattern in the native brain is the well-known neurodegenerative disease Alzheimer’s disease (AD), which still lacks effective treatments. In the AD brain, disease progression is observed from one brain region to another, eventually influencing the whole brain. This disease model can be mimicked *in vitro* within microdevices to assist neuroscientists in gaining a better understanding of the mechanisms of AD spreading in the native brain.

In this thesis, we designed and fabricated compartmentalized microfluidic devices to build a co-pathological model to study the propagation of Tau pathology, which is one of the key pathological hallmarks of neurodegenerative disorders. Besides the morphological characteristics that we observe using our microfluidic device, microelectrode arrays (MEAs) technology, which is based on microtechnology and allows for recording extracellular neuronal activity, was integrated with the microfluidic device in this work. Together, the microfluidic and the integrated microfluidic-MEA devices provide us the possibility to monitor respectively time-variant morphological and electrophysiological alterations during disease spreading. We are therefore able to distinguish the contribution of neuron-to-neuron transmissions, observe different patterns of disease propagation with high and low drug-induced AD models, and observe the order in which the structural and functional alterations occur during AD progression. Based on the results that were achieved during our investigation of AD in this thesis, these microfluidic and integrated microdevices may potentially be used to study neurodegenerative diseases and perform pharmaceutical drug tests.

Keywords: compartmentalized microfluidic device, microelectrode array (MEA) device, PDMS and SU-8 bonding technology, integrated microfluidic-MEA device, Alzheimer's disease propagation, hyperphosphorylated-Tau protein, neural activity, neural morphological and electrophysiological observations, beads-based 3D neuronal culture

Résumé

Depuis que la première culture cellulaire de neurones compartimenté fût décrite par Robert B. Campenot en 1977, les dispositifs microfluidiques compartimentés ont beaucoup été utilisés pour le contrôle de l'environnement cellulaire dans la culture de cellule. Dans les travaux de Dr. Anja Kunze, un dispositif microfluidique permettait de construire un modèle "co-pathologique" de culture de cellules neuronales pour l'étude de maladie neurodégénératives. Dans ce modèle, deux populations de neurones sont mises en culture dans des compartiments indépendants. Les axons peuvent grandir vers un compartiment commun qui se trouve entre les deux compartiments contenant les deux populations de neurones. Quand une population de neurones est exposée à une drogue et exprimait un état spécifique d'une maladie, différents états de cette maladie ont pu être observés dans le compartiment des axons, vers la population non-exposée de neurones. Ce schéma co-pathologique a été réalisé et les premières étapes de la propagation de la maladie ont été observées dans ce dispositif microfluidique compartimenté. Un exemple très connu de cette forme de propagation dans le cerveau est la maladie d'Alzheimer, qui n'a pas de méthode de traitement efficace pour l'instant. Dans le cerveau affecté par la maladie d'Alzheimer, la propagation de la maladie est observée d'une région du cerveau vers une autre, pour finalement influencer tout le cerveau. Ce modèle de la maladie peut être imité *in vitro* dans des micro-dispositifs pour aider les neuroscientifiques à mieux comprendre les mécanismes de la propagation de la maladie d'Alzheimer dans le cerveau.

Dans cette thèse, nous avons conçu et fabriqué des dispositifs microfluidiques compartimentés pour générer un modèle co-pathologique pour l'étude de la propagation de pathologie Tau, qui est une des principales caractéristiques des troubles neurodégénératifs. Mise à part les caractéristiques morphologiques que nous observons dans notre dispositif microfluidique, la technologie des matrices de microélectrodes (MEAs), qui est basée sur la microtechnique et permet de mesurer et d'enregistrer l'activité neuronale extracellulaire, a été intégrée avec le dispositif microfluidique durant cette thèse. Ensemble, les dispositifs microfluidiques et microfluidique-MEAs nous permettent d'observer en fonction du temps respectivement les altérations morphologiques et les altérations électrophysiologiques pendant la propagation de la maladie. Nous sommes alors capable de distinguer la contribution des transmissions neurone à neurone, d'observer les différentes formes de propagation de la maladie pour des modèles d'Alzheimer avec haute et basse induction par des drogues ainsi que d'observer dans quel ordre les altérations structurelles et fonctionnelles se produisent pendant la propagation de la maladie d'Alzheimer. Basé sur ces résultats qui découlent de notre investigation de la maladie d'Alzheimer dans cette thèse, ces micro-dispositifs microfluidiques et intégrés pourraient potentiellement être utilisés pour étudier les maladies neurodégénératives et pour effectuer des tests pharmaceutiques de médicaments.

Mots-clés : dispositifs microfluidiques compartementalisés, dispositifs avec des matrices de microélectrodes (MEAs), technologie de collage de PDMS et SU-8, dispositifs intégrés microfluidique-MEAs, propagation de la maladie d'Alzheimer, protéine Tau hyperphosphorylée, activité neuronale, Observations morphologiques et électrophysiologique neuronale, culture de cellule 3D basée sur des billes

Table of Contents

Acknowledgements.....	i
Abstract.....	iii
Résumé.....	v
1. Introduction.....	1
1.1 Alzheimer's disease	2
1.1.1 AD and its hallmarks.....	2
1.1.2 Formation of NFTs from Tau protein	5
1.1.3 Propagation of Tau pathology in AD	6
1.2 Morphological studies.....	7
1.2.1 <i>In vivo</i> and <i>in vitro</i> models to study AD	7
1.2.2 Microfluidic technology for <i>in vitro</i> neuroscience research.....	7
1.2.3 Characteristics and fabrication techniques for a microfluidic device.....	7
1.2.4 Microfluidic device and its application on neuronal culture	10
1.2.5 Microfluidic device for AD studies.....	12
1.3 Electrophysiological studies	13
1.3.1 Development of technologies for neural activity recording.....	13
1.3.2 Intracellular recording methods <i>in vitro</i>	15
1.3.3 Extracellular recording methods <i>in vitro</i>	15
1.3.4 Microelectrode array recording technology	19
1.3.5 Glass-substrate based MEA device	20
1.4 2D and 3D neuronal culture.....	21
1.4.1 Comparison of 2D and 3D neuronal culture environments.....	21
1.4.2 3D neuronal culture.....	21
1.4.3 3D neuronal culture for AD studies.....	23
1.5 Building an AD propagation model.....	25
1.5.1 Concept of co-pathology in building AD propagation model.....	25
1.5.2 Co-pathological model in microfluidic and MEA platforms to study AD	26
1.6 Scope of the thesis.....	30
1.7 Thesis structure	30
2. Microfluidic, MEA and integrated microfluidic-MEA devices fabrication	33

Table of Contents

2.1	Introduction.....	34
2.1.1	Integration of microfluidic device and MEA device.....	34
2.1.2	PDMS and SU8.....	34
2.1.3	PDMS and SU8 bonding methods.....	35
2.1.4	Aminosilane-mediated silanization bonding method.....	35
2.2	Methods.....	37
2.2.1	Microfluidic device design and fabrication	37
2.2.2	MEA device design and fabrication	39
2.2.3	Primary cortical neuron dissection.....	42
2.2.4	Experimental materials.....	42
2.3	PDMS and SU-8 bonding tests.....	42
2.3.1	Bonding tests	42
2.3.2	Analysis of chemical reactions on the PDMS.....	44
2.3.3	Manual tensile strength test.....	46
2.3.4	Ultimate tensile strength test for the bonding.....	46
2.4	Microfluidic-MEA device	49
2.4.1	Surface silanization of the PDMS part from the device.....	49
2.4.2	Fabrication of the SU-8 part from the device	49
2.4.3	PDMS and SU-8 bonding for the microfluidic-MEA device.....	49
2.4.4	Device preparation for neuronal culture	50
2.4.5	Morphological and electrophysiological observations from the microfluidic-MEA device.....	50
2.5	Conclusion.....	52
3.	Propagation of Tau pathology in microfluidic and integrated microfluidic-MEA devices.....	53
3.1	Introduction.....	54
3.1.1	Importance of building a microfluidic-MEA device for studying AD.....	54
3.1.2	Building a diseased cell model based on Tau pathology	54
3.1.3	Disease propagation studies by using microfluidic and microfluidic-MEA devices ..	55
3.2	Materials and Methods.....	55
3.2.1	Design and fabrication process of microfluidic and microfluidic-MEA devices	55
3.2.2	Preparation and plating procedure for the devices.....	57
3.2.3	Induce Tau hyperphosphorylation via OA exposure	57
3.2.4	Immunocytochemistry staining for morphological studies.....	58

Table of Contents

3.2.5	Extracellular recording method and parameters settings.....	59
3.2.6	Recording data analysis and statistical analysis	60
3.3	Results.....	60
3.3.1	Control experiment.....	60
3.3.2	Cytoskeleton alterations after OA exposure	60
3.3.3	Propagation of Tau hyperphosphorylation between diseased and healthy neural populations by axonal connection	63
3.3.4	Spontaneous firing rate and burst rate during the disease propagation.....	64
3.4	Discussion.....	65
3.4.1	Structural characteristics alterations during disease propagation.....	65
3.4.2	Different functional patterns under different concentrations of OA exposure.....	66
3.4.3	Order of occurrence of structural and functional alterations during disease propagation	70
3.5	Conclusions and future prospects	70
4.	3D beads-based neuronal culture in microfluidic device	73
4.1	Introduction.....	74
4.2	Methods	74
4.2.1	Design of layer pattern in microfluidic device.....	74
4.2.2	Experimental set-up	76
4.3	3D Silica beads culture in microfluidic device.....	76
4.3.1	SHSY-5Y cell line culture on silica beads.....	76
4.3.2	Primary neural cell culture on silica beads and patterned in microfluidic device	77
4.3.3	cAMP and cGMP guidance experiment using 3D silica beads culture.....	81
4.4	3D agarose-alginate beads culture in microfluidic device	83
4.4.1	Agarose-alginate beads	83
4.4.2	Agarose-alginate beads fabrication.....	84
4.4.3	3D agarose-alginate beads culture in layered-pattern in microfluidic device	85
4.5	Conclusion.....	88
5.	Conclusions and perspectives	89
5.1	Conclusions	90
5.1.1	PDMS and SU-8 bonding method for microfluidic-MEA device integration.....	90
5.1.2	Applications of using microfluidic and microfluidic-MEA devices for AD propagation studies.....	90

Table of Contents

5.1.3	Building a layer-pattern neuronal culture model in a microfluidic device.....	91
5.2	Perspectives.....	92
5.2.1	Axonal transmission mechanisms	92
5.2.2	Relation between Tau and A β	92
5.2.3	3D cell culture model for AD studies	93
5.2.4	Towards building a brain-on-a-chip	94
5.2.5	Benefits from using miniaturized devices	94
Bibliography		95

List of Figures

Figure 1: Medical information of brain scans from an AD patient from 1993 to 2003 by Magnetic resonance imaging (MRI).....	3
Figure 2: Plaques and tangles in the cerebral cortex in AD.....	4
Figure 3: Comparison between healthy neuron and Alzheimer diseased neuron.....	4
Figure 4: Comparison between healthy neuron and Alzheimer diseased neuron on Tau protein.	5
Figure 5: AD spreading through the brain.....	6
Figure 6: The first compartmentalized microfluidic device for neuronal culture.....	8
Figure 7: Schematic diagram of the manipulation with microfluidics for neural culture.....	9
Figure 8: Variation of the junction channels (150 μm , 450 μm , 900 μm) for the microfluidic device to isolate neurite or axon.	9
Figure 9: Schematic fabrication process of a microfluidic device made of PDMS for neuronal culture..	11
Figure 10: Microfluidic neural culture platform.	11
Figure 11: Images of primary cortical neural network in compartmentalized PDMS microfluidic device after OA treatment.....	13
Figure 12: Intracellular recording of the squid giant axon.....	14
Figure 13: Four methods for patch clamp including cell-attached recording, inside-out recording, whole-cell recording and outside-out recording.	16
Figure 14: Schematic of the design of the planar patch clamp system.	17
Figure 15: Theory of MEA recording and an example of MEA device.....	17
Figure 16: Neuronal network on a microelectrode array (MEA) device and the illustration on the basic concepts of electrophysiological activity.....	18
Figure 17: The illustration of spike train and burst train with an example of a raw signal.....	18
Figure 18: The MEA device invented in 1972.....	19
Figure 19: The manipulation of the MEA recording system.....	21
Figure 20: Schematic image of the guidance concept of 3 layers beads.....	24
Figure 21: Schematic picture of the hanging drop formation process.....	24
Figure 22: Designing principle of the 3D layer hydrogel scaffold for neural cell cultures.....	25

List of Figures

Figure 23: The schematic pictures on the experimental region inside a microfluidic device to show the steps to achieve a co-pathological “diseased” and “healthy” neural network.....	28
Figure 24: Microtubule-associated Tau protein equilibrium in the brain.....	28
Figure 25: Fluorescent images of healthy and diseased cells after OA treatment.	28
Figure 26: Schematic picture of the simplified model of AD propagation.....	29
Figure 27: Microfluidic-MEA device.	36
Figure 28: Theoretical reactions during the bonding. (A) Reaction between APTES molecule and the O ₂ plasma activated PDMS surface and (B) reaction between the -NH ₂ group from the APTES molecule on the PDMS surface and the epoxy group from the SU-8 surface.....	36
Figure 29: Designs of microfluidic device and MEA device.	38
Figure 30: A representative microstructured silicon wafer contains multiple microfluidic designs for PDMS master molding.	38
Figure 31: Process flow for microstructuring PDMS devices in the cleanroom.....	40
Figure 32: PDMS device fabrication process.....	40
Figure 33: Design of a normal MEA device with 60 electrodes.....	41
Figure 34: Schematic diagrams of the fabrication of MEA device.	41
Figure 35: The N1s spectra of the PDMS surfaces by XPS under different surface modifications	45
Figure 36: PDMS and SU-8 bonding strength testing sample.	47
Figure 37: The set-up for the manual tensile strength test.	48
Figure 38: Tensile strength test for the bonding.....	48
Figure 39: Design of microfluidic-MEA device and recording result.....	51
Figure 40: Schematic picture of the experiment process.	56
Figure 41: Image of the microfluidic-MEA device and its internal structures.	56
Figure 42: Control experiment for drug diffusion effect test.	61
Figure 43: Cytoskeleton alteration visualized by MAP2 immunocytochemistry staining as green color.	62
Figure 44: Disease propagation patterns during recovery period (0 h, 6 h, 24 h, 48 h) under high concentration of OA exposure (600 nM).	65
Figure 45: Disease propagation patterns during recovery period (0 h, 6 h, 24 h, 48 h) under low concentration of OA exposure (60 nM).....	66

List of Figures

Figure 46: Spike rate acquired by extracellular recording under two concentration of OA treatment (600 nM, 60 nM) which represented the functional patterns during the disease propagation.....	67
Figure 47: Burst rate acquired by extracellular recording during two concentration of OA treatment (600 nM, 60 nM) which represented the network synchronous pattern changed during disease propagation.....	67
Figure 48: Preliminary results from loading beads into the microfluidic device without pillars pattern in the middle channels.	75
Figure 49: Four-layer pattern design of microfluidic device.	75
Figure 50: The cell seeding setups for cell culture in a microfluidic device in a sterile environment....	76
Figure 51: Images of the silica beads with neural culture on the surface, from the top surface focus plane towards the bottom direction.....	78
Figure 52: Neurons growing on the surface of silica beads inside the layer-pattern microfluidic device.	78
Figure 53: A microfluidic device with 4 layers pattern and fully filled with silica beads (Fig. A) and a 3D neural cell culture on silica beads captured from a 3D imaging result of one channel (Staining: MAP2, neurite) (Fig. B).	80
Figure 54: Cell density analysis and cell position in gel analysis based on a 3D image of the beads with cells in a microfluidic device (DIV 6) (one layer of beads).	80
Figure 55: The experiment design of the arrangement of the beads layers	81
Figure 56: Systematic diagram of loading different layers of beads into microfluidic device	82
Figure 57: Cell culture on silica beads in microfluidic device on day 6, 9 and 12.	82
Figure 58: Layer pattern 3D silica beads culture I microfluidic device on 12 DIV.	84
Figure 59: Collected gel-beads without cells inside.....	85
Figure 60: Agarose-alginate beads with cells inside were patterned into two layers inside a microfluidic device that has pillars for layer pattern (DIV 12).	87
Figure 61: Cell density analysis and cell position in gel analysis based on a 3D image of the beads with cells in a microfluidic device (DIV 12) (one layer of beads).....	87
Figure 62: Three possible models of interesting interaction between A β and Tau.....	93

Introduction

1

“Never lose a holy curiosity.”

by Albert Einstein

Alzheimer's disease (AD) is a well-known neurodegenerative disease of the brain. One of the main characteristics of AD is its aggressive propagation between the involved regions, but the mechanisms of disease propagation remain obscure. In order to understand AD progression *in vitro*, innovative tools that can allow interaction-controlled neuronal cultures and can distinguish complex functions in the neuronal network are required. Microfluidic technology, which is developed for precise manipulation of fluids through compartmentalized microchannels, has been widely applied in cell morphological studies, including neuroscience research. Microelectrode arrays (MEAs) technology, which allows for action potential recordings in excitable cells through the use of multiple microelectrodes, has been applied in neuronal electrophysiological studies as well. In this thesis, we integrate these two microtechnologies of combined microfluidic and MEA platforms to investigate AD disease propagation *in vitro* in a more comprehensive manner. Through the use of a compartmentalized channels structure within our microfluidic device, we build diseased and healthy "co-pathological" neuronal networks to mimic AD disease propagation and attempt to observe the alterations of morphological and electrophysiological characteristics during disease progression. We are moving towards building a "brain-on-a-chip" using microfluidic and MEA platforms, which may potentially make significant contributions to disease studies and pharmaceutical tests.

1.1 Alzheimer's disease

1.1.1 AD and its hallmarks

Alzheimer's disease (AD) is one of the most healthcare cost-intensive neurodegenerative diseases in the world with no efficient cure existing at present. The disease mechanism is still uncertain after many years of debate. The first symptoms for Alzheimer's disease (AD) were described at a conference in Germany by Dr. Alois Alzheimer in 1906. Later, in 1910, these symptoms were named "Alzheimer's disease" by Emil Kraepelin [111]. AD is a progressive neurodegenerative disease in the brain. Often, AD lesions propagate through the patient's brains for years before any symptoms appear. As the disease develops, impaired judgment, disorientation, confusion, abnormal behavior and difficulties in speaking, swallowing and walking start to appear, and gradually, AD gives patients more troubles in daily life, with cognitive and functional abilities declining and finally leading to death [3]. Under the situation that the disease mechanism is unclear, the diagnosis for the AD patients is uncertain and requires a series of medical assessments. After inquiring into a patient's symptoms in detail, physicians also need to analyze the patients' family's medical history, undertake cognitive tests, physical and neurological exams and biomarker tests (e.g., blood test, magnetic resonance imaging). However, more scientifically relevant diagnostic criteria are required for the clinical diagnosis of AD, such as biomarkers focusing on essential AD hallmarks.

AD, like the other neurodegenerative diseases, displays a spreading pattern through

anatomical connection across memory-related brain regions. It starts from the entorhinal cortex and progresses to all the hippocampal related sub-regions (including dentate gyrus, CA3, CA1 and subiculum) and finally spreads to the cortical areas via anatomical connections (Figure 1) [97, 57, 17]. During AD propagation, two major pathologies play an important role in the brain: the deposition of extracellular amyloid-beta ($A\beta$) plaques, and intracellular hyperphosphorylated Tau (hp-Tau) neurofibrillary tangles (NFTs) (Figure 2) [9, 124]. $A\beta$ plaques are composed of peptides cleaved by β -secretase and γ -secretase from the amyloid precursor protein (APP) (Figure 3) which is an integral membrane protein probably in charge of synapse formation [130], neural plasticity [151] and iron export [35]. NFTs are composed of aggregated and fibrillary hyperphosphorylated (hp) microtubule-associated protein (MAP) Tau protein (MAPT) (Figure 4). More recent hypotheses have explored the role of Tau oligomers and their toxic effects [155], and have focused on the correlation between $A\beta$ and Tau protein [68]. Based on the theories of $A\beta$ and NFTs, neuroscientists are focusing on promising therapeutic approaches such as anti-amyloid or tau based drug development to reduce amyloid-beta production, prevent amyloid-beta aggregation, and promote amyloid-beta clearance [101]. As the common histopathological hallmark of AD, the “ $A\beta$ cascade hypothesis” was first proposed to explain the pathological mechanism of $A\beta$ neurotoxicity, which strongly contributed to the development of AD therapy [61, 56, 55]. The current therapeutic approaches in clinical trials are mainly focused on reducing of $A\beta$ level, but unfortunately, remain unsuccessful after several treatment candidates [50, 51, 33]. Hp-Tau, another potential therapeutic target is attracting the attention from researchers as well because of its strong correlation to cognitive decline in AD compared to $A\beta$ [97, 17]. The hallmarks of AD provide clues (e.g., determining the level of $A\beta$ accumulation in the brain) that should be investigated in order to better diagnose AD early and accurately [147].

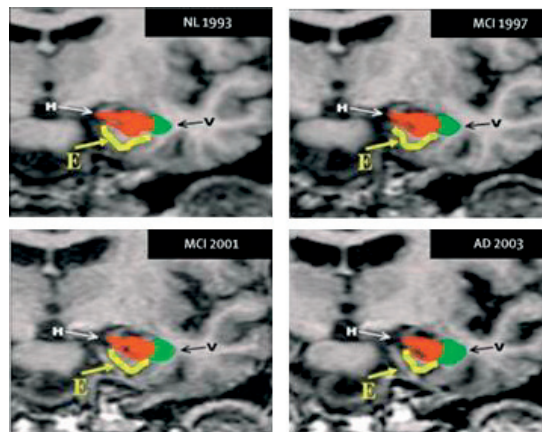


Figure 1: Medical information of brain scans from an AD patient from 1993 to 2003 by Magnetic resonance imaging (MRI). This evidences showed how the disease progresses: Hippocampus (red) and entorhinal cortex (yellow) shows an apparent shrink, meanwhile the ventricular system which contains cerebrospinal fluid (green) increased in volume during the 10 years of disease propagation. Reprinted from [9] with permission

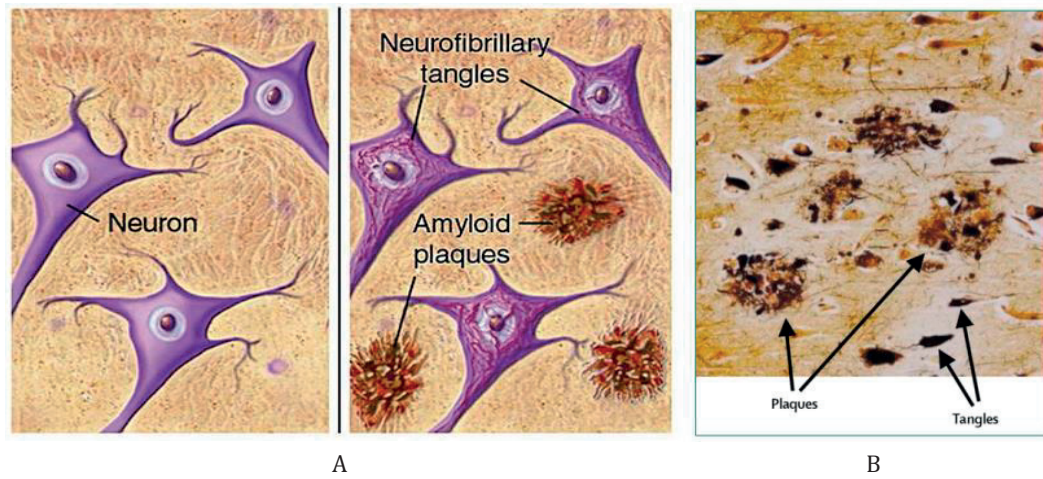


Figure 2: Plaques and tangles in the cerebral cortex in AD. (A) Schematic pictures of healthy neurons (left) and diseased neurons in AD brain (right) (B) Stained tissue from a diseased brain. A β plaques are the round structures. The triangular shapes are the neurofibrillary tangles made of hp-Tau. Reprinted from [4] with permission from Elsevier

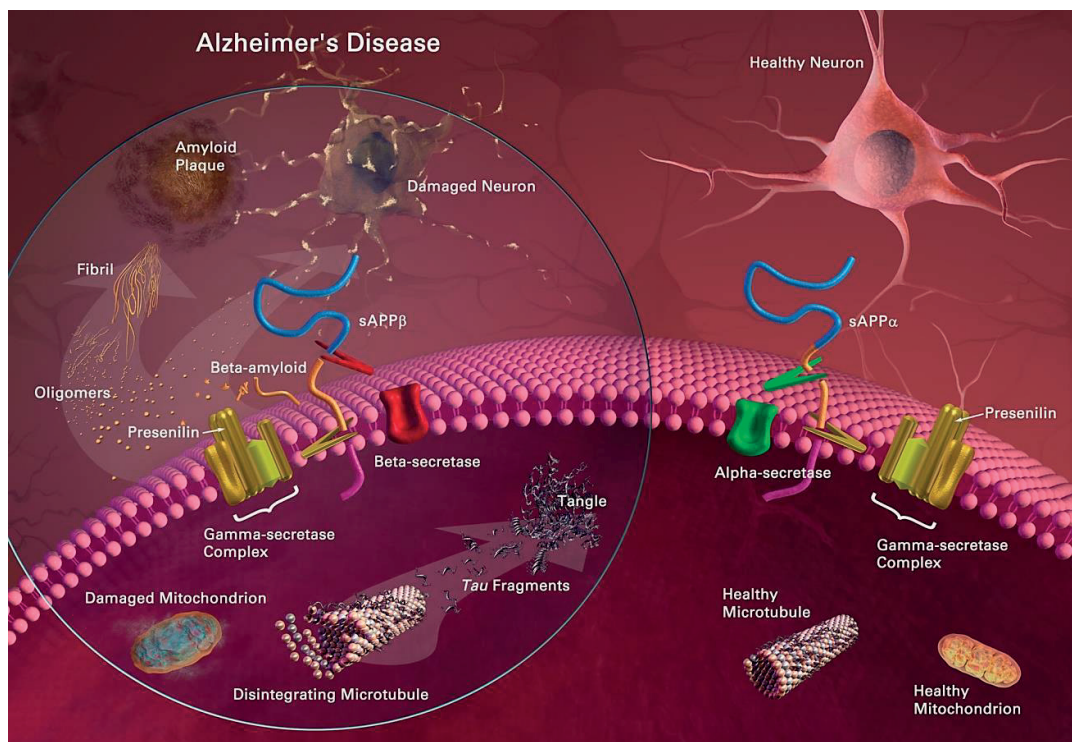


Figure 3: Comparison between healthy neuron and Alzheimer's Disease neuron. Image courtesy of the National Institute on Aging/National Institutes of Health.

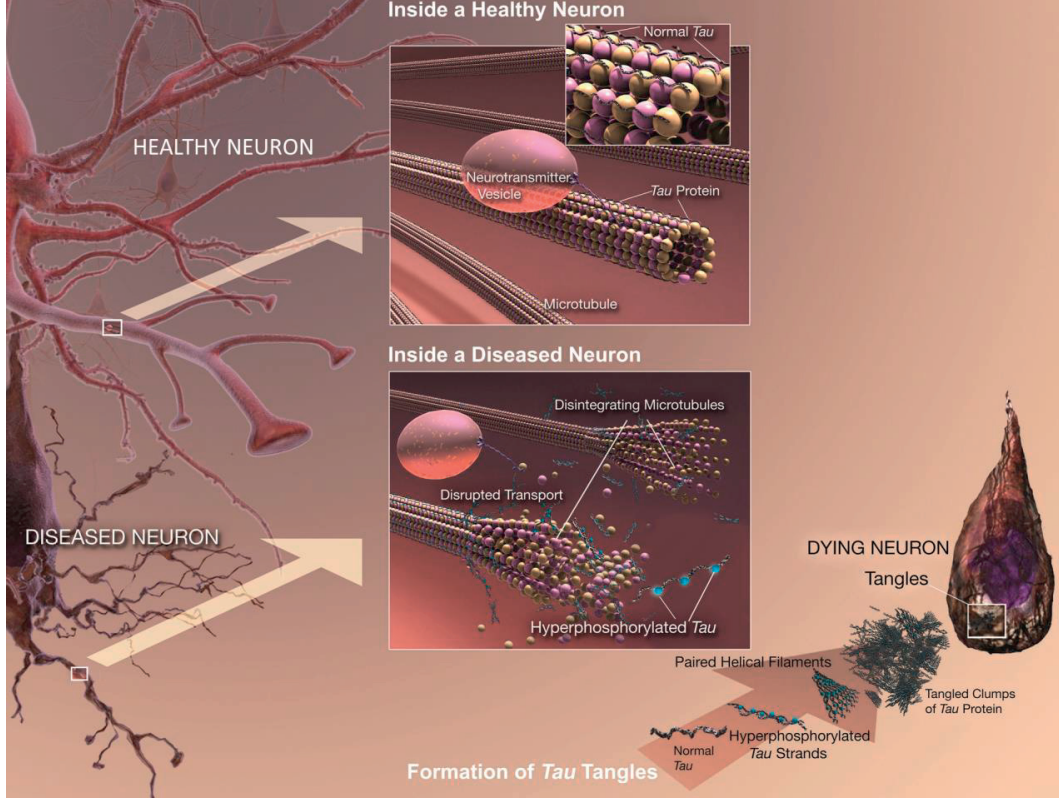


Figure 4: Comparison between healthy neuron and Alzheimer diseased neuron on Tau protein. Image courtesy of the National Institute on Aging/National Institutes of Health

1.1.2 Formation of NFTs from Tau protein

In this thesis, we focus on the Tau pathology of AD. Inside a healthy neuron, MAPs are the proteins that can interact with the microtubules of the cellular cytoskeleton to regulate the stability of the microtubules. Tau protein is one type of MAPs also called microtubule-associated protein Tau (MAPT). It can interact with tubulin to stabilize the microtubules and promote the tubulin assembly into microtubules [90]. Tau protein is a highly soluble MAP, not present in the dendrite and is primarily in the distal portions of the axon [8, 79] where it stabilizes the microtubules [15]. It is a vital factor in regulating microtubule dynamics, axonal transport and neurite outgrowth, and all these functions of Tau are modulated by site-specific phosphorylation [72]. Tau protein dephosphorylation helps to prevent dimerization and subsequent PHF formation [7]. When Tau protein is regulated in an abnormal way, it becomes highly phosphorylated Tau (hyperphosphorylated-Tau, hp-Tau). Afterwards, the aggregation of hp-Tau becomes the major component of the paired helical filaments (PHFs) [7] and together with straight filaments [53] forms NFTs, one of the hallmarks of AD and other Tauopathies [26]. During this spreading of AD, the neuron-to-neuron transmission has been proposed to be important [109]. More specifically, the spreading of Tau pathology was observed along the synaptically connected circuits in a transgenic mouse model and this indicates that the secretion of Tau by

presynaptic neurons and its uptake by the postsynaptic neurons could be the sequential events leading to the propagation of Tau pathology in the brain [109].

We investigate this neuron-to-neuron transmission theory during AD progression in an AD model *in vitro* using compartmentalized microfluidic device. In order to further study the function of the axonal network during disease propagation, we distinguish the axonal network from the other parts from the neuronal network to exclude other factors, e.g., the dendrite-axon interaction and the soma-axon interaction, only focus on the axon-axon transmission of Tauopathy during the disease propagation.

1.1.3 Propagation of Tau pathology in AD

Degeneration in AD starts from the transentorhinal cortex (A), spreads to the hippocampal formation, anterior temporal cortex and polymodal and unimodal association areas, (Figure 5 B) and eventually invades the entire cerebral cortex in the final disease state (Figure 5 C) [36]. Neurofibrillary tangles (NFTs) as a hallmark of AD, have been tracked to observe disease propagation *in vivo* by following the microtubule-associated Tau protein (MAPT) in a transgenic mouse model, and it has been observed that Tau pathology has evolved in the same predictable pattern as the early neuropathological development of AD [17]. More specifically, the spreading of Tau pathology was observed along synaptically connected circuits, and this result indicates that secretion of Tau by presynaptic neurons and its uptake by postsynaptic neurons could be the sequential events leading to the propagation of tau pathology in the brain [109]. All these data support the hypothesis that the local Tau aggregation can be transmitted from neuron to neuron, which plays an important role in the progression of Tau pathology.

To date, there is no cure for AD and no pharmaceutical company has succeeded in developing a fully effective treatment against the progression of AD symptoms. This pressing situation encourages us to develop novel experimental approaches to better understand AD. It is imperative to acquire proper models and tools, which allow for more accurate control and multifunctional tests both on disease mechanism and diagnosis studies, based on the mechanisms of A β plaques or NFTs have already been identified.

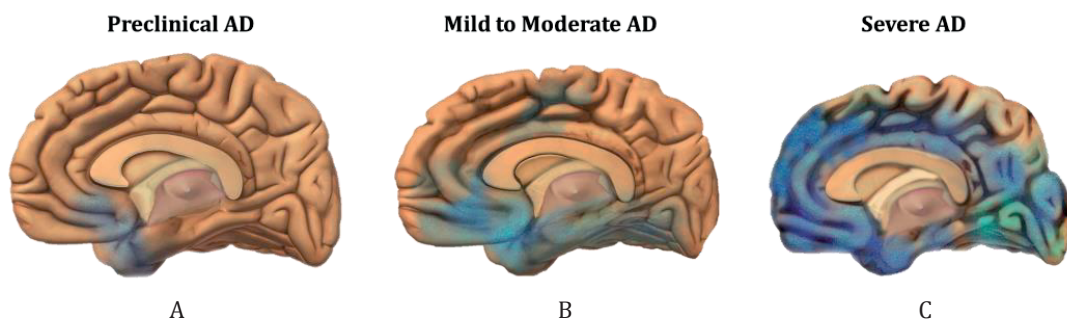


Figure 5: AD spreading through the brain. Image courtesy of the National Institute on Aging/National Institutes of Health

1.2 Morphological studies

1.2.1 *In vivo* and *in vitro* models to study AD

In order to understand AD mechanisms comprehensively, both *in vivo* and *in vitro* models have been developed [99]. *In vivo* studies take advantage of the full complexity of the brain structure and function; however, the functional and molecular pathways still cannot be clearly understood. To understand structural connections and their impact on the diverse range of brain functions during neurodegeneration processes, *in vitro* models that allow for controlled interaction are indispensable. They open the possibility of better understanding the mechanisms of the propagation of AD in a more controllable environment, where we are able to study cellular and molecular mechanisms in a simplified and controlled way. Nowadays, studies on AD are usually performed in conventional cell culture tools such as plastic petri dishes or multi-well plates for a large number of experiments. In order to understand AD progression *in vitro*, novel tools that help to distinguish the different functions of each component in the neuronal network and their contribution during disease progression are required.

1.2.2 Microfluidic technology for *in vitro* neuroscience research

Micro-electro-mechanical systems (MEMS) is a technology which combines miniaturized mechanical and electrical components developed from microfabrication. Lab-on-a-chip (LOC) is a subset of MEMS that provides high sensitivity and resolution in experiment by manipulating small amounts of sample in a single chip. Microfluidics, which is related to LOC, is developed for precise manipulation of fluids at the submillimeter scale and was first applied in cell biology in the 1980s [104]. Nowadays, microfluidic devices have been widely used in biological and biomedical applications, and have involved in neurological studies as well. The first *in vitro* compartmentalized neuronal culture was described by Robert B. Campenot in 1977 (Figure 6) [119]. In this three-chamber neuron culture system, neurites from the sympathetic neuron somata grow through the engraved glass to other chambers built by fluid impermeable barriers, so that the neuron soma and their neurites still keep their physical connection, but are cultured in different environments [18]. Campenot's isolated chamber model gave the possibility of culturing neurites and somata separately in compartmentalized environments in the scale of millimeters to micrometers. This was when the compartmentalized neuronal culture concept started and has since been better implemented in microfluidic devices because of the rapidly advances in microtechnology.

1.2.3 Characteristics and fabrication techniques for a microfluidic device

Our microfluidic devices are produced in a cleanroom from the Centre of Micro and Nano technology of Swiss Federal Institute of Technology (Lausanne, Switzerland). In this cleanroom, the working environment provides controlled level of contamination,

specified by the number of particles per cubic meter. This can largely avoid the environmental particles on our device such as dust and chemical vapors. This is crucial for microfabrication because the functional elements from the products are at the microscale, which makes it sensitive to pollutants. Our microfluidic device for neuronal culture requires several microfabrication techniques including Photolithography, Wet oxidation, Si DRIE etching, Si and SiO₂ RIE etching and device molding. Benefitting from the use of these techniques, we have the ability to fabricate chambers of different heights in a single device. By adequately choosing the heights of different chambers in a microfluidic device, we can isolate the neuron body (around 20 μm in diameter) in one compartment and only allow the neurite (which may be either a dendrite or an axon) to grow through a narrow channel, which we call the junction channel. The theory of using junction channels for neuronal culture is shown in Figure 7. Depending on the length of the junction channel, we can also isolate the dendrite and axon, which have very different lengths. In the case of a long junction channel, the dendrite is not long enough to grow out of the channel and only the axon can grow out of the junction channel and reach another isolated compartment (Figure 8) [144]. By using junction channels, we can obtain and observe an isolated axonal network without interaction from the cell soma and dendrite, and this is one of the main advantages of using microfluidic devices for neural culture. In brief, for our morphological study on AD propagation, the microfluidic device allows us to mimic disease propagation patterns with an isolated axonal network. The culture medium and drug exposure are precisely and locally controlled at the microscale.

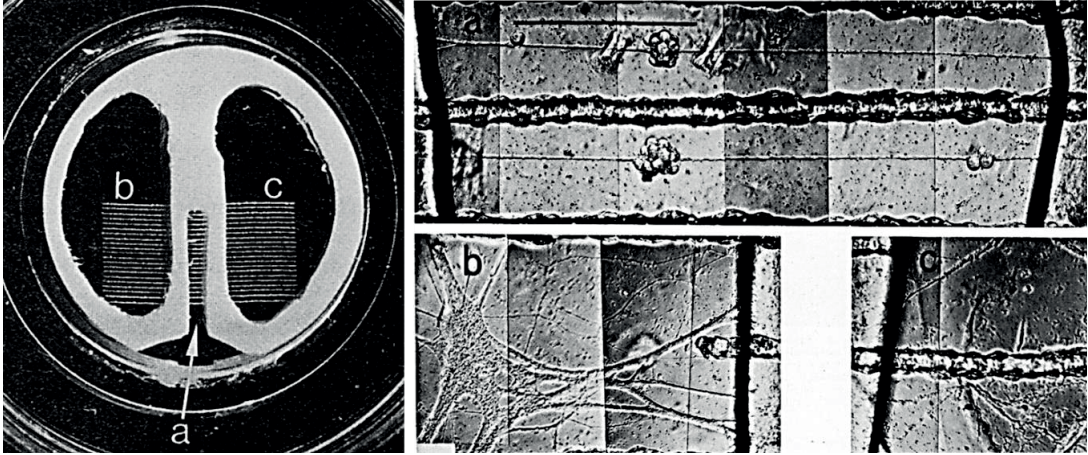


Figure 6: The first compartmentalized microfluidic device for neuronal culture. The three chambers were divided by a Teflon set-up which is sealed to the petri dish with silicone grease. The neurons were plated in chamber a and the neurites grew into lateral chambers b and c by the guiding of a series of scratches in parallel [15].

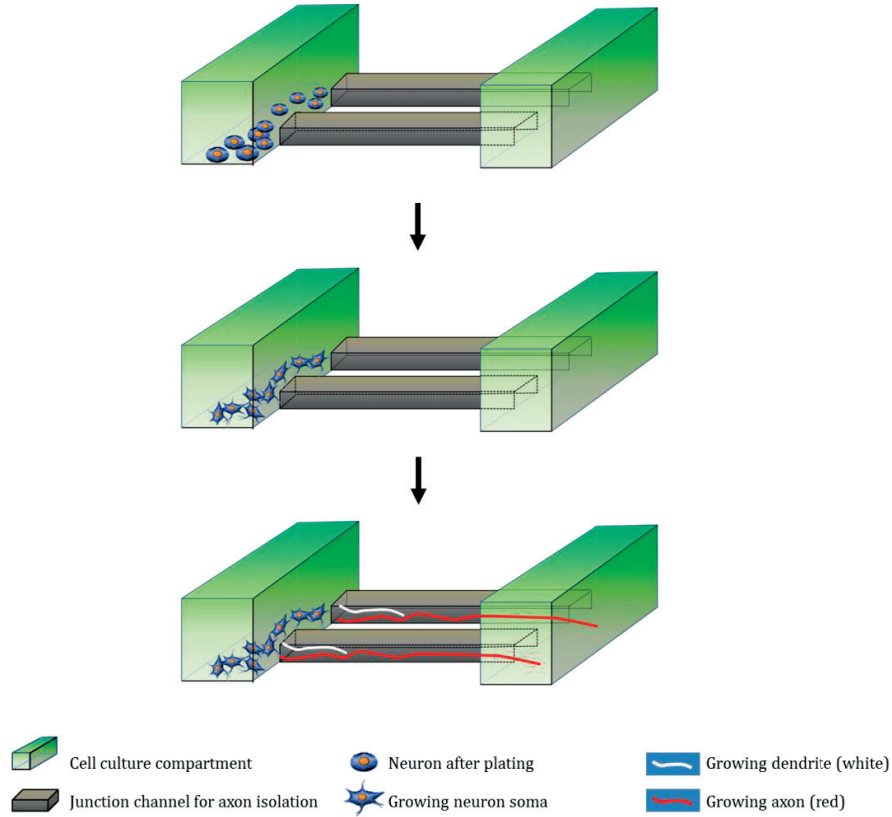


Figure 7: Schematic diagram of the manipulation with microfluidics for neural culture. The channel that blocks the cell soma and let the axon to pass through is called the junction channel. The height of the junction channel is smaller than the diameter of the neuron, so that we can use the junction channels to isolate the axon from the neural soma and build an isolated axonal network in a different environment

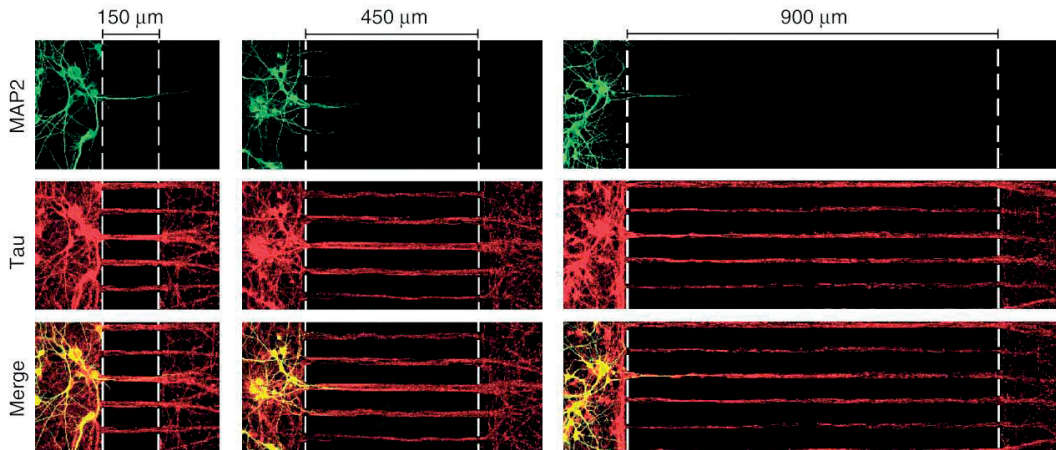


Figure 8: Variation of the junction channels (150 μm , 450 μm , 900 μm) for the microfluidic device to isolate neurite or axon. When the junction channels is 450 μm or more (14 DIV), the dendrite cannot grow through the junction channel (green, MAP2), and the axon (red, Tau) was observed growing through to the end of the junction channels (dashed lines indicate the end of the junction channels). Reprinted from [16] by permission from Macmillan Publishers

1.2.4 Microfluidic device and its application on neuronal culture

Microfluidics, a multidisciplinary field involving manipulation of liquids and gases in micro-scale channels, has become one of the central technologies in miniaturized systems and has been applied in many disciplines such as physics, chemistry and biology. The miniaturization using microfluidics produces a lot of advantages, for instance, small quantities of samples and reagents, carrying out separations and detections with high resolution and sensitivity, low cost, short time for analysis and portability. Historically, silicon has been the most widely used as the base substrate material for fabricating microfluidic devices [93] benefitting from its suitable electrical and mechanical properties for microfabrication. However, Si is relatively expensive for mass production of disposable devices and its opaque property makes it less compatible for microscopy analysis [107]. Many new types of material have been used for microfabrication, especially polymers such as polycarbonate (PC), polymethylmethacrylate (PMMA), polyvinylchloride (PVC) and polyethylene (PE) [105]. One of the most used polymers is polydimethylsiloxane (PDMS). PDMS is a silicone elastomer with desirable properties such as transparency, gas permeability, biocompatibility and low cost, which make it attractive for microfabrication. All these aspects make PDMS an excellent material for the fabrication of microfluidic devices for biological use. PDMS is viscoelastic and the solidification of PDMS can be accelerated by adding a curing agent. That is the reason that we usually use a PDMS base together with a curing agent to make PDMS mixture. When the temperature increases, the PDMS mixture becomes cross-linked and solidified and this property of PDMS makes it a good material for molding devices. When it becomes solidified, the pattern from the mold (e.g., silicon wafer with pattern on its surface can be used as a mold) is replicated to the PDMS surface. For fabricating the silicon wafer for PDMS devices, the procedures are shown in Figure 9 that involves photolithography, etching and molding. PDMS is used for the molding step to make the bulk of the device. The pattern from the silicon wafer is inversely replicated on the PDMS surface (Figure 9 E) [42]. The micro-scale channels become present on the PDMS surface, for instance, the junction channels from the microfluidic device for axon isolation are fabricated in this way.

For the microfluidic device for neuronal culture, PDMS serves as a very suitable material. The junction channels from the microfluidic device can isolate the axon from the neuronal soma and this gives the microfluidic device a big advantage for neural cell culture compared to normal culture dishes (Figure 10) [119, 121, 84]. Microfluidics technology has already been widely applied in cell morphological studies and it has become an innovative culture device to build compartmentalized neuronal culture for neuroscience studies. For neurite isolation by the microfluidic device, different lengths of junction channels can be used to distinguish the dendrite and axon because of the faster growth and greater length of the axon compared to dendrite [34]. Longer junction channels ($>300\text{ }\mu\text{m}$) can distinguish the axon from the dendrite. The junction channels with small cross-section have a smaller volume compared to the large channels, which also

makes them a barrier between two compartments to slow down the chemical diffusion effect between two compartments.

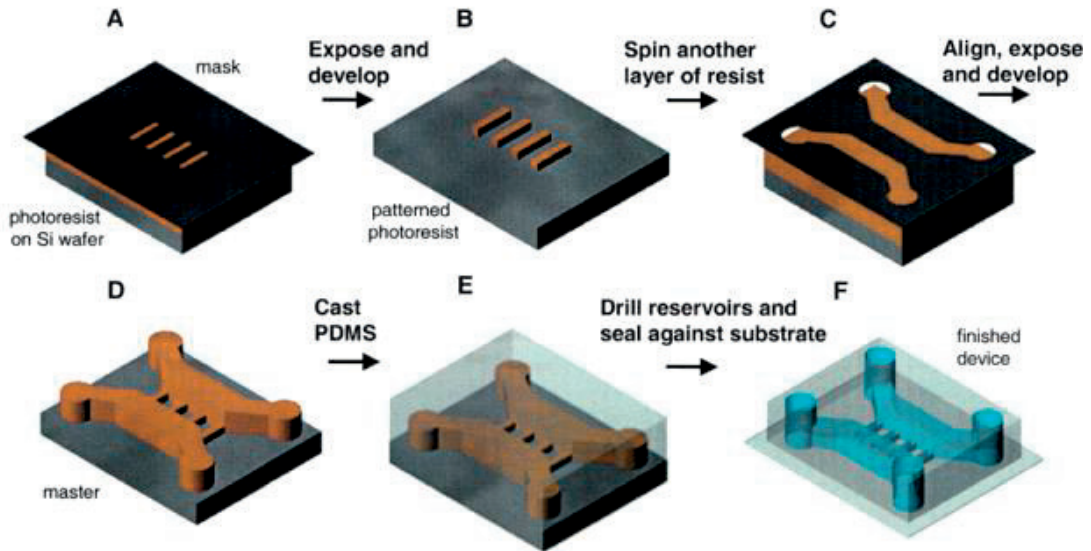


Figure 9: Schematic fabrication process of a microfluidic device made of PDMS for neuronal culture. The double photolithography steps create two different heights of channels. The first photolithography makes the junction channel, and the second photolithography makes two big compartments. Reprinted from [146] with permission

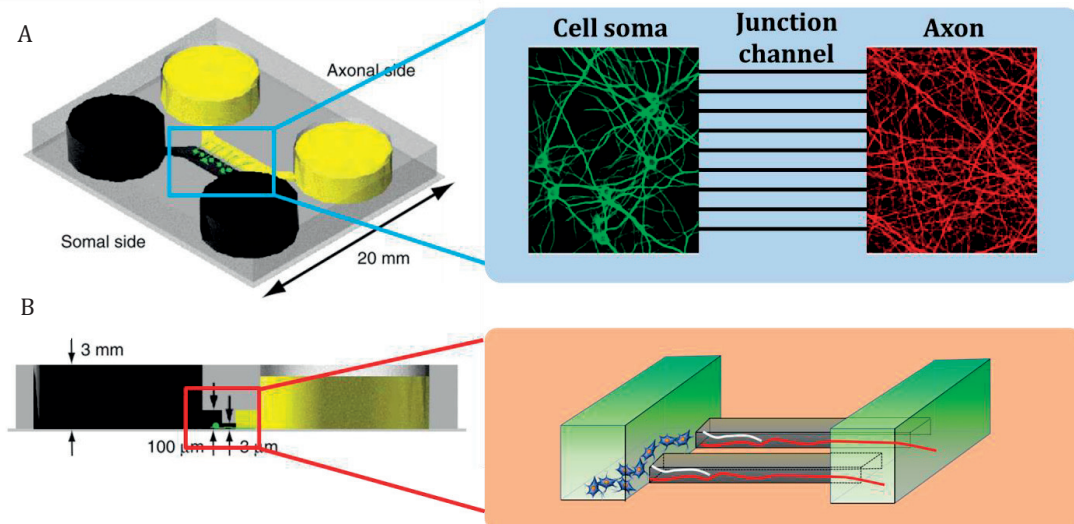


Figure 10: Microfluidic neural culture platform. (A) Perspective picture of the PDMS device with two chambers (black and yellow) which are connected by many junction channels (10 μm in width and 3 μm in height, 450 μm in length) to let the axon to grow through. (B) Side view of the device. The cell soma is isolated on the left side of the junction channel and only the axon (in red) grows through the junction channel and reaches at another chamber. Reproduced from [144] with permission

1.2.5 Microfluidic device for AD studies

Benefitting from the compartmentalized chambers and the neurites isolation design, microfluidic device has been used for neurodegenerative diseases studies, including AD studies. In AD, the disease spreads from one region to another in the brain. Tau pathology has evolved in the same predictable pattern as the early neuropathological development of AD [17]. There is a hypothesis stating that the local Tau aggregation can be transmitted from neuron to neuron, which plays an important role in the progression of Tau pathology [36, 109]. It was also reported that the secretion of Tau by presynaptic neurons and its uptake by postsynaptic neurons could be the sequential events leading to the propagation of Tau pathology in the brain [109]. This indicates that the axonal transportation participates in the disease propagation. These neuron-to-neuron and presynaptic-to-postsynaptic models can be simplified and built into microfluidic devices with compartments by using the junction channels to distinguish the axonal network from the whole neuronal culture, in order to exclude the other factors that also potentially to contribute to AD propagation and focus on the axonal transportation for Tau pathology studies.

In 2011, Anja Kunze used a compartmentalized microfluidic device to build a co-pathological model for Tauopathy study (Figure 11) [85]. In this model, a diseased cell population communicated with a healthy cell population from another compartment through culturing their axons in the same compartment, which was isolated from the two cell population compartments. The diseased cell population was induced by okadaic acid (OA), an inhibitor of Tau dephosphorylation. As an example, OA infused into the right lateral dorsal hippocampus area of ovariectomized adult rat induced NFTs-like AD pathology *in vivo* [158], which we replicated *in vitro*. During the drug exposure, OA diffused through the junction channel and created a gradient in the middle channel where axons were growing (Figure 11 A). As a result, the OA-induced cell population exhibit hp-Tau aggregates in the neurites and the soma. The axonal network under gradient exposure of OA presented different phosphorylation states (Figure 11 B). The un-exposed cell population revealed a homogeneous Tau distribution and hp-Tau was heavily increased after 24 h. All these results demonstrate that a novel experimental model to generate co-pathological states within two separated primary cortical cell compartments that are connected through a neurite network. This device opens the possibility of study cellular and molecular propagation mechanisms in neurodegeneration in Tauopathies (e.g., in Alzheimer), as well as simultaneous drug effects on connected healthy and diseased cell populations.

Building a co-pathological neuronal network in a compartmentalized microfluidic device has been proved as an appropriate simplified model to mimic the disease propagation *in vitro*. It is reasonable to continue using this model for neurodegenerative disease studies. This microfluidic device could also integrate with other microdevices to investigate more characteristics of AD during disease propagation. For example, a re-

cording device could be added to observe the electrophysiological alterations besides the morphological observations from the microfluidic device. This will help us to understand sequential occurrences of structural and functional change, which will potentially promote research on AD early diagnosis.

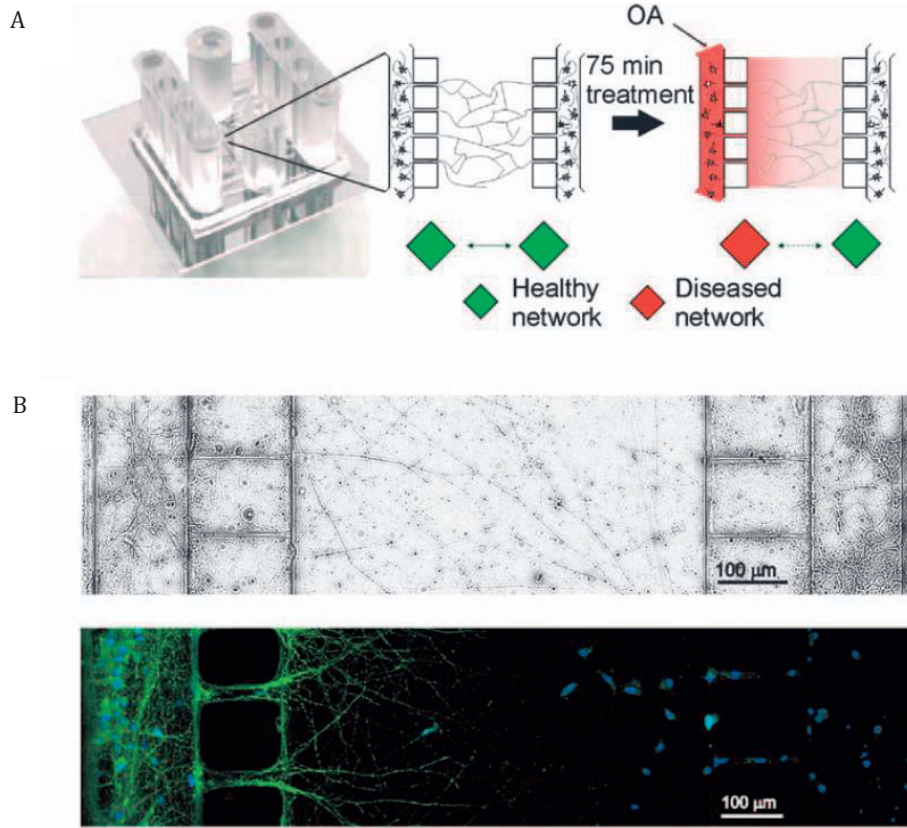


Figure 11: Images of primary cortical neural network in compartmentalized PDMS microfluidic device after OA treatment. (A) Differential interference contrast (DIC) image of the primary cell culture in the microfluidic device before OA treatment (B) Immunocytochemical staining image of primary cortical neurons in the microfluidic device after OA treatment (600 nM) for 75 min on the left cell population. (Green: CY-2, blue: DAPI) Reprinted from [85] with permission

1.3 Electrophysiological studies

1.3.1 Development of technologies for neural activity recording

Besides the morphological characteristics, electrical properties play an indispensable role in living beings, from a single ion channel on the cell membrane to whole organs like the heart. In 1939, Prof. Andrew Fielding Huxley first started to study the squid giant axon, and with the large nerve fibre from the axon, he found keys to understanding the electrical activity that excites biological cells which had been a mystery since the 18th century [45]. Kenneth Cole and George Marmont invented the first voltage clamp and the first experiments with this equipment were made in 1947 [65]. They made an internal

electrode to be inserted into a squid giant fibre. The current would be fed to the electrode under feedback control and Cole added an arrangement by which alternatively the potential of the electrode could be controlled electronically. Based on this voltage clamp technique, Prof. Andrew Fielding Huxley established that the ions carry electrical signals in nerves (Figure 12) [63, 62], and received the Nobel Prize with Alan Lloyd Hodgkin and John Carew Eccles “for their discoveries concerning the ionic mechanisms involved in excitation and inhibition in the peripheral and central portions of the nerve cell membrane” in 1963 [45]. At the same time period, microtechnology started to progress and the patch clamp technique was invented in the 1980s by Erwin Neher and Bert Sakman, which was essentially a more refined version of the voltage clamp [134]. It allowed the study of ion channels in a wide range of excitable cells. They won the Nobel Prize in Physiology or Medicine in 1991. Meanwhile, new recording technologies were required which could be more reliable, have lower noise and higher throughput than the patch clamp technology, even though planar patch clamp had been commercialized at that time [135]. During the past decades, several technologies have been developed to record the action potential, including current clamp, voltage clamp, patch clamp. However, these technologies are based on intracellular recording techniques. Compared to the new extracellular recording technologies, intracellular recording technologies are limited to recording individual neurons by inserting electrode into the intracellular environment and it is regarded as an invasive method [139]. New technologies that allow for long term recording and large number of cells recording are required. Based on the fast development of microtechnology in the past decades, new techniques such as microelectrode array (MEA) have brought us into a new era in ion channel research. This technology of recording extracellular neural activities is applied in this thesis to study the electrophysiological alteration during AD propagation.

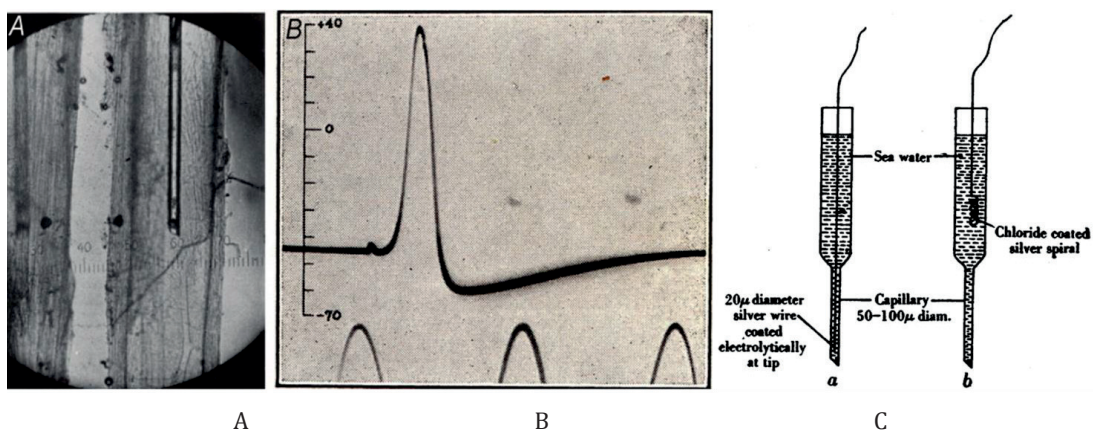


Figure 12: Intracellular recording of the squid giant axon. (A) Photomicrograph of an electrode inserted inside a squid giant axon (around 500 μm diameter). (B) The first intracellular recording of an action potential. (C) Types of microelectrode employed. Images were taken from Hodgkin and Huxley in 1945. Reprint from [63] with permission

1.3.2 Intracellular recording methods *in vitro*

As mentioned previously, it has been a long way to understanding the physiology of neural activity and inventing new tools to assist our exploration on electrophysiology. In 1947, Kenneth Cole and George Marmont did the first experiment with the voltage clamp and detected that the action potential is generated by sodium ions moving down their concentration gradient [65]. Voltage clamp measures how much ionic current passes the cell's membrane under a certain voltage and this mechanism is strongly related to the natural characteristics of voltage-gated ion channels. This is an invasive method, which requires inserting microelectrode inside the cells. Instead of inserting a sharp microelectrode inside the cell, the new patch clamp technique applies a glass micropipette tip and an electrode together to attach to the cell membranes in different ways (Figure 13) with advantages and disadvantages [96]. Intracellular patch clamp and techniques which allow direct measurement inside the cell, are still the prime tool to characterize the sub-threshold synaptic potentials, membrane oscillations and action potentials [139] even though they have some limitations (e.g., cell invasion and limited number of cells for recording). The new planar patch clamp has been developed based on patch clamp technique (Figure 14). It is based on microfabrication technology which provides greater than two orders of magnitude increase in throughput compare with the traditional voltage clamp techniques [82]. This type of automated patch clamp can avoid a mass of manual work on inserting the electrode for the operators. In general, patch clamp has greatly contributed to neuroscientists on intracellular recordings until now, including on Alzheimer's disease studies [67, 136] to illustrate the electrophysiological properties of AD.

1.3.3 Extracellular recording methods *in vitro*

Meanwhile, the noninvasive extracellular recording techniques have been invented. Nowadays, substrate-integrated MEAs technique is an innovative methodology in studies on neuronal circuit-connectivity, physiology and pathology *in vitro* and *in vivo* [139]. MEAs technique enables simultaneous recording of the electrophysiological signals and stimulation in a neural network from native brain slices or neuronal cultures by a certain quantity of recording electrodes [139] for days and months. This recording system combines a neuron, a cleft between the neuron and the substrate, and the recording electrode at bottom to monitor and stimulate the activity (Figure 15). The obtained signals are amplified by the amplifier and sent to the data acquisition system for further analysis. The substrate is coated with chemicals depending on the cell type for cell adhesion like in a normal culture dish. Figure 16 and Figure 17 present some basic concepts of neuronal activity, e.g., spike and burst, from the MEA recording.

Complementary metal oxide semiconductor (CMOS)-based MEA can achieve higher signal resolution by increasing the number of the electrodes (e.g., 16,384 electrodes per MEA [88]) and reducing the diameter of the electrode tip. It allows extracellular recordings at a very high spatio-temporal resolution. By including amplification on the chip it-

self, noise is minimized and a high signal quality is guaranteed. However, increasing the number of neurons results in the need for sorting out the single neural activity from the neural network. This is referred to spike sorting, which is a time consuming task [95]. This challenge is specially true happened for the MEA device with a huge number of electrodes, such as the CMOS technology [38]. Recent developments in measurement techniques and in spike sorting algorithms help to overcome some of the limitations of extra-cellular recordings, which enable high-density MEAs (HDMEA) to obtain clear and reliable signals [41].

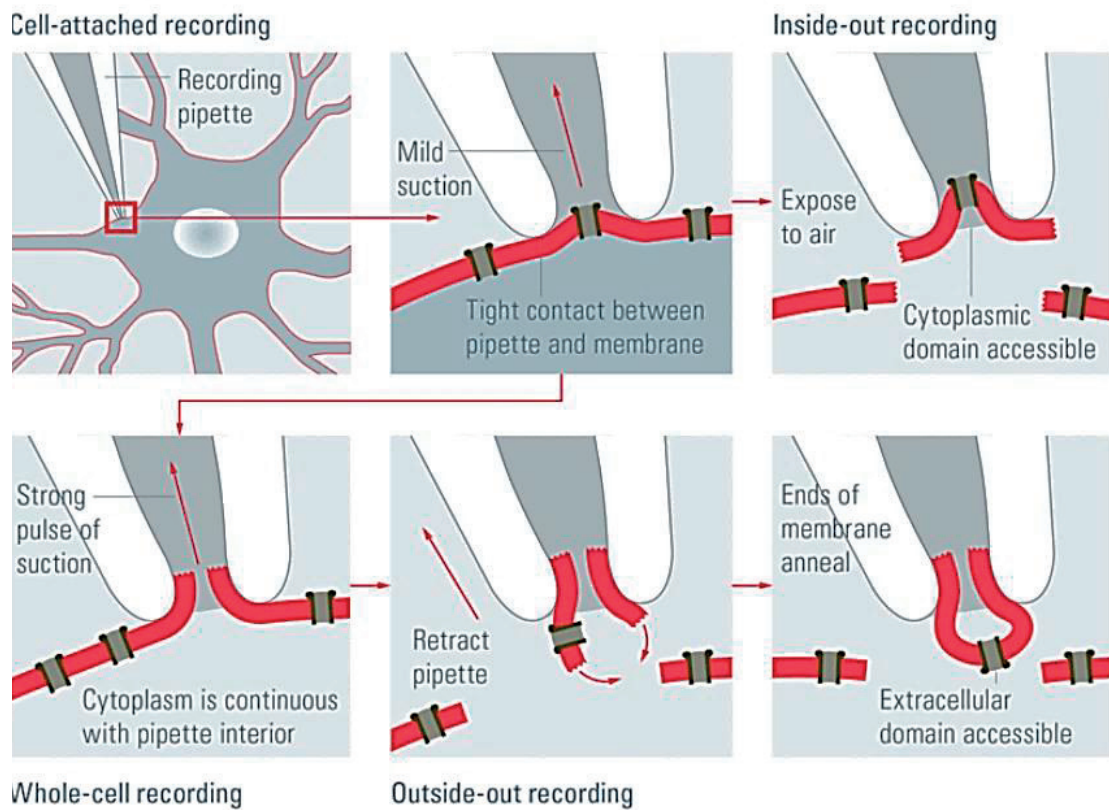


Figure 13: Four methods for patch clamp including cell-attached recording, inside-out recording, whole-cell recording and outside-out recording. Source: <http://www.leica-microsystems.com/science-lab/the-patch-clamp-technique/>

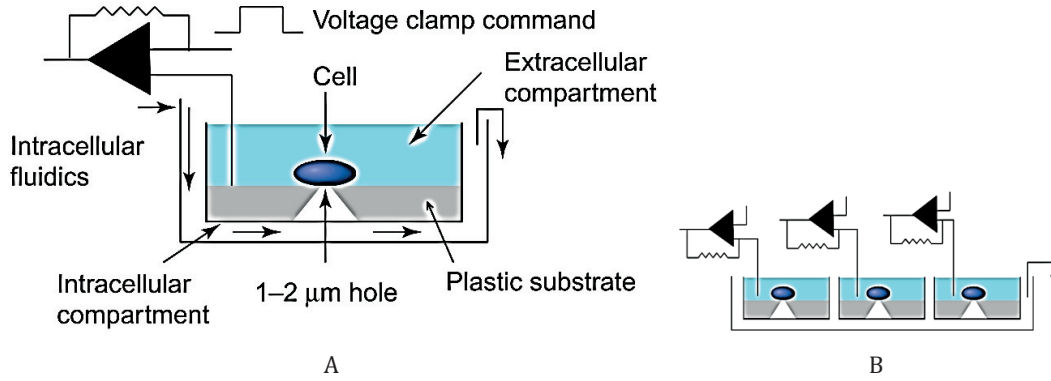


Figure 14: Schematic of the design of the planar patch clamp system. (A) A single chamber showing the compartments and a cell. Cell is loaded into its chamber and negative pressure is applied to pull the cells into the holes to form high-resistance seals like the “tip” from the patch clamp. The membrane within the hole is subsequently mechanically, electrically or chemically perforated to obtain a whole-cell recording configuration. (B) An array of three chambers. An actual array might have between 2 and 384 wells. Reprinted from [6] with permission

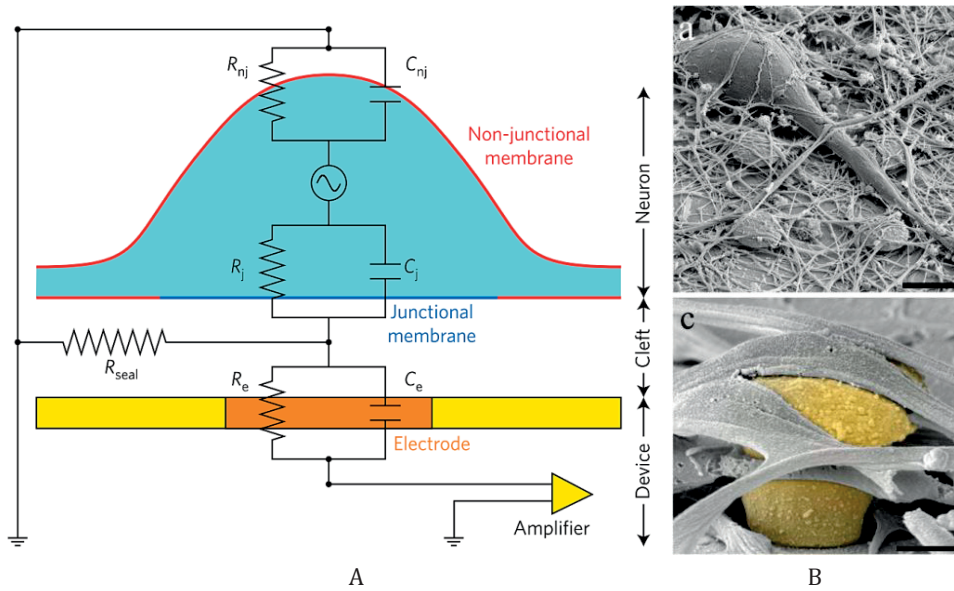


Figure 15: Theory of MEA recording and an example of MEA device. (A) Schematic layout depicting the spatial relationships between a neuron and a substrate-integrated electrode and the analogue passive electrical circuit. Reprinted from [139] with permission. (B) Scanning electron microscope images of neurons grown on a matrix of gM μ Es. Reprint from [116] with permission

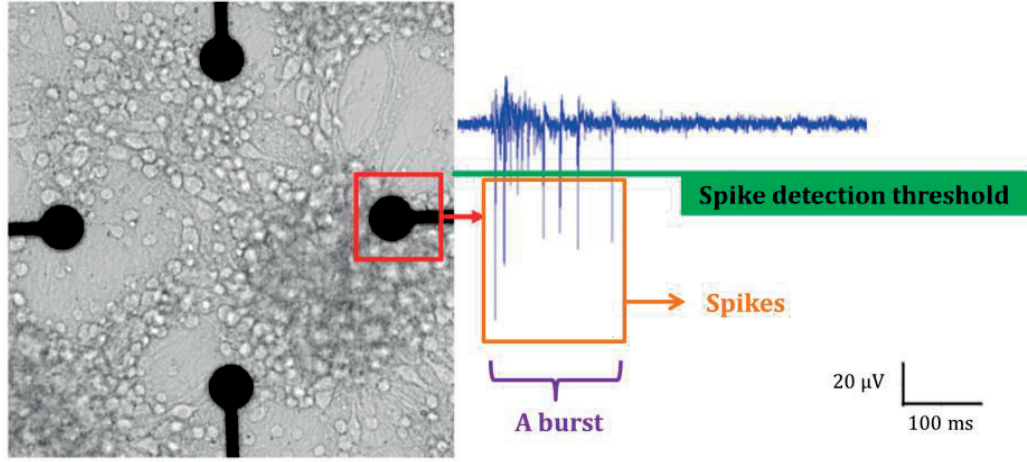


Figure 16: Neuronal network on a microelectrode array (MEA) device and the illustration on the basic concepts of electrophysiological activity. Reproduced from [114] with permission

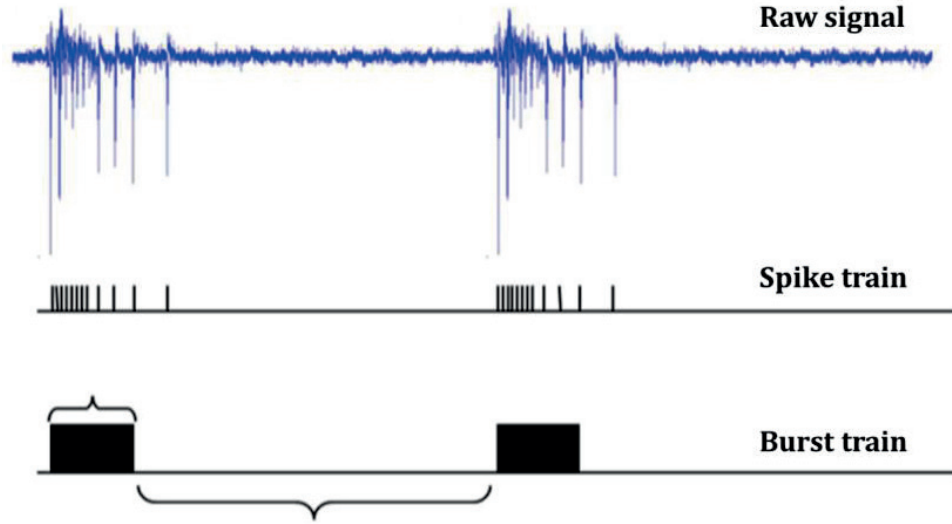


Figure 17: The illustration of spike train and burst train with an example of a raw signal. Reproduced from [114] with permission

Comparing the CMOS-based MEA to our glass-substrate based MEA, our device cannot allow large numbers of electrodes. However, the material used for CMOS is opaque and it cannot be used with inverted microscopy technology. MEA devices are fabricated on a transparent glass substrate, which means it is more compatible for microscope imaging than a CMOS device. This transparency is a particular indispensable property for our integrated microsystem that aims synchronous for morphological and electrophysiological observations. At the same time, our glass-substrate based MEA is more flexible and fabrication costs are lower.

Another important property of the recording device is the signal-to noise ratio [66]. There are two main factors that influence the cell-chip coupling: the cell adhesion and the input impedance of the electronic interface [12]. A large sealing gap between the recording neuron and the electrode increases the resistance and decrease the signal amplitudes [133]. The electrode itself with a big impedance can lower the signal quality as well [12]. These are the reasons that other shapes of 3D electrodes have been developed, e.g., the gold mushroom-shaped microelectrodes (gM μ Es) (Figure 15 B) [54]. These gM μ Es electrodes enable simultaneous electrical recordings from many individual neurons at a quality comparable to intracellular recordings by sharp or patch electrodes.

1.3.4 Microelectrode array recording technology

Microelectrode arrays (MEAs) technology is an extracellular recording and stimulation technology based on microtechnology. The development of MEA technology started from C. A. Thomas Jr. in 1972 (Figure 18) [148]. By using a planar multi-electrode array, field potentials from spontaneously contracting sheets of cultured chick cardiac myocytes could be recorded, whereas recording of activity from single cells was not possible [129]. Today, MEA devices are used in neuroscience laboratories to characterize electrophysiological signals from either natural brain slices, or *in vitro* neural networks from dissociated neurons. MEA recorded data can be analyzed to extract functional connectivity and functional links in *in vitro* neural networks using statistical algorithms [43].

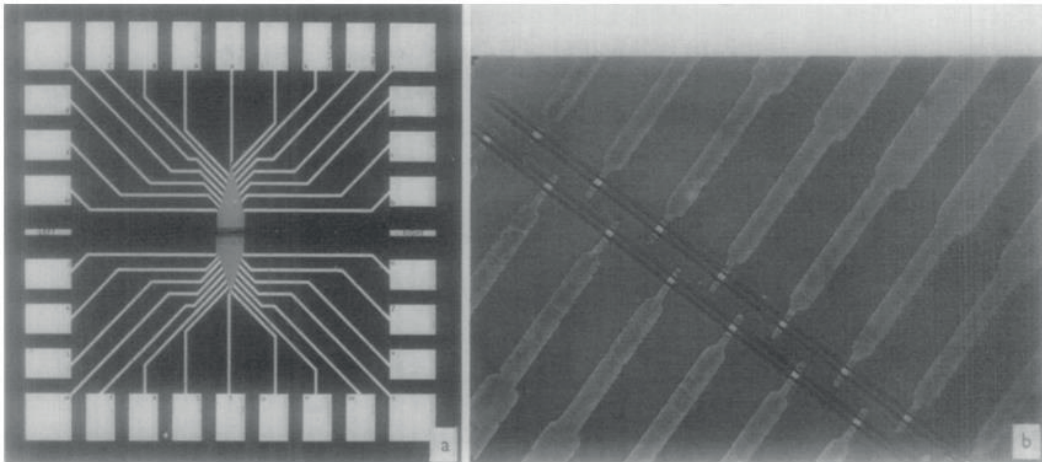


Figure 18: The MEA device invented in 1972. (A) The plan view of the completed MEA device which contains 30 electrodes. (B) The electrode tips covered with photopolymer insulation [19]

The MEA devices we used in this thesis were fabricated in a cleanroom as well as the microfluidic device. It contains 60 electrodes, which allow for simultaneous recording from multiple points in the neuronal network. The compatibility of MEA and microfluidic fabrication processes allows us to integrate neural electrophysiological studies into compartmentalized microfluidic devices [37]. The pattern of the 60 electrodes is

adapted to the compartmentalized design from the microfluidic device. Using this device, we recorded neuronal activities from the soma area and the isolated axon area. These recorded data extend our knowledge of functional alteration during AD propagation, and together with morphological data from the microfluidic device, we are able to observe the relation between morphology and electrophysiology during AD progression.

1.3.5 Glass-substrate based MEA device

Nowadays, 2D and 3D MEAs are being applied in neuroscience studies [60] and have shown great potential for *in vitro* neuronal network studies in neurotoxicity and neuropharmacology evaluations [114]. The brain slice with native networks or dissociated neural cell culture will be simultaneously recorded and response to stimulation for long periods without mechanical damage to the plasma membrane [139]. Dissociated neuronal networks lacking of many features of a real brain is inevitable, but they still retains some other functions. They can develop organotypic synaptic connections and exhibit a rich variety of distributed patterns of electrical activity and all these extracellular signals from the neural network can potentially be recorded by the MEA system [129].

The electrode array is designed by Clewin Software and fabricated in the clean-room, containing 60 electrodes (Figure 19 A). Glass is chosen as the substrate material for our device because of its transparency, biocompatibility and insulation characteristics [60]. Then it is mounted to a printed circuit board (PCB) by conductive glue which transfers the measured signals to the external data acquisition system [60]. Cells are placed close to or on the top of a metallic electrode (Figure 19 B) and the electrical field around the cell can be recorded [60]. Afterwards, the MEA device is connected with a data acquisition system (Multi Channel Systems, Germany) with an integrated amplifier and a stimulus generator (Figure 19 C), and this system is further connected to a computer for data visualization and analysis (Figure 19 D). The MC_Rack software (Multi Channel Systems, Germany) is installed in the computer and is used for data acquisition and analysis.

The MEA device used in this thesis, it is based on the MEA fabrication technology from Qwane Biosciences SA in Switzerland. It is integrated with the compartmentalized microfluidic device to obtain additional electrophysiological information during AD propagation. We design the pattern of the electrodes from the MEA device adapting to the compartmentalized design from the microfluidic device, so that the electrodes are located at the compartments for neuronal culture and axonal network instead of the junction channels area.

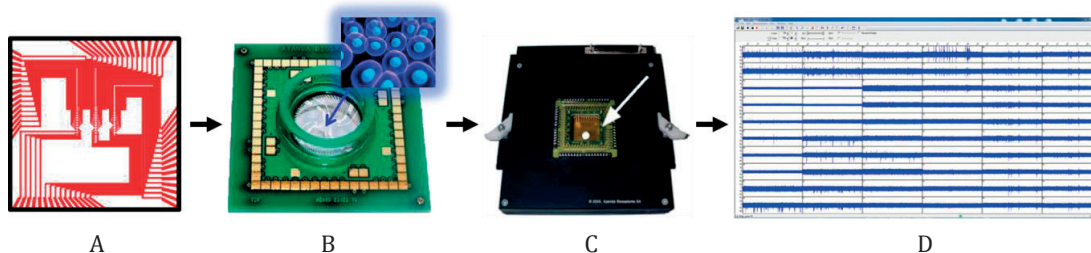


Figure 19: The manipulation of the MEA recording system. (A) The design of the board of 60 electrodes MEA. (B) MEA device for cell loading. (C) Recording system with amplifier and stimulus generator. (D) Window of data visualization and analysis system from a computer (60 electrodes for 10 minutes recording)

1.4 2D and 3D neuronal culture

1.4.1 Comparison of 2D and 3D neuronal culture environments

Depending on the objectives of the cell culture experiment, 2D and 3D cell culture have their advantages and limitations. It is necessary to select the proper cell culture model depending on the objectives of experiments. In AD studies, both 2D and 3D neural culture models have their advantages when combined with microfluidic device. Traditional 2D neuronal culture on the substrates (e.g., glass, plastic surface) can be used as a simplified model without producing the anatomy or physiology of a native brain tissue [59]. It is more suitable for experiments requiring an axonal network isolation function from the microfluidic device, uniform and quick removal of the drug exposure in the matrix for absolute control and better imaging quality. However, some experiments cannot be realized in a 2D culture, like tracing extracellular material secreted from the cells, e.g., A β plaques. 2D cell culture is also not sufficient for drug testing because it does not really present the drug efficacy and toxicity compared to a real tissue. 3D scaffolds can provide the intricate cell-cell and cell-environment interactions and better mimic the structure and mechanism property of the brain tissue. Neurons are a type of process-extending cells with outgrowth in all directions, and 3D scaffolds lead to longer neurite outgrowth, higher density of cells and neural network formation, higher cellular survival, more realistic gene expression and cellular behaviours [89]. By entering the third dimension, cells in the artificial scaffold will have relatively comprehensive external conditions, like multiple extracellular matrix (ECM), mechanical stimulation, soluble signals from neighbour and remote cells [52]. This requires the organization of the cells and the nutrient and waste product exchange [59] which brings complexity into the experiment and makes it less convenient for manipulation.

1.4.2 3D neuronal culture

In 3D cell culture, the scaffold material and architecture will determine the effective mechanical and mass transport properties that can significantly influence tissue regen-

eration [70]. For neuronal culture specifically, the ECM influences diverse mechanisms including mechanical or adhesive interactions and charge interactions via electrically charged ECM components [31]. The relation between properties of the ECM and the neural functions is still not fully understood. So far, the choice of bulk materials used for 3D scaffold includes metals, glasses, polymers, and ceramics [58]. Polymers are the most popularly applied materials due to the feasibility to control their chemical and structural properties. Both synthetic and natural derivatives polymers play vital roles in tissue engineering since 1980s [156]. Synthetic polymers include poly(ethylene glycol)(PEG), poly glycolic acid (PGA), poly lactic acid (PLA) and poly(caprolactone) (PCL) [126] and so on. Natural polymers include collagen, gelatin, elastin, silk fibroin, chitosan, chitin, fibrin and fibrinogen [132] and so on. In order to choose a proper material for a scaffold, several parameters need to be considered, including fabrication, architecture, mechanical properties, biocompatibility, and biodegradability [21, 70]. Specifically, architecture is defined to include pore shape, pore size, and pore interconnectivity which interrelate strongly with scaffold characteristics.

Agarose hydrogel is widely used in tissue engineering for cell immobilizations and it has the necessary physiochemical structure to support 3D neurite extension from primary neural cells. Compared to collagen, agarose has shown better result for cell survival and neural outgrowth, and it can provide better stiffness to mimic a soft organ such as brain which is near 260-490 Pa [108, 94, 115]. The 0.5 % (w/w) agarose gel we apply for our 3D culture has the stiffness between 2 kPa and 5 kPa, while the stiffness of a typical concentration of collagen is above 10 kPa [157]. For experimental manipulation with gel, the curing temperature and duration is another important factor. Agarose has short transition time and its mechanical properties are independent of the speed of the curing process. It takes less than 10 s. to cool down some preheated agarose, while collagen is reported to take more than 30 min following a standard protocol [13, 157]. However, using agarose alone does not provide good neuronal survival [115], it is necessary to add other factors to promote the neural growth or neurite outgrowth. Alginate is a natural polymer derived from algae and it is a linear polysaccharide composed of (1-4)-linked β -D-mannuronic acid (M) and α -L-guluronic acid (G) [10]. It has been shown that alginate hydrogel strongly supports the neurite growth and protects the neurons against oxidative stress [106]. The combination of agarose and alginate will become a proper scaffold to build 3D neural culture in microfluidic device.

Some hydrogel-free methods have been developed in addition. For example, 3D neural networks built with silica beads was reported by Sophie Pautot in 2008 (Figure 20) [125]. Primary rat hippocampal neurons were cultured on micro-beads (several dozen microns in diameter) made of silica that provides a growth surface. Like a normal cell culture dish, the surface of the silica bead was treated with poly-L-Lysine (PLL) coating solution to enhance the cell adhesion and support neural maturation. Meanwhile, some other beads were treated with attractant signalling molecule cyclic AMP (cAMP) to guide

the axonal growth [138]. The axon grows at a speed 50 $\mu\text{m}/\text{d}$ over the cAMP coated beads surface. They managed to guide process extension from one population of neurons to another by inserting guiding beads in the assembly. It was proved that these micro-beads can be used as carriers for the cells and allow for neural growth, neural maturation, transfection and manipulation. This method brings more flexibility for cell manipulation than the hydrogel-based ones. Based on this 3D beads-culture technology, we explore culturing primary cortical neurons on these silica beads and pattern them inside a compartmentalized microfluidic device to mimic the layer pattern in cortex. At the same time, we also consider the shortcomings of commercial glass particles and try to use soft microgel particles (MGPs) instead [127]. We further develop our micro-beads with agarose-alginate gel inspired by the Hanging Drop Arrays technique (Figure 21) [150]. Our gel beads can provide a portable 3D scaffold for brain studies. Together with microfluidic device, we manipulate the gel-beads and build layer pattern 3D culture.

1.4.3 3D neuronal culture for AD studies

The conventional 2D culture has some drawbacks for AD studies. For instance, secreted A β can continuously diffuse into the culture medium instead of being aggregated and form A β plaques in 2D culture. 3D culture can avoid this problem because of its solid scaffold. It is reported that 3D culture would accelerate A β deposition by limiting diffusion of A β , allowing for aggregation [24]. In 2015, the characterization of a novel 3D culture system was reported which exhibits key events in AD pathogenesis, including extracellular aggregation of A β and accumulation of hp-Tau. This is the first human cellular model that showing the A β driven Tauopathy in 3D culture comprehensively. This model can be used to examine many other key questions of AD pathogenesis *in vitro*, including the molecular mechanisms underlying the production of high concentrations of A β , the accumulation of extracellular A β , the deposition of A β aggregates, the hyperphosphorylation of Tau and hp-Tau aggregation. More conditions can be tested under controlled conditions in this 3D AD model. For instance, microglia cells can be added to study its crucial effect in A β clearance, brain inflammation and synaptic and neuronal damage [100]. Overall, this is a big advance on building 3D neural cell culture model for AD studies. More important characteristics from the real AD brain should be added to mimic the brain comprehensively, and this may have an effect on the results.

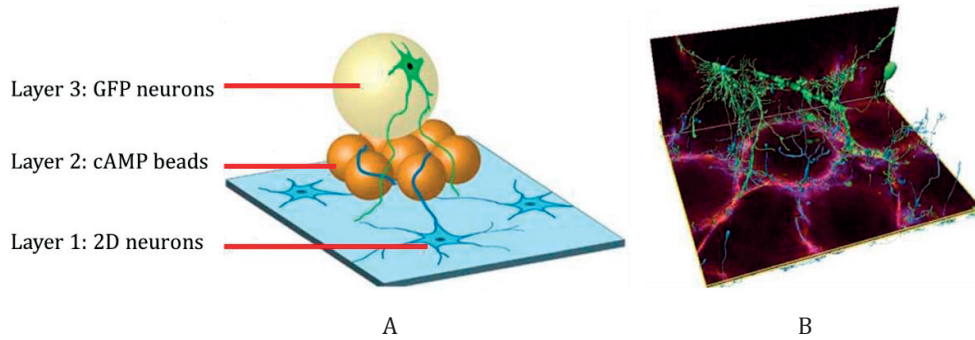


Figure 20: Schematic image of the guidance concept of 3 layers beads. (A) On layer 1, 2D neurons are growing on the coverslip and their axons (in blue) are growing through the Layer 2 cAMP coated beads. The GFP-expressing neurons from beads Layer 3 descend their dendrites (in green) down through the Layer 2 beads and encounter the extended axon from 2D neurons on Layer 1. (B) Image of the 3D reconstruction neural network described in Figure A. Reprinted from [125] by permission

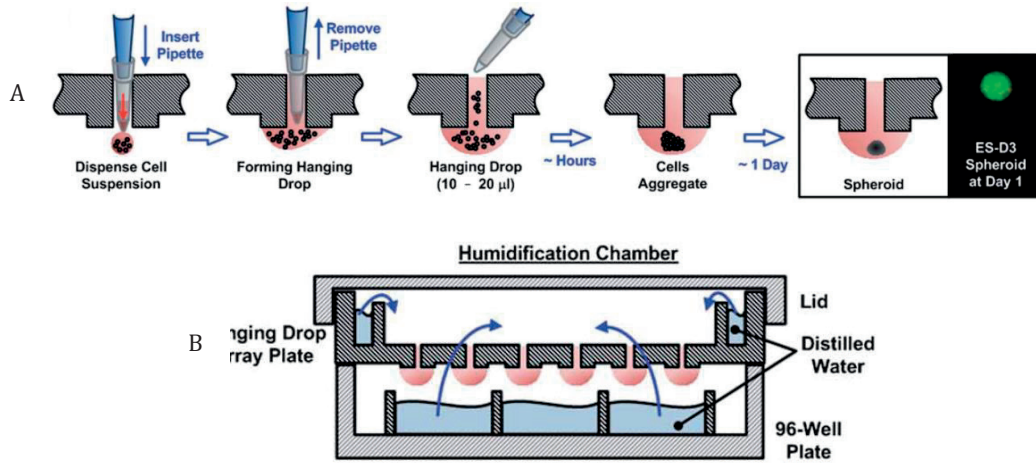


Figure 21: Schematic picture of the hanging drop formation process. (A) and the humidification chamber used to culture 3D spheroids in the hanging drop array plate (B). Reproduced from [150] with permission

For 3D cell culture, compartmentalized microfluidic device can be used for the construction of brain models [32] mimicking some specific patterns in the brain. In 2011, Anja Kunze reported a 3D layer hydrogel scaffold mimicking the layer structure of cortex inside a microfluidic device (Figure 22) [83]. This work intended to control laminar flows of agarose-alginate gel with and without primary cortical neurons, and freeze the hydrogel when it achieved the multi-layer pattern. In order to build layer-pattern in the microfluidic device, flow-controlling system was required for the laminar flow in microfluidic device. Rich experience is required with this work because of the gel solidification under temperature variations and laminar flow control by a pump that makes it more difficult on gel manipulation. This is a successful model of mimicking brain structure by combining hydrogel culture and microfluidics technology. This 3D cell culture model can be used

for AD studies by patterning cell layers in the microfluidic device to observe cell-cell and cell-environment interactions during disease propagation.

In this thesis, the microfluidic device with layer patterning design is combined with the 3D beads culture including silica beads and agarose-alginate beads. This layer-pattern 3D neuronal culture model using microfluidic device mimicking the cortex structure that has layers of different compositions, can be used to study the neuron-to-neuron interactions in an *in vitro* 3D environment. This will represent a novel model to study neurodegenerative diseases including AD.

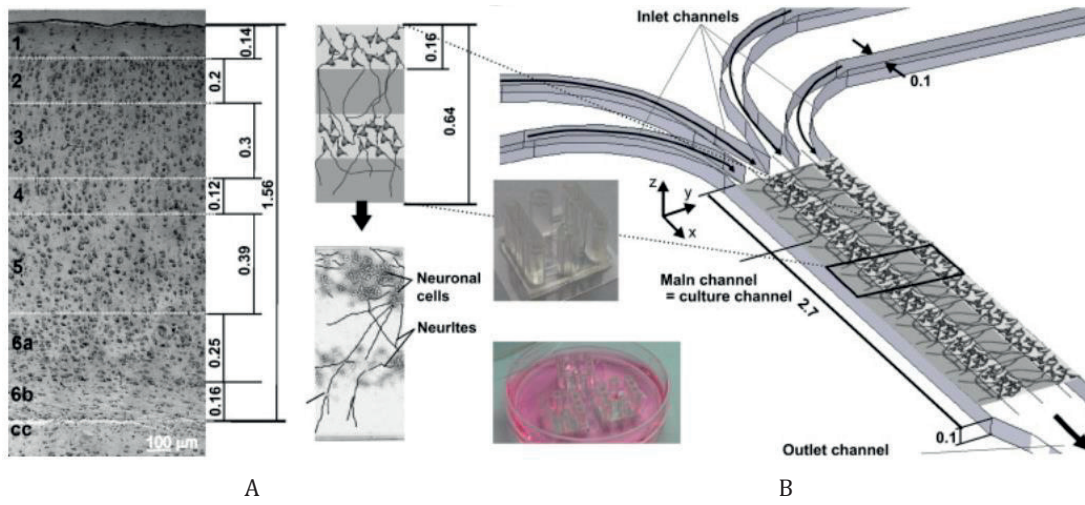


Figure 22: Designing principle of the 3D layer hydrogel scaffold for neural cell cultures. (A) Image of a native cortical brain slice showing the six different cell layers after staining for cell bodies and closed dendrites. The engineered model consists of two cell layers interlaced by two cell-free layers. (B) Schematic drawing of the layer structure of the 3D neural cell culture. There are 4 inlet channels for gel loading, through the main channel and exit the outlet channel. The two inserts show the final microfluidic device and three devices placed in a Petri dish for incubation during cell culture. Reprinted from [83] with permission

1.5 Building an AD propagation model

1.5.1 Concept of co-pathology in building AD propagation model

During disease progression, neurons from different regions in an AD patient's brain have abnormal functions and these regions probably affect each other through the neural networks. NFTs and A β , two major hallmarks in AD, are very likely involved during this propagation in the neuronal network between different brain regions. During the development of AD, NFTs follow the pattern of disease spreading in the brain, from the transentorhinal cortex, followed by the hippocampus and cortical areas. There is evidence that the local Tau aggregation can be transmitted from neuron to neuron through synaptic connections, which is an important role in the progression of Tau pathology [36, 109, 16]. A β does not follow this spatiotemporal propagation pattern in the brain, however,

the soluble oligomeric A β is still directly transferred from neuron to neuron [113]. It becomes obvious from the evidence above, that transportation from neuron to neuron plays an important role in the neuronal network. We call the pattern of the diseased and healthy neuronal populations with interaction a “co-pathological” model (Figure 23). In this model, two neuronal populations grow separately, while their axons are connected and the disease spreads from the diseased neuronal population towards the healthy one. In order to focus on the axonal transportation during disease propagation, the axonal network needs to be distinguished from the other parts of each neuronal population to exclude some other possibilities on transportation. First, two neuronal populations are cultured separately while the axons from each cell population can grow out of their own environment. Afterwards, the axons from each cell population grow into another isolated environment and meet there. In the end, one of the two cell populations is treated with a drug to induce a diseased cell population model while the observations on the disease spreading continue. This co-pathological model with only axonal interactions helps to isolate the axon interaction spatially and enables us to study the axonal transport function separately. To achieve this goal in real experiments, comprehensive designs for experiments and multifunctional devices for targeted characteristics are required for these *in vitro* studies.

1.5.2 Co-pathological model in microfluidic and MEA platforms to study AD

1.5.2.1 Example of co-pathological model in microfluidic platform for AD studies

Microfluidic devices for neuronal culture application provide compartmentalized chambers that allow 1. the neurons to grow in different regions with precise local control of medium and drug, and 2. the axonal network to be isolated by the junction channels from the cell soma and dendrites to observe the axonal transport. Benefitting from this compartmentalized design of the microfluidic device, we build a co-pathological model of diseased and healthy neuronal populations in separated compartments in the microfluidic system, to create the neuron-to-neuron interaction. By using the junction channel from the microfluidic device for neuronal culture in general, the axons from the diseased and healthy neuronal populations are isolated in to another compartment, so that providing an environment that the axons from the diseased neuronal population can communicate with the axons from the healthy neuronal population.

The approach for our compartmentalized microfluidic device was presented by Anja Kunze in 2011 [85] as mentioned before in this thesis. This microfluidic device consists of three parallel compartments, each of the two-neighboring compartments are connected by small junction channels. Neurons are plated in the two lateral compartments and the axons grow through the junction channels into the middle compartment forming a neuronal network. One population was drug-induced to become a diseased

neuronal population. To detail the microfluidic device manipulation and drug exposure, the liquid from the lateral compartments were removed first, and then the drug-enriched medium was injected into the inlet of the left lateral chamber to induce the cells and make them become diseased neuronal population. The outlet of the chamber was kept not filled. For the right lateral compartment, fresh normal neural culture medium was injected to the inlet of the right side lateral compartment. A time variant flow generates inside each lateral compartment because of the pressure difference between the inlet and outlet. During the time variant flow, a concentration gradient established across the main chamber and through the junction channels (Figure 23). The drug exposure lasted for 75 min and okadaic acid (OA), as a phosphatase inhibitor of the serine/threonine (Ser/Thr) phosphatases that can induce hyperphosphorylation of Tau protein (Figure 24) [75], was used for drug-induction at 600 nM. The sample was fixed at 6 h after the drug exposure. In the left chamber where cells were treated by OA, it was observed that hp-Tau aggregation in the neurites and accumulation in the soma on the diseased cell population side using Ser262-Tau immunostaining (Figure 25 A). On the contrary, in the right chamber, the Tau distribution in the cells has lower fluorescence intensity and no accumulation (Figure 26 B). This was the first 2D *in vitro* co-pathological model on observations on neurodegenerative disease propagation in a compartmentalized device and it opened the possibility to study cellular and molecular propagation mechanisms of neurodegeneration in Tauopathology in a microfluidic device.

1.5.2.2 Our co-pathological model in microfluidic and MEA platforms for AD propagation studies

Inspired from Anja's co-pathological model above, we decide to continue this co-pathology arrangement with the diseased and healthy cell populations and their isolated axonal network (Figure 26). At the same time, based on our hypotheses on neuron-to-neuron transmission and axonal transmission during disease study, we build our microfluidic device.

Compared to Anja's previous experiment using a gradient in the compartment for axonal network, we try to avoid this gradient by continuously replacing the drug in the compartment with fresh culture medium. In this way, we can exclude the fact that the axons are affected by a gradient of drug in the same compartment and furthermore ensure an unexposed environment for the healthy cell population. A publication showed much lower concentrations (1.5, 3, 6.25, 12.5, 25 and 50 nM) of OA can induce Tau phosphorylation [102], so additionally, we intend to try a lower concentration in our experiment as well as the concentration that was previous used (600 nM) to observe the different drug effect at different concentrations. One of our hypotheses is that under low concentration OA, the disease could propagate more slowly compared to the high concentration condition and it is highly possible that we observe more information that is detailed

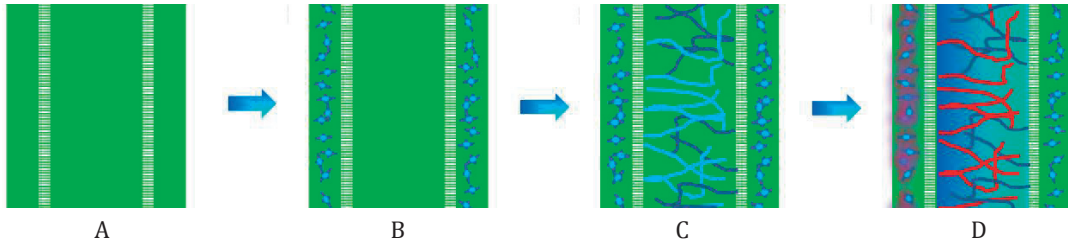


Figure 23: The schematic pictures on the experimental region inside a microfluidic device to show the steps to achieve a co-pathological “diseased” and “healthy” neural network. (A) PDMS microfluidic device with three compartments connected by junction channels. (B) Neurons were injected inside the two lateral chambers. (C) After 1 week continuous culture, the neurites grew through the junction channels and build up a neurite network in the middle chamber. (D) The left neuronal cell population was exposed to a drug and this will generate a drug gradient in the middle chamber by diffusion through the junction channels, while keeping the right cell population unaffected

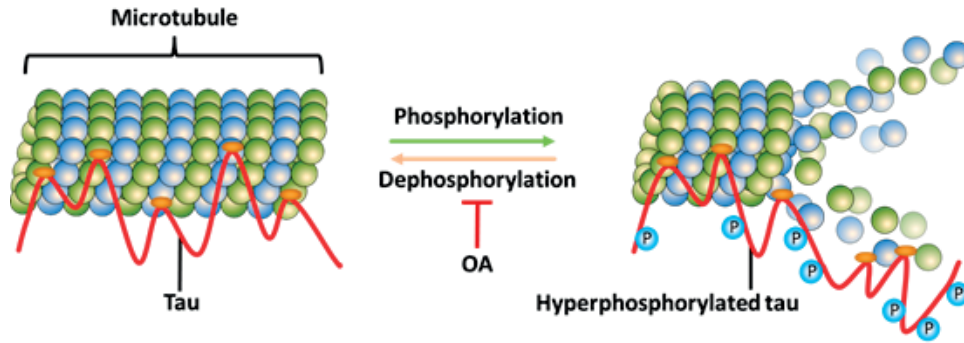


Figure 24: Microtubule-associated Tau protein equilibrium in the brain. By phosphorylation, Tau protein becomes hp-Tau, and after dephosphorylation, it comes back to be normal Tau protein. When OA is induced to the cells, it inhibits the dephosphorylation of the phosphorylated Tau. Then the phosphorylated Tau becomes hp-Tau and highly accumulated inside the brain which is a hallmark of AD

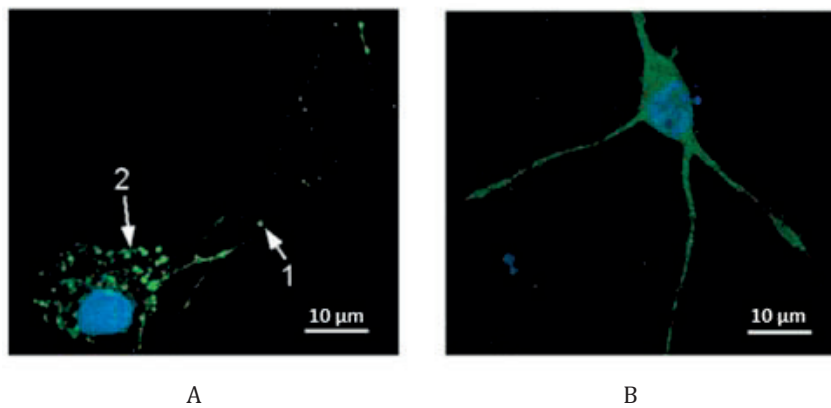


Figure 25: Fluorescent images of healthy and diseased cells after OA treatment. (A) Diseased cell from left compartment and (B) Healthy cell from right compartment from same microfluidic device with Immunocytochemical staining. (Green: Ser262-Tau, blue: DAPI). Diseased neurons presented accumulation of phosphorylated Tau clusters in neurites (arrow 1) and soma (arrow 2). Reprinted from [85] with permission

in the neuronal soma and axon under slower disease propagation. More observation time points and longer observation times are added in our experiment compared to previous work. In addition to the morphological observations from the microfluidic device, electrophysiology observations are achieved by MEA recording technology as well. In this way, we can analysis the alteration of neural activities and obtain the sequential occurrence between structural and functional alterations during AD propagation. By adding the MEA device into our experiment, it is required to have a more mature neuronal network (>14 days neuronal culture) to allow us to record the neural activities. That is one of the reasons that we drug-induce the neuronal population on the 21 DIV instead of 8 DIV from previous experiment. Another difference is that our junction channel is designed with $500\text{ }\mu\text{m}$ length to further isolate the axon from the dendrite. It can better isolate the medium from the compartments as well. However, the axon will take longer time to grow out of the junction channels than the $150\text{ }\mu\text{m}$ from the previous device. Together with the microfluidic and MEA platforms we fabricated, a co-pathological AD model was built with diseased and healthy interaction in the neuronal network to study the AD propagation. All these modification to the device will assist us to prove our hypotheses and have a better understanding of AD propagation in Tauopathy.

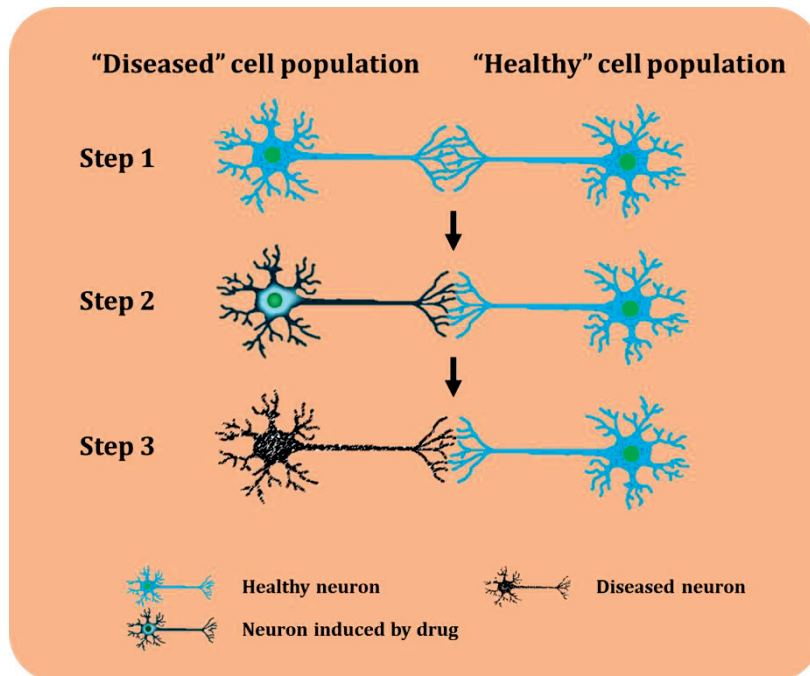


Figure 26: Schematic picture of the simplified model of AD propagation

1.6 Scope of the thesis

Based on the microfluidic and the MEA technologies, scientists were able to fabricate PDMS devices and MEA devices individually to do compartmentalized neuronal culture and record the neural activities respectively. In previous work [85], a microfluidic device was developed and applied to build a co-pathological model and mimic some characteristics of AD for disease propagation studies. The early stage of hyperphosphorylated Tau (hp-Tau) spreading was observed in the drug induced diseased cell population. MEA device has been applied in general AD studies for extracellular neuronal activity recording as well, but it has not been utilized in AD progression studies [47].

In this thesis, we preserve this co-pathological pattern for AD propagation. We combine these two microtechnologies (microfluidics and MEA) together and fabricate our integrated microfluidic-MEA device. The microfluidic device part can provide compartmentalized channels to extract the axonal network for individual culture and drug exposure. We observe the hp-Tau propagation from the diseased cell population to the healthy cell population through the axonal network. This proves our hypotheses on the neuron-to-neuron transmission, axonal network communication and concentration-dependent effect of drug during AD propagation. The MEA recording device provides electrodes at the bottom of the microfluidic channels to record from the neurons growing in the microfluidic channels. This integrated microfluidic-MEA device allows us to observe time-dependent alterations in neuronal morphology and electrophysiology synchronously during AD progression. This helps us to understand the order in which the structural and functional alterations occur (order of occurrence) during AD progression. This microfluidic-MEA device is promising in studies of neurodegenerative disease mechanism. AD, as a neurodegenerative disease and the most common type of dementia, is an appropriate disease example to start to test our microfluidic-MEA device.

Some detailed preparative and exploratory work is presented as well, including developing 2-dimensional (2D) and 3-dimensional (3D) neural culture in microfluidic devices as well as our microfabrication technique for microfluidic and MEA devices and the bonding technology for microfluidic-MEA devices.

1.7 Thesis structure

In this thesis, the whole process for preparing, fabricating and applying microfluidic and MEA techniques for hp-Tau propagation studies of AD is presented.

In **Chapter 2**, we present the fabrication methods of microfluidic and MEA devices and the bonding method for making the microfluidic-MEA device. This bonding method involves the bonding between the PDMS material from the microfluidic device and the SU-8 material from the surface of MEA device. After the quantified bonding tests from surface analysis and tensile strength test, we find the key factors for this irreversible

bonding method between PDMS and SU-8. This bonding method solved our challenges in integrating the microfluidic and MEA device. The theory of this bonding method is explained and this bonding process is detailed in the fabrication of microfluidic-MEA device part. The preliminary neural culture and neural activity recording test from this microfluidic-MEA device are presented as well.

Chapter 3 is the core chapter in this thesis. It presents the experiment of applying the integrated microfluidic-MEA device for morphological and electrophysiological observations during the propagation of AD. The results give us more clues about the phenomenon during neural network degeneration as well as the relation between morphology and electrophysiology during AD progression. This work provides valuable observations and confirms our hypotheses on the neuron-to-neuron transmission, axonal network communication, concentration-dependent effect of drug and the order of occurrence of structural and functional alterations during AD propagation. This highlights the advantages of the microfluidic and the MEA technologies.

After the experiments of 2D neuronal culture in microfluidic and MA devices, **Chapter 4** presents some exploratory work on the 3D neuronal culture in microfluidic device. Neurons are cultured on/in two different types of micro-beads (silica and agarose-alginate) and they are patterned into layers inside the microfluidic device to build 3D neuronal cultures mimicking the layer pattern from the cortex. By culturing neurons with the beads, cell sedimentation, which is caused by gravity during the gel solidification, can be avoided, and the distribution of the neurons inside the microfluidic device is relatively homogeneous. These 3D silica and agarose-alginate beads culture models in microfluidic device with layer pattern can be used for cell patterning in 3D environment. For AD studies, these two methods will allow us to build co-pathological in 3D mimicking the disease propagation and observe the formations of the NFTs and the A β plaques that might not achieve in 2D neuronal culture.

Finally, **Chapter 5** concludes the work we have achieved so far on morphological and electrophysiological observations during AD propagation with microfluidic and microfluidic-MEA devices. It gives some perspectives for the study of AD propagation using microfluidic and MEA devices as well as the concepts of building a brain/cortex-on-a-chip, like other organ-on-a-chip projects. We are attempting to build a "brain-on-a-chip" using microfluidic and MEA platforms, which may potentially make significant contributions to disease studies and pharmaceutical tests.

Microfluidic, MEA and integrated microfluidic-MEA devices fabrication

2

“If I have seen further it is by standing on the shoulders of giants.”

by Isaac Newton, in a letter to Robert Hooke in 1676

2.1 Introduction

2.1.1 Integration of microfluidic device and MEA device

Based on our hypotheses about importance of neuron-to-neuron transmission, axonal network communication and concentration-dependent effect of drug during AD propagation, compartmentalized microfluidic device can serve as a suitable tool to assist us to investigate on these assumptions by building a simplified co-pathological disease propagation model for *in vitro* morphological alteration observations. Meanwhile, the MEA neural activity recording device allows for non-invasive simultaneous recording on neuronal culture. This MEA device brings great help to understand the electrophysiological signals alteration during AD propagation. Together with the compartmentalized microfluidic device, an integrated microfluidic-MEA device is built (Figure 27 A) which can provide compartmentalized neuronal culture, record and distinguish neural activities from different locations in the neuronal network. This will help us to observe electrophysiological alterations in the co-pathological model and perceive the sequential occurrences on the structural and functional degeneration during AD propagation, which will potentially promote the research on AD early diagnosis.

This microfluidic-MEA device combines a compartmentalized microfluidic device made of PDMS and a MEA device with a 5 μm layer of SU-8 as an insulation layer on the top of the wires for recording electrodes and glass substrate (Figure 27 B). In order to integrate the microfluidic device that is made of PDMS and the MEA device which has SU-8 on its top, the irreversible bonding technique for PDMS and SU-8 is required.

2.1.2 PDMS and SU8

PDMS is an elastomeric material that is widely used for rapid prototyping microfluidic systems and cell-chip devices, due to its chemical inertia, thermal stability, permeability to many gases, simple preparation, optical transparency, and low cost [105]. It can be easily integrated with electrodes, heaters, and sensors, which are fabricated on substrates, to generate multifunctional devices for biomedical applications [42]. SU-8 is an epoxy-based negative photoresist initially developed for the microelectronics industry [98]. Currently, SU-8 becomes widespread in the development of microfluidic devices due to its ease of use, the high aspect ratio it allows to create, its high chemical stability, and mechanical properties [19]. It has become a material of choice for microelectromechanical systems (MEMS) and microfluidics, from the fabrication of single components to complete lab-on-chip devices [2]. Since PDMS and SU-8 are both popular materials in the microfabrication field [42, 98], researchers have started to integrate PDMS and SU-8 together more and more to benefit from both of their advantages [122, 123, 117]. In the fabrication of microfluidic devices made of PDMS, the PDMS component is generally bonded to a glass coverslip to obtain closed microfluidic channels by using an oxygen (O_2) plasma surface treatment on the PDMS and glass surfaces. This results in a permanent covalent siloxane (Si-O-Si) bond between the PDMS and glass surfaces. However,

using O_2 plasma is not sufficient to bond PDMS and SU-8 surfaces irreversibly as the oxidation of the SU-8 surface does not result in the creation of $-SiOH$ groups.

2.1.3 PDMS and SU8 bonding methods

Recently, different bonding methods for PDMS and SU-8 have been reported in the scientific literature, such as nitrogen plasma treatment [160] or spin coating SU-8 on the PDMS surface [122]. Nevertheless, nitrogen plasma is not available in all labs, and spin coating, which requires layer-by-layer processing during device fabrication, does not provide the flexibility of bonding two fabricated individual devices. Some researchers also choose to bond PDMS and SU-8 reversibly [76]. However, for long-term cell culture devices where liquid leakage is to be avoided during the whole duration of the experimentation, a solid sealing is necessary which reversible bonding cannot provide. Instead of aligning the devices every time before each use, in the case of reversible bonding, irreversible bonding can also save time and effort on repeating micro-scale design alignment for the devices before each use as this step is time-consuming. As it is increasingly demanded of integration between PDMS and SU-8 devices, irreversible bonding of PDMS and SU-8 becomes an important technology.

2.1.4 Aminosilane-mediated silanization bonding method

Silanization is one of the widely applied surface modification methods. It generates a self-assembled monolayer of alkoxy-silane molecule, which has methoxy (CH_3O-), or ethoxy (CH_3CH_2O-) groups onto a substrate. Aminosilane, one of the alkoxy-silane molecules, has an amino (NH_2-) group as well. Aminosilane-mediated silanization has been applied on silica surfaces as a coupling agent for functionalization due to its bifunctional nature [161]. (3-Aminopropyl)triethoxysilane (APTES) is one of the highly-selective effective aminosilanes, which has been widely applied in bonding materials for microdevice fabrication and protein immobilization for biological applications [159, 64, 141]. It has been used for bonding PDMS to various thermoplastic materials including polycarbonate (PC), cyclic olefin copolymer (COC), polymethylmethacrylate (PMMA), polystyrene (PS) and others [143, 142, 141]. SU-8 is an epoxy-based negative photoresist and the epoxy groups that remain on the SU-8 surface could be sufficient to react with the aminosilane molecule from the PDMS surface and form a covalent bond. In this way, PDMS and SU-8 bonding can be realized by introducing APTES molecules between the two materials (Figure 28). It is promising to apply this theory to the irreversible bonding of PDMS and SU-8 for our integrated microfluidic-MEA device.

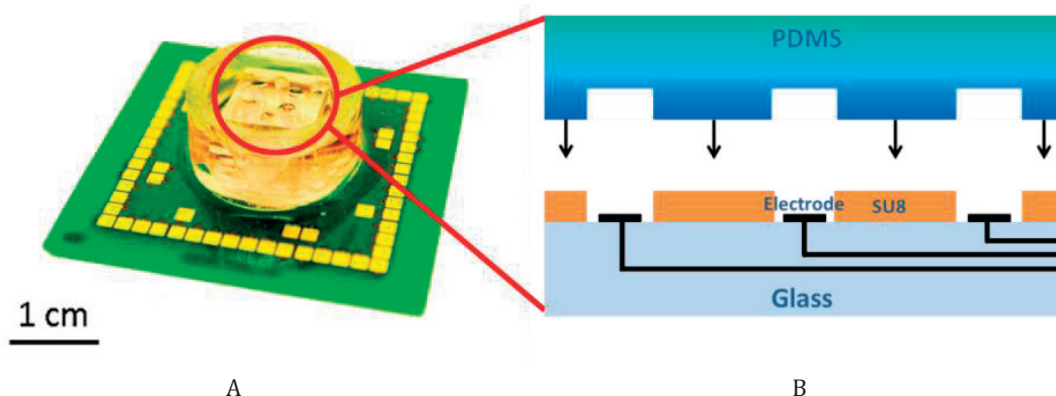


Figure 27: Microfluidic-MEA device. (A) Picture of this integrated microfluidic-MEA device for our neural culture bonded with our PDMS and SU-8 bonding method. (B) Schematic of the cross-section of the device

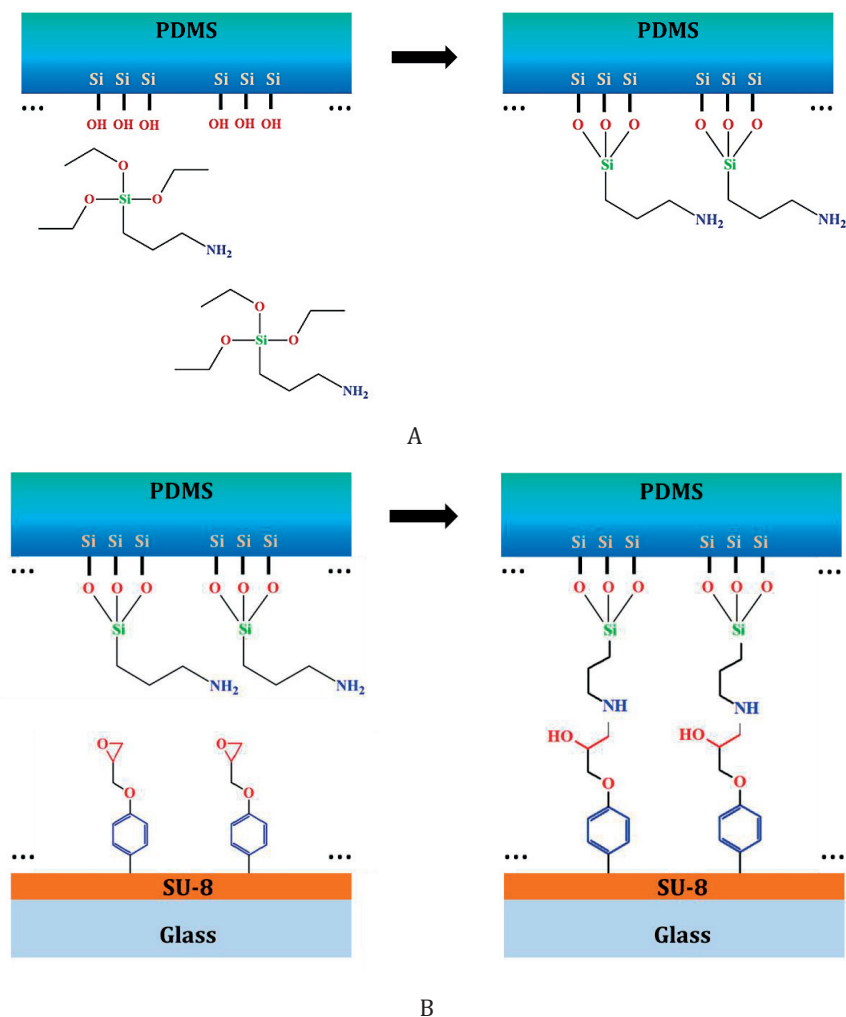


Figure 28: Theoretical reactions during the bonding. (A) Reaction between APTES molecule and the O₂ plasma activated PDMS surface and (B) reaction between the -NH₂ group from the APTES molecule on the PDMS surface and the epoxy group from the SU-8 surface.

In this chapter of device fabrication, we first describe the fabrication methods of microfluidic and MEA device. Then we investigate on the bonding technique of microfluidic and MEA devices, focusing on PDMS and SU-8 bonding technique. We try to find a simple and reliable bonding method for PDMS and SU-8, based on the elements and chemical bonds from the modified PDMS surface through the XPS analysis and the tensile strength test for the SU-8 processed with and without a hard bake step. In addition, we detail this bonding method with a practical microfluidic device example. This device combines a compartmentalized microfluidic device made of PDMS and a MEA neural activity recording device with SU-8 as its insulation layer. We name it a microfluidic-MEA device. The design of the electrode array is adapted to the compartmentalized design from the microfluidic PDMS device. This allows us to distinguish the neural activity from different cell populations, which can potentially present different disease status. Axons can be isolated from the neuronal network and be recorded separately. This combination of compartmentalized PDMS device and MEA device provides a multifunctional platform for neuroscience research. Our bonding technology is used to bond the PDMS and SU-8 surfaces irreversibly for this microfluidic-MEA device. The cell compatibility of this bonding method is proved through neural electrophysiological results using this integrated device. It is promising to apply this simple and reliable irreversible bonding method to integrate microdevices with PDMS and SU-8 surfaces for biological use. This type of microfluidic-MEA device has proved an innovative tool for neural electrophysiological studies.

2.2 Methods

2.2.1 Microfluidic device design and fabrication

We designed the compartmentalized PDMS device with three chambers (Figure 29). Each two chambers are connected by junction channels of 20 μm width, 10 μm height and 500 μm length. The low dimensions on width and height allow the microfluidic PDMS device to segregate the neural soma in one chamber and allow its axon to grow through the junction channel to the neighbour chamber. We placed the primary neural cells into the two lateral chambers (Region 1 and 3) and the axon from the cells will grow through the junction channels and built a neural network in the middle chamber (Region 2) with axonal contacts from the two lateral cell populations.

We choose PDMS as the material for our microfluidic device based cell culture. The pattern of chambers and channels on the bottom surface from the PDMS device is molded by using a silicon wafer (Figure 30). The silicon wafer is fabricated in a cleanroom with a mask that has the pattern for the microfluidic device. The mask was designed using Clewin 4 and produced in the LASER lithography system (Heidelberg DWL200). For the silicon wafer fabrication, two types of wafer fabrication processes can be used (Figure 31), depending on whether different heights are necessary for the channels. In order to isolate the neurites, we need to use different heights of channels to make the barriers, for example some low height junction channels (e.g., 10 μm in height that is smaller than the size of neuron soma), to block the neu-

ron soma and let the neurites to grow through to other compartments in the device. In this case, junction channels require a different height compared to normal channels, only to let the neurites to grow through. A two-step dry etching process can be used to fabricate the wafer to mold PDMS device, which requires different heights (Figure 31 B). After the first etching step, the channels are 10 μm high for the junction channel. With the second etching step, another 90 μm high etching is made so that the total channel height becomes 100 μm . Otherwise, if junction channels are not applied, one-step dry etching process is enough and all the channels are in the same height (Figure 31 A).

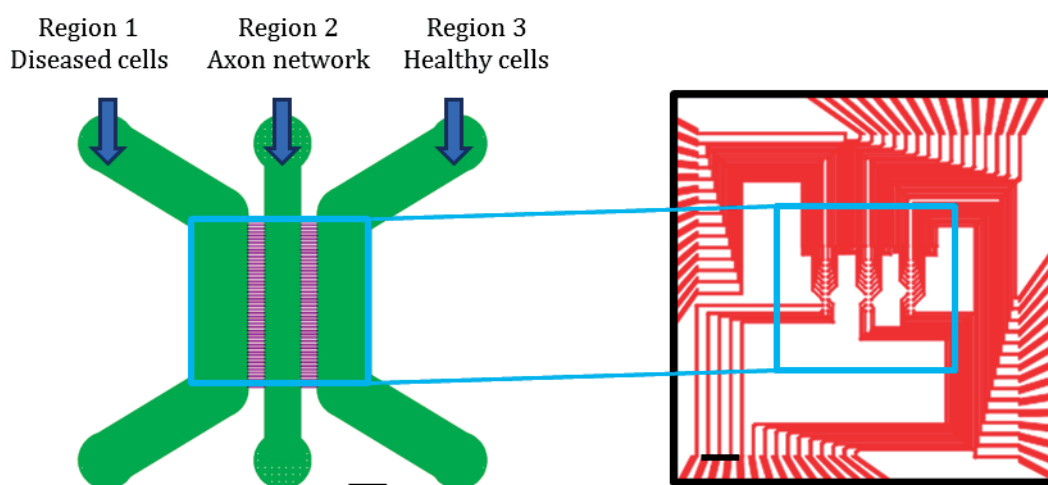


Figure 29: Designs of microfluidic device and MEA device. (A) Design of microfluidic device and illustrations. (B) Design of MEA device with 60 electrodes in 3 columns in parallel. Scale: 1000 μm

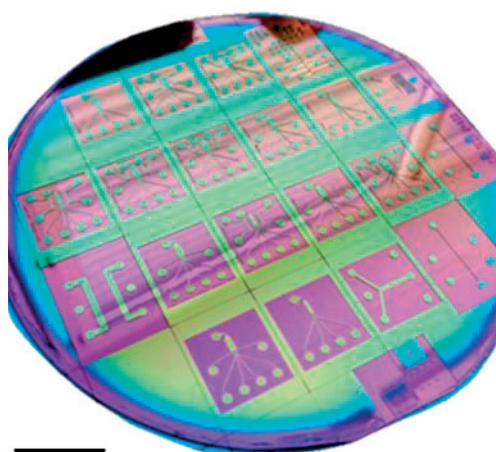


Figure 30: A representative microstructured silicon wafer contains multiple microfluidic designs for PDMS master molding. Scale: 1000 μm

Once the silicon wafer is fabricated, it is used as a mold for making PDMS devices. Before we use it for molding, we deposit a thin layer of SiO_2 to make a protection layer on top of the silicon wafer to allow for longer usage as a mold for PDMS device. (Figure 31 B ⑪) PDMS sticks to the silicon wafer's surface and the PDMS cannot be peeled easily from the silicon wafer. To solve this problem, a silanization should be done for the silicon wafer surface before the first use. This makes the wafer's surface hydrophobic and allows the PDMS to be easily unmolded from the silicon wafer.

After the silicon wafer is ready for PDMS device molding, the next step is to prepare the PDMS mixture (Figure 32). The silicone elastomer (PDMS base) and curing agent are mixed using a 10:1 ratio (Figure 32 A), then pour the mixture onto the silicon wafer with the pattern, up to a height of 5 mm or even higher. Then put the silicon wafer with the PDMS mixture on its top into a desiccator (Figure 32 B). The PDMS elastomer can be cured at 80 °C for one hour (Figure 32 C). Then the design from the silicon master is molded at the bottom surface of the PDMS device. The PDMS part is cut and detached from the silicon wafer (Figure 32 D). The opening reservoirs from the device that connect micro channels to the outside environment are created by holes puncher tools, and then the device is ready for use (Figure 32 E). Glass cover slips of 0.17 mm thickness are applied to close the channels and chambers for the PDMS device and to obtain better biological imaging quality. This cover slip bonding is done by an Oxygen Plasma treatment for both the PDMS device's and cover slip's surfaces at 40 Pa (300 mTorr), 50 Watt for 45 seconds. Immediately after this treatment, both parts are pressed against each other to complete the bonding process and kept in the oven for 3 minutes. Then, the PDMS device is filled with 70 % ethanol for sterile cleaning for 20 minutes, and then rinsed by sterile water 3 times to wash away residual ethanol on the surfaces inside the PDMS device. UV exposure for 20 minutes is the last step to sterilize the PDMS device and dry the chamber inside the device. In summary, after the fabrication of the PDMS device, the PDMS device and the cover slip need to be sterilized by ethanol cleaning or by an autoclave machine, water washing several times and UV exposure.

2.2.2 MEA device design and fabrication

For a normal MEA device for neuronal activity recording, 60 electrodes from the MEA device are arranged by 10 rows and 6 columns (Figure 33). For compartmentalized neuronal culture, the positions of the electrodes need to be modified. Together with the three chambers, there are two columns of electrodes in parallel in each chamber. These are electrodes made of Platinum on the MEA device, which allow for simultaneous recording of extracellular potentials from the neuronal culture. At the same time, both the microfluidic PDMS and MEA devices were designed to provide a good fitting of their functions and their integration.

The microelectrodes had a diameter of 50 μm and each two microelectrodes were separated by a distance of 200 μm . The fabrication of MEA device was using a process developed by Qwane Biosciences SA, Switzerland (Figure 34). First, the glass was cleaned by photoresist remover and ultrasound. Secondly, a photoresist layer was spin-coated onto the surface with a

thickness of 2 μm for the metal lift-off process. Then a thin layer of titanium (150 \AA) was sputtered onto the wafer to serve as an inter-metallic adhesion promoter. Next, a layer of platinum (1500 \AA) was sputtered onto the wafer surface. Afterwards, with the ultrasonic removal of photoresist, metal traces with electrode and connection pad for external PCB were formed. In the end, 5 μm thick SU-8 was spin-coated on top as insulation layer and with no final hard baking step. The fabricated multi-layered wafer was then diced and assembled with the external PCB by a screen printing technique. This MEA device is successfully fabricated in the clean-room and ready for a further test.

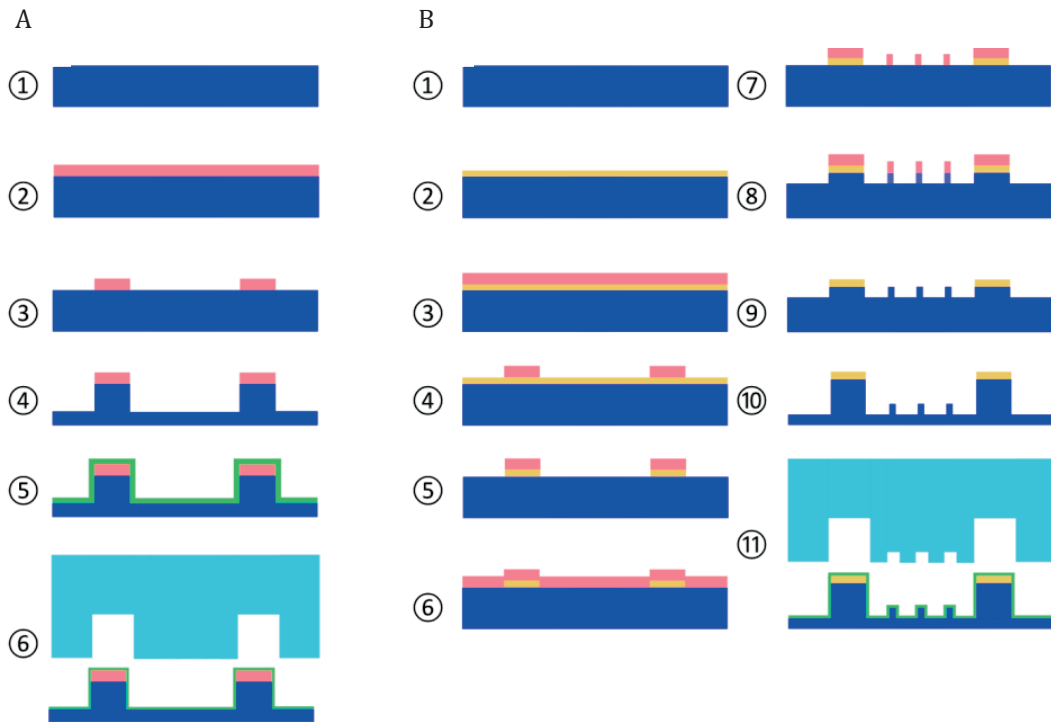


Figure 31: Process flow for microstructuring PDMS devices in the cleanroom. (A) One depth channel PDMS device fabrication process flow: ① Silicon wafer, 10 mm ② Photoresist coating, 5 μm ③ Photolithography ④ Si DRIE etching, 100 μm ⑤ Wet oxidation, 300 nm ⑥ PDMS molding. (B) Two different depths of channels PDMS device fabrication process flow: ① Silicon wafer, 10 mm ② SiO_2 deposition, 1 μm ③ First photoresist coating, 2 μm ④ First photolithography ⑤ SiO_2 RIE etching ⑥ Second photoresist coating, 5 μm ⑦ Second photolithography ⑧ Si RIE etching, 10 μm ⑨ Remove photoresist ⑩ Si DRIE etching, 90 μm ⑪ Wet oxidation, 300 nm and PDMS molding (RIE: Reactive ion etching; DRIE: Deep reactive ion etching)



Figure 32: PDMS device fabrication process

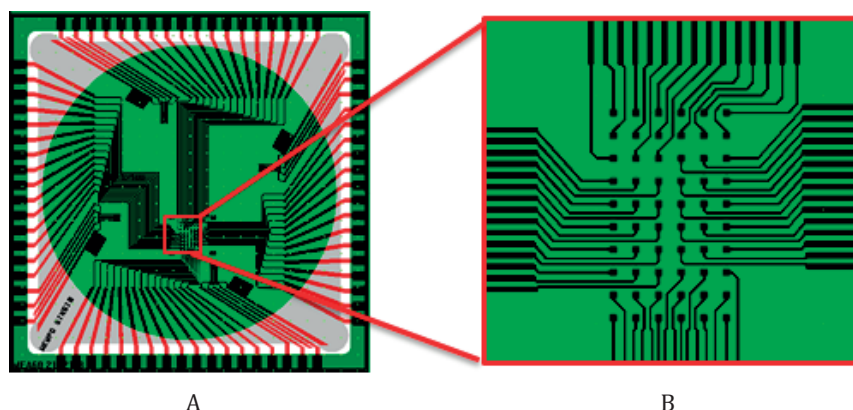


Figure 33: Design of a normal MEA device with 60 electrodes. (A) MEA device design by Clewin (B) Close-up of the 6 x 10 electrodes array in Clewin software

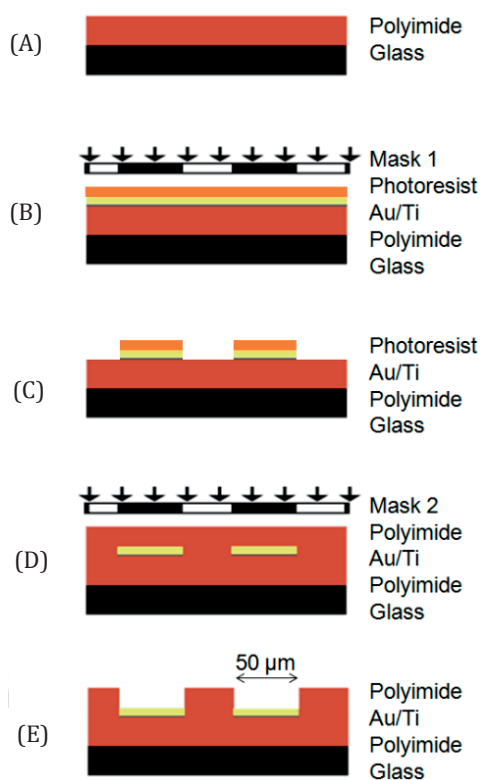


Figure 34: Schematic diagrams of the fabrication of MEA device. (A) A 15 μm thick photosensitive PI film was utilized as the substrate for the deposition of metals. (B) A gold layer (2000 \AA) was then deposited after a titanium layer (200 \AA) as the adhesion layer above the PI. Mask 1 was used to create the trace of electrodes by wet etching. (C) A gold electrode and pad trace pattern was formed by etching away not wanted metal then followed by removing the photoresist. (D) 20- μm -thick spin-coated PI film was used to encapsulate the electrodes. Mask 2 was then applied to expose microelectrodes and contact pads. (E) MEA device was then baked at 100 $^{\circ}\text{C}$ for 1 h. The fabricated MEA device has 60 microelectrodes in total and each active electrode site has diameter of 50 μm in circle. Image from my partner Shun-Ho Huang.

2.2.3 Primary cortical neuron dissection

Our microfluidic system allows culturing a variety of cells of different types (e.g., astrocyte, primary neuron) [84], from different regions of the brain (e.g., hippocampus, cortex), or from different transgenic animal models (e.g., Amyloid precursor protein transgenic mouse models, or tau transgenic mouse models). In our experimental procedure, we cultured dissociated neurons from the cerebral cortex of embryonic mice at day 19 (E19).

Cortical neurons are dissected from rat embryonic brains and be kept inside Petri dishes with PBS solution. Embryonic brain tissue is cut into smaller pieces to avoid clustering after digestion. The enzymatic digestion solution (2 ml Segal's medium with phenol red as pH indicator, add 200 μ l papain and drops of NaOH for adjusting pH to 7.3) needs to be heated up to 37 °C, intermixed with brain tissue at 37 °C for 15 minutes and swirled lightly by hand every 5 minutes. After the brain tissue settles down, the supernatant is removed and 1 to 3 ml protease inhibitor solution (10 % horse serum and 90 % neurobasal culture medium, adding 2 % B27 supplement and 1 % antibiotics) is added. The brain tissue is then pipetted through a 1000 μ l pipette tip five times to triturate the tissue and the supernatants containing suspended cells are transferred into a fresh falcon tube through the strainer. Afterwards, the cell suspension is flowed through a 40 μ m cell strainer to remove the debris, and some medium is then added and centrifuged at 0.6 u/min for 6 minutes. The supernatant is then discarded and cells are transferred into an eppendorf tube to count cell density. In the end, the cells are transferred into a falcon tube, some 37 °C pre-warmed cell culture medium (neurobasal medium, 2 % (v/v) B27, and 1 % (v/v) GlutaMAX are added and finally can be diluted into the desired concentration for the experiment.

2.2.4 Experimental materials

PDMS Sylgard® 184 Silicone Elastomer Kit from Dow Corning Corporation (Midland, MI, USA) was sold as two components, the PDMS base and its curing agent. SU-8 (GM 1060) was ordered from Gersteltec Sàrl (Pully, Switzerland). (3-Aminopropyl)triethoxysilane 99% (APTES) was purchased from Sigma-Aldrich GmbH (Buchs, Switzerland).

2.3 PDMS and SU-8 bonding tests

2.3.1 Bonding tests

2.3.1.1 Bonding theory based on the chemical reactions

In this irreversible bonding method (Figure 28), APTES molecules, which are both CH₃CH₂O- and -NH₂ terminated, are bound both to the PDMS and SU-8 interfaces. The CH₃CH₂O- group reacts with the -SiOH group from the O₂ plasma activated PDMS. The NH₂-group from the other end of the APTES molecule reacts with the epoxy group on the SU-8 surface. Two factors that play important roles during this bonding process were investigated experimentally: (1) the way the silanization is carried out, either in a liquid-phase or vapor-phase method; and (2) the degree of reticulation of SU-8 achieved before performing the

PDMS and SU-8 bonding step. These two factors have effects on the efficiency of bringing APTES molecules on the PDMS surface and the amount of epoxy groups on the SU-8 surface after the baking process, respectively. Since the microfluidic device bonded with this method will be used for neural cell culture in the future, and the neurons will grow on the surface of SU-8, we decided to have the surface modification on the PDMS surface instead of the SU-8 surface to have less effect on the cell culture.

For general use of SU-8 on microfabrication, SU-8 is first spin-coated and soft baked at low temperature (65 °C to 95 °C) allows evaporating the solvents. Then standard photolithography technique is used to reveal the pattern on the SU-8 surface. During the SU-8 exposure process of photolithography, the photoacid catalyst facilitates the epoxy group cross-linking. Following the exposure, a post exposure bake is performed to selectively cross-link the exposed regions, and the SU-8 resin is developed in a solvent to reveal the fabricated pattern. In the end, the SU-8 is generally baked again at 140 to 200 °C for a further crosslink of SU-8 and obtains good mechanical properties of the final components. This step is called hard bake. For our PDMS and SU-8 bonding, this hard bake step for the SU-8 should happen after the PDMS and SU-8 bonding. This is because the hard bake process can further cross-link the remaining epoxy groups on the developed SU-8 surface and result in less epoxy group left to react with the -NH₂ group from APTES molecule.

2.3.1.2 Sample preparation for the bonding test

We prepared our test samples by a combination of PDMS and SU-8 samples under different processed conditions: for the PDMS surfaces, they were first activated by O₂ plasma (50 W, 0.6 mbar, 30 s) to create the -SiOH group on the PDMS surface. After the surface activation, the APTES molecules were brought in contact with the activated PDMS surface immediately. In the literature, different methods to achieve a surface silanization using APTES have been described, such as liquid-phase silanization with deionized (DI) water followed by heating to a temperature of 85 °C [81], or by mixing with anhydrous toluene [159] or ethanol [141] and vapor-phase silanization [137]. To avoid the use of toxic chemicals, such as toluene [110], and provide a bonding method that is compatible with the requirements of the cell culture on a chip, we decided to use directly 99 % APTES in liquid-phase or vapor-phase for the silanization step. The protocol we used for liquid-phase silanization is the following: PDMS surface was immersed for 5 min into 99 % APTES immediately after the O₂ plasma, then washed in DI water DI water and dried. The protocol for vapor-phase silanization is the following: PDMS samples were exposed for 0.5 h or 1.0 h of APTES vapor by placing them into a desiccator containing a few drops of liquid 99 % APTES and reaching a vacuum environment so that APTES evaporates.

To obtain SU-8 surfaces showing different degrees of reticulation, some samples were used in the bonding tests without hard bake, while others were submitted to a 2 h hard bake at 150 °C on a hotplate. XPS analysis was performed on the surface of the PDMS obtained by different silanization methods, including vapor-phase and liquid-phase. The bonding strength

was evaluated for different degrees of reticulation for the SU-8, including SU-8 with and without the hard bake process.

2.3.2 Analysis of chemical reactions on the PDMS

2.3.2.1 XPS analysis instrument and spectra calibration

In order to prove the APTES molecules were bound onto the PDMS surface by liquid- and vapor- phases silanization, the elements and the chemical bonds on the tested PDMS surfaces have been determined by XPS analysis. The samples were analyzed using an ESCA KRATOS AXIS ULTRA Surface Analysis System. Data were analyzed by software MultiPak Version 9.5 (ULVAC-PHI Inc. Chigasaki, Japan). All spectra were calibrated in reference to the aliphatic C 1s component at a binding energy of 285.0 eV.

2.3.2.2 Evidence of APTES binding to PDMS

Among all the molecules present in the bonding protocols studies here, the N 1s is only present in the -NH₂ group of the APTES molecule, so its presence in the XPS spectra proves the presence of the APTES molecule on the tested sample. Figure 35 shows the N 1s binding energy from different samples: Sample 1 corresponds to a PDMS sample without any chemical surface treatment, Sample 2 is a liquid-phase silanized sample under 5 min immersion in 99% APTES, Samples 3 and 4 are vapor-phase-silanized PDMS surfaces, exposed for 0.5 h and 1.0 h to the APTES vapor, respectively. A peak in the XPS spectra close to an energy of 400 eV corresponding to the C-NH₂ bond can be seen only for Sample 2, proving the efficiency of the liquid-phase silanization method. No significant peak at this value of the energy can be observed for the other samples, which indicate that tested vapor-phase silanization of PDMS is inefficient in our experiment. Interestingly, the composition measurement of the main elements from Sample 2 (C 1s 44.7%, O 1s 30.9%, N 1s 7.3%, Si 2p 17.1%) is very close to the main elements composition of the APTES molecule (C 1s 48.9%, O 1s 21.7%, N 1s 6.3%, Si 2p 12.7%). This is a further indication of the presence of the APTES molecules on the surface of this PDMS sample after the liquid-phase silanization.

2.3.2.3 Analysis of the effect after hard bake process on the SU-8 material

There are typically three heating steps involved during the microfabrication of compounds in SU-8, a soft bake step at low temperature (65 °C to 95 °C) allows to evaporate the solvents, a post exposure-bake is performed at temperatures similar to the soft bake step and accelerates the SU-8 polymerization, and a hard bake step after development to further cross-link the epoxy groups of the SU-8 resist. This final baking step result in significant changes in the chemical bonds involved and cannot be easily monitored by XPS analysis. After the hard bake step, the SU-8 interface has a much higher Young's modulus [71], a higher stiffness and less changes on its shape under strength. On the other hand, the SU-8 without hard bake is more flexible and can provide better contact for adhesion [20]. When binding PDMS to SU-8,

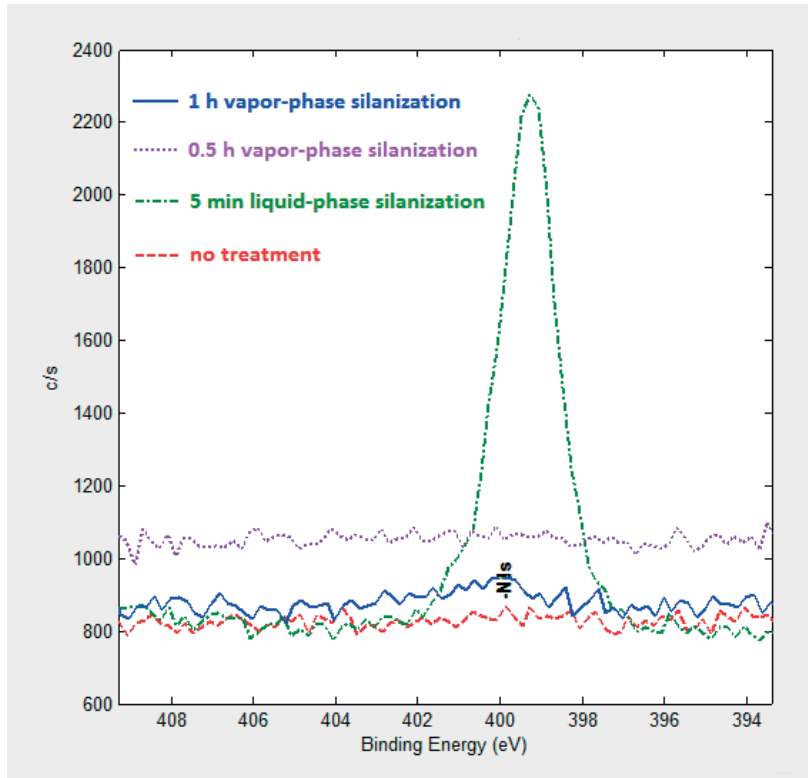


Figure 35: The N1s spectra of the PDMS surfaces by XPS under different surface modifications

it is clearly an advantage to have a large number of the epoxy groups on the surface of SU-8, and those groups can react with the APTES molecules bound to the PDMS component. To obtain a good binding, the SU-8 and PDMS compounds are maintained in close contact and pressure is applied to the assembling, while increasing the temperature in a similar way as for the conventional hard bake of SU-8, which simultaneously favours the binding reaction and the further cross-link of SU-8.

2.3.2.4 Summary of liquid- and vapor- phases silanization effects on the PDMS surface and hard bake effect on the SU-8 surface

To summarize, the XPS analysis suggests some important characteristics of the PDMS surfaces under solution- and vapor- phases silanization, which can assist us towards a good bonding method. From the N 1s spectrum result, APTES molecules were brought onto the O₂ plasma activated PDMS surface only under the condition of liquid-phase silanization. The alkoxysilane groups from the APTES molecule can potentially react with the -OH group from the activated PDMS surface and form Si-O-Si covalent bond. Secondly, before the hard bake at a high temperature, the SU-8 surface is less cross-linked and could contain more unreacted epoxy resin, which can potentially react with the -NH₂ groups from the APTES molecule. Furthermore, the SU-8 surface without a hard bake is more flexible mechanically and can provide

a better surface contact with the PDMS surface. In brief, the liquid-phase silanization method is selected as treatment for the PDMS surface, and the difference between with and without hard bake SU-8 surfaces will be compared at the following tensile strength test part.

2.3.3 Manual tensile strength test

2.3.3.1 Test sample preparation and manual tensile test set-up

SU-8 without hard bake can provide a larger number of epoxy groups and better contact for adhesion, which can potentially achieve a better bonding quality. To verify the difference of SU-8 with and without hard bake in our bonding method, we performed a manual tensile strength test on the assembled PDMS and SU-8 samples obtained by combining PDMS samples resulting from liquid-silanization of APTES and SU-8 samples with and without hard bake. The samples submitted to the tensile test were prepared by bonding a 1 cm in diameter PDMS device to a 5 μm thick layer of SU-8 deposited on glass (Figure 36). The contact surface between PDMS and SU-8 is 0.785 cm^2 in circular shape. The surface of the PDMS device was activated by O_2 plasma and processed with liquid-phase APTES surface silanization. SU-8 samples with and without hard bake were both individually bonded with the modified PDMS device and tested in this tensile strength test.

2.3.3.2 Building of manual tensile test set-up and the theory of manual test

The testing set-up (Figure 37 A) was built manually. As shown in Figure 37 A, a scale carrying a piece of metal of 3.530 kg was attached to a transparent plastic holder with a square hole on its top to maintain the tested the PDMS sample part. A lifting-jack was inserted into the glass part of the tested sample moved in the vertical direction and can lift up to 6 kg. With this set-up, by lifting up the SU-8 coated glass part of the sample, we created a separating force between the SU-8 and the PDMS that was attached to the metal plate. This force was decided by the change of mass indicated by the scale.

2.3.3.3 Summary of the manual tensile strength test

With this tensile strength test, we observed the difference in bonding strength between the SU-8 with and without hard bake. The samples with hard baked SU-8 broke at the interface of PDMS and SU-8 during the lifting by the lifting-jack. However, the samples where SU-8 was placed in contact with PDMS without hard bake showed a good adhesion until the separation process applied reached 440 kPa, which is the highest value the test set-up can provide, without failure. This is substantially higher than the working pressure for typical microfluidic devices. This manual tensile test revealed that SU-8 is required without a hard bake before contacting with the silanized PDMS surface. After the two surfaces were in contact and processed by the final baking step (150 $^{\circ}\text{C}$ for 1 h), a strong irreversible bonding that can reach 440 kPa was made between the PDMS and SU-8. This manual tensile strength test setup is flexible and convenient for quick tensile testing in the lab as a preliminary result.

2.3.4 Ultimate tensile strength test for the bonding

2.3.4.1 Set-up and testing sample preparation

From the manual tensile strength test shown above using the tensile setup made in the lab, the bonding with combination of liquid-phase silanized PDMS and SU-8 without hard bake reached the 440.6 kPa separation limit without any sign of breaking. To investigate the limit of the tensile strength for our bonding method by using liquid-phase silanized PDMS surface and the SU-8 surface without hard bake. A tensile test machine from Walter + Bai AG (Lönnigen, Switzerland) was used and the test was conducted under force control until the breaking point of the bonding. The tested sample was attached between two metal sample holders (Figure 38). The separating force on the tested sample was increased by the machine until the PDMS and SU-8 bonding interface broke.

2.3.4.2 Ultimate tensile strength test result and analysis

The tensile strength force measured during the tensile strength test was 116 ± 5 N, with most of the deformation occurring on the PDMS. This result corresponds to a stress of around 1.5 MPa at the point where the breaking occurred. This is reasonable when we consider the tensile strength of PDMS that is much higher than this bonding breaking point. [73]. The published result of tensile strength for PDMS and SU-8 bonding reach around 1 MPa [159]. Compared to this value, our method provided a slightly higher strength of the irreversible bonding.

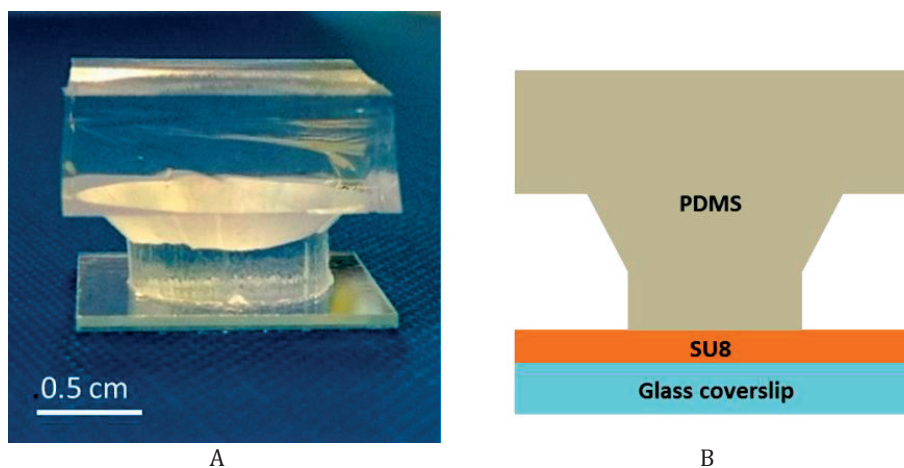


Figure 36: PDMS and SU-8 bonding strength testing sample. (A) PDMS and SU-8 samples for the bonding strength test. (B) Schematic of the testing sample. The lower part is a piece of 1mm thick glass coated with a 5 μ m thick SU-8. The upper part is a piece of PDMS obtained by molding

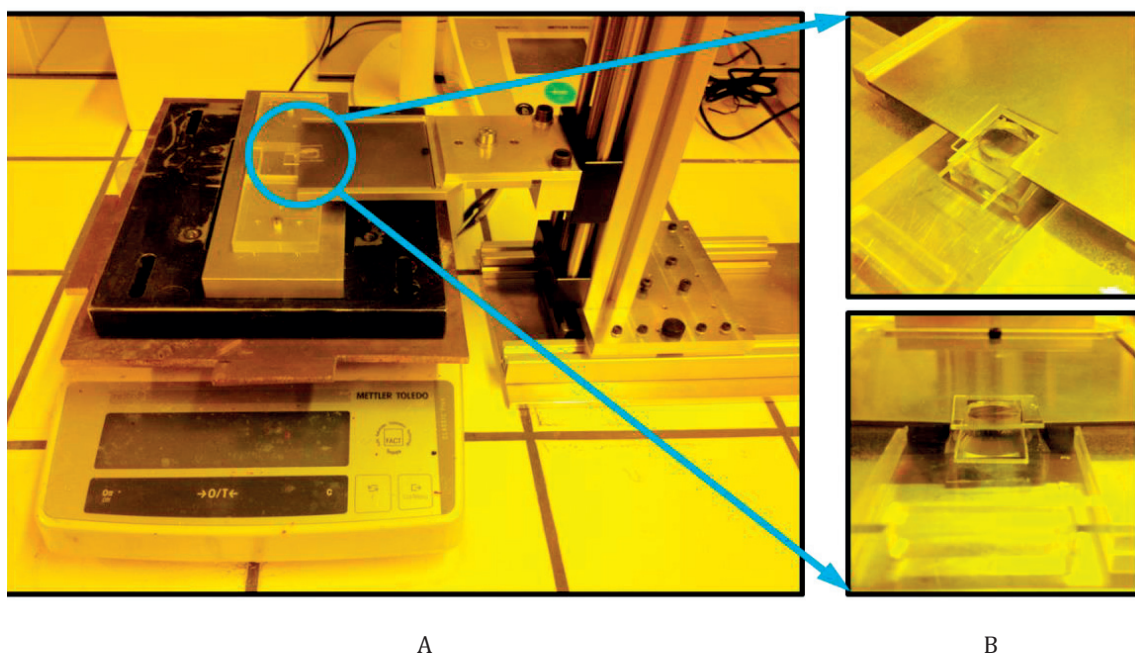


Figure 37: The set-up for the manual tensile strength test. It includes a scale, a piece of metal mass with a plastic PDMS chip fixer on top and a lifting-arm (Fig. A). Detail of the manual tensile test set-up during test and its side view (Fig. B)

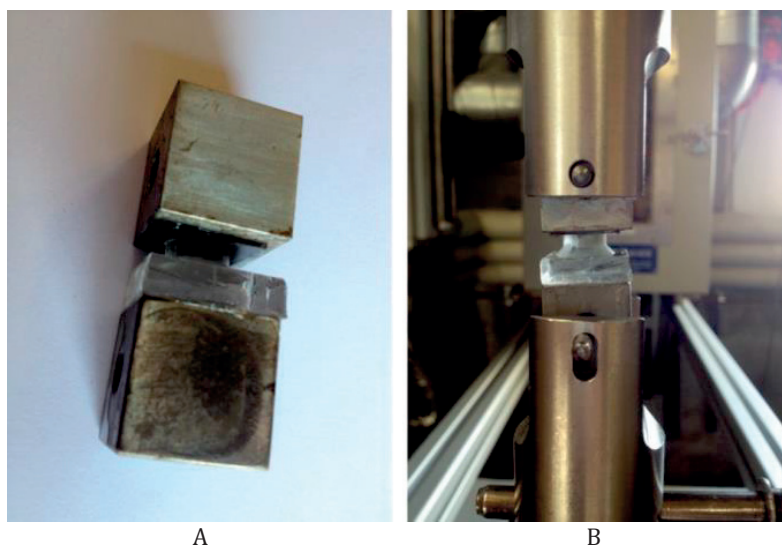


Figure 38: Tensile strength test for the bonding. (A) Test sample was fixed between the two metal parts from the tensile test machine for the bonding strength limit test. (B) A sample during the test

2.4 Microfluidic-MEA device

2.4.1 Surface silanization of the PDMS part from the device

For the compartmentalized PDMS device fabrication, the PDMS base and the curing agent were mixed at a ratio of 10:1. The mixture was poured onto a silicon wafer with structured patterns, degassed in a desiccator for 20 min until the air bubbles were gone, and cured in an oven at 80 °C for 1 h to solidify the PDMS mixture and replicate the pattern on the surface of the PDMS device. Subsequently, a PDMS puncher was used to perforate the PDMS device to create reservoirs, which connect the microchannels to the macro world for the injection of fluids into the device. The PDMS surface was first cleaned using adhesive tape to remove small particles generated from the hole-punching step. It was then sonicated in an ultrasonic bath for 5 min and the surface was dried. The PDMS device was placed in the O₂ plasma machine to activate the surface (50 W, 0.6 mbar for 30 s). This surface modification step creates -SiOH groups on the PDMS surface. Afterwards, the PDMS device was immediately immersed into the 99% APTES solution for 5 min and then washed with DI water and dried. The CH₃CH₂O- groups from APTES molecule can attach and react with the -SiOH group from the activated PDMS surface and form a covalent Si-O-Si bond [40].

2.4.2 Fabrication of the SU-8 part from the device

For the MEA part in this microfluidic-MEA device, the SU-8 epoxy photoresist was coated on top of the electrode wires, as it acts as an insulation layer between the cell layer and the electrode array layer. Polymer coatings, such as SU-8, are widely used on metals for insulation and protection for circuit boards and wires in electronic devices to provide high electrical insulation and protection from environmental damage [22]. This SU-8 insulation layer is essential for this neural activity recording device because it can also reduce the parasitic capacitance between the electrode wires and the culture medium (conductive saline solution) for better signal recording [23]. A 5 µm thick layer of SU-8 was first spin-coated on the MEA surface, and baked by a hot plate at 60 °C for 15 min and another 15 min at 95 °C for a soft bake. Then it was exposed to UV light and polymerized by a hot plate at 80 °C for 20 min for a post-exposure bake, and developed in PGMEA solvent. The SU-8 surface (without the hard bake process) from the MEA device also needs to be cleaned using isopropyl alcohol to remove the residual particles on the surface. Subsequently, the SU-8 surface was carefully rinsed by DI water and dried.

2.4.3 PDMS and SU-8 bonding for the microfluidic-MEA device

When the surface modification of the PDMS device has finished, the PDMS device was taken out of the APTES solution, washed by DI water and dried. Then the PDMS device was immediately aligned onto the MEA device under a microscope without touching the silanized surface before alignment was achieved. Afterwards, the microfluidic-MEA device was placed on a flat surface inside an oven and a pressure of 2 N/cm² was applied on the top of the device to generate a force between the PDMS and MEA parts to keep these two surfaces fully in contact. The temperature of the oven was slowly increased with a ramp of 2 °C per min to 150 °C

and kept at 150 °C for 1 h. Then, the temperature was decreased back to 30 °C naturally. The reason for increasing and decreasing the temperature slowly is to avoid structural deformations, as well as the generation of cracks inside the SU-8 material, which would create leakage. During this bake time, a chemical reaction occurs between the -NH₂ group from the APTES molecule on the PDMS surface and the epoxy group from the SU-8 surface [24]. The bonding for this integrated microfluidic-MEA device was completed.

2.4.4 Device preparation for neuronal culture

The device needed to be sterilized before its use for cell culture. 70 % ethanol was injected into the reservoirs using a syringe, which generated a flow inside the device to both wash away the particles remaining inside the chambers and junction channels and sterilize them. It was kept inside the device for 20 min, and then sucked out by a vacuum aspirator. The ethanol was then replaced with DI water. The chambers and junction channels were washed with DI water three times and emptied by using the vacuum aspirator each time. The device was then placed in a sterile petri dish (100 mm diameter) and exposed under UV light for 1 h. Like normal neural culture in well plates, the cell adhesion surface inside the device needs to be treated with a coating solution for faster neuronal adhesion and more homogeneous cell distribution. The coating solution, 0.05 % (v/v) polyethyleneimine (PEI), was injected into the device from the reservoirs and kept in the chambers and junction channels for 2 h at 37 °C inside a sterile closed petri dish. Then, the PEI coating solution was removed and the device was washed three times with DI water and replaced with Laminin (20 µg/ml) coating solution and kept at 37 °C for another 20 min. Finally, the Laminin coating solution was removed, and the device was washed three times with DI water, and replaced with neural culture medium (neurobasal, 1 % GlutaMAX, 2 % B27, 1 % penicillin/streptomycin) and kept inside a petri dish in the incubator (37 °C, 95% air, 5 % CO₂ and 65 % relative humidity), getting ready for the cell placing.

Primary cortical neurons were extracted from E17 embryos on the day of cell placing. The cell suspension was concentrated to 10 million cortical neurons per ml of neural culture medium. The prepared microfluidic-MEA device was first emptied, and then filled with the freshly prepared cell suspension into the lateral chambers (Region 1 and 3) in the PDMS, carefully avoiding air bubbles. The middle chamber (Region 2) which contains no cells was filled with the normal neural culture medium. The device and the freshly placed cortical neurons were kept inside the incubator for long-term cell grow and neural network development.

2.4.5 Morphological and electrophysiological observations from the microfluidic-MEA device

After 23 days of continuous culture *in vitro*, spike activities from the neural network were recorded with a MEA 1060 System (Multi Channel Systems, Germany) with 60 recording channels at 10 or 20 kHz sampling frequency and 10 to 3000 Hz hardware bandpass filter. Data acquisition and analysis were obtained using the MC_Rack software (Multi Channel Systems, Germany). The activity signals from the neuron soma and the axons were recorded indi-

vidually by the 60 electrodes (Figure 39). The healthy neural network confirms that this bonding method is compatible for cell culture since the chemicals introduced by the PDMS and SU-8 bonding do not have a big effect on the cell culture. The device did not show any leakage or crack under microscope, and the bonding could not be separated afterwards in the vast majority of cases (with very rare failures occurring possibly due to the roughness or flatness of the PDMS surface). Concerning the device re-use, the device was aspirated first, then washed with DI water and treated with trypsin after use to detach the cells. In the end, the device was emptied, dried and kept in a sterile environment until the next use.

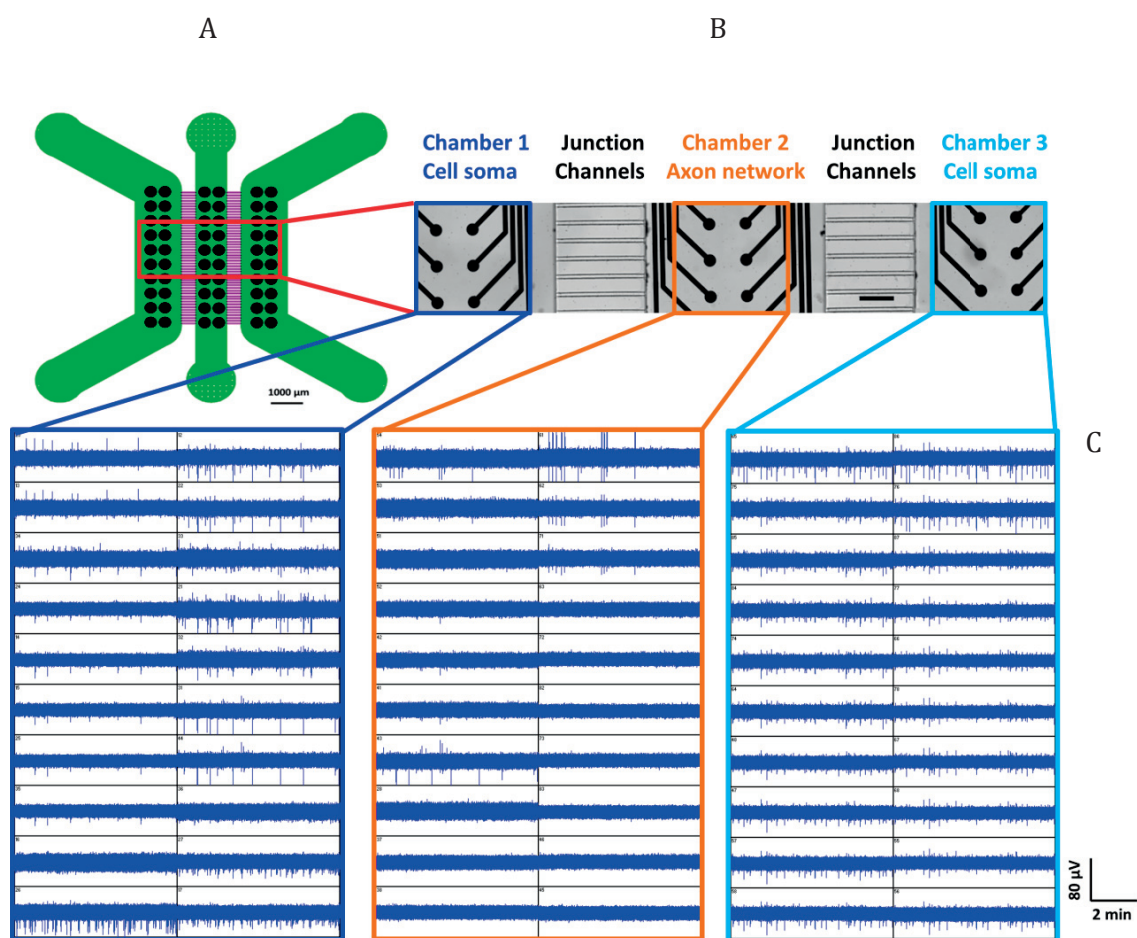


Figure 39: Design of microfluidic-MEA device and recording result. (A) Schematic of the chambers and junction channels from the PDMS device and the six columns of electrodes from the MEA device. (B) Picture of the interface of PDMS and SU-8 from the device taken by wide field microscope. The functions of each part are indicated. Scale: 200 μm. (C) Neural activities recorded by 60 microelectrodes from this microfluidic-MEA device. The colors are correlated to the regions with the same colors in Fig. b. Each sub-window corresponds to one individual electrode. The signals from the chamber 1 and 3 were recorded from cell soma region, and the axon activities were recorded by the electrodes from Chamber 2

Comparing to other technologies such as spin-coating SU-8 onto the PDMS surface, our bonding method is simple and convenient as shown in the example of our microfluidic-MEA device, and requires only a chemical hood and an oven. The microfluidic PDMS device and

MEA device can be fabricated individually and synchronously, and integrated together at the end of the process without any limitations. This flexible combination characteristic of this bonding method allows an easy fabrication of microfluidic systems and sealed chambers based on PDMS and SU-8, while avoiding leakages and allowing the obtained systems to be re-used after being cleaned. Concerning the device re-use, the device was aspirated first, then washed with DI water and treated with trypsin after use to detach the cells. In the end, the device was emptied, dried and kept in a sterile environment until the next use.

2.5 Conclusion

In this chapter, we detailed the fabrication process of microfluidic and MEA devices, and especially focusing on our bonding technique of PDMS and SU-8 for the integration of the microfluidic and MEA devices. This simple and reliable PDMS and SU-8 irreversible bonding method, which was based on the covalent bonds, was obtained by introducing aminosilane molecules by liquid-phase silanization and SU-8 without hard bake. This bonding method was determined by XPS analysis and validated by tensile strength tests. Comparing to other technologies such as spin coating, our bonding method is simple and flexible for individual devices bonding which means the devices can be fabricated individually and synchronously and integrate the devices together at the end of the process without any limitations. This irreversible bonding method can furthest avoid leakages and allowing the obtained systems to be re-used after being cleaned.

This PDMS and SU-8 bonding technique solved our issue on the fabrication of our integrated microfluidic-MEA device, which can be used to observe the morphology and electrophysiology of neural networks *in vitro* simultaneously. The result from our microfluidic-MEA device proved that this bonding method is robust on its quality, flexible for integration, simple and user-friendly for manipulation and compatible for *in vitro* cell culture. This makes it very useful for many applications related to PDMS and SU-8 materials, in particular microfluidics and lab-on-a-chip device where handling of fluids needs to be performed without leakage. On the other hand, this type of integrated devices will give the possibility for neuroscientists to study the morphology and electrophysiology of neurodegenerative diseases more thoroughly and comprehensively.

Propagation of Tau pathology in microfluidic and integrated microfluidic-MEA devices

3

“To raise new questions, new possibilities, to regard old problems from a new angle, requires creative imagination and marks real advance in science.”

by Albert Einstein

3.1 Introduction

3.1.1 Importance of building a microfluidic-MEA device for studying AD

In 2011, Anja Kunze used a compartmentalized microfluidic device to build a co-pathological model and present different phosphorylation states in the axonal network under a gradient of OA between the diseased and healthy neuronal populations [85]. This cell morphological study opened the possibility of study cellular and molecular propagation of AD in a compartmentalized microfluidic device. However, morphological degradation is not the only issue that is happening in an AD brain. The neuropathological, electrophysiological and neuroimaging data have suggested that AD exhibits both functional and structural abnormalities across anatomically distinct brain regions. This requires innovative tools to extend our research to functional studies for neuronal culture *in vitro* and to observe electrophysiological patterns within the neuronal network. This concept guided us to combine the microfluidic device with the MEA device [76, 78, 77, 49]. This combination allows us to observe unique features of the electrophysiological properties of the compartmentalized neuronal network, such as the depression of neural activity of two distinct neuronal populations during AD propagation [37, 118], the functional neuronal circuitry between specific type of neurons [76, 78, 49] and some selective pharmacological administrated effects [77]. The microfluidic-MEA device is designed as a multifunctional tool for neuroscientists to observe the neuronal network dysfunctions simultaneously during the propagation of neurodegenerative diseases such as AD. Several hypotheses are expected to prove with our microfluidic and microfluidic-MEA device: 1. the neuron-to-neuron transmission during disease propagation. 2. the function of axonal network during disease propagation. 3. the concentration-dependence drug effect on building a diseased model to mimic AD propagation. 4. the order in which the structural and functional alterations occur during AD propagation. Based to Anja's previous work on building co-pathological model to study AD, we make several modifications as described in Introduction Section adapting the requirements for proving our hypotheses. Briefly, it includes the longer junction channels to absolute control at the axon region to isolate axon and exclude drug effect on the axon, low and high concentrations of OA exposure for concentration-dependence drug effect studies, longer observation duration from early stage to the late stage during disease propagation and the integration of microfluidic device and MEA recording device which provide innovative information on the order of occurrence of structural and functional alterations.

3.1.2 Building a diseased cell model based on Tau pathology

Microtubule-associated Tau protein (MAPT) is a type of microtubule-associated proteins [44] and it mainly works on stabilizing the microtubule function and maintaining the cytoskeleton plasticity in neurons [5]. The phosphorylation and the dephosphorylation characteristics of Tau protein play important roles in maintaining proper axonal connectivity, synaptic function as well as neuronal survival [7, 112]. Under AD conditions, the Tau protein is phosphorylated at 3 to 4 times increased (6-8 mol phosphate/mol Tau) compared to the healthy

situation (1.9 mol phosphate/mol Tau) [80, 11] and the abnormal highly phosphorylation of Tau protein leads to hp-Tau which then aggregates into NFTs [87]. NFTs trigger axonal swellings and dystrophic neuritis which is related to axonopathy and neuronal transport deficits [46, 5]. In order to build our AD model, the neurons are induced with okadaic acid (OA), which is an inhibitor of protein Ser/Thr phosphatases PP1 and PP2A. This effect will further inhibit the Tau dephosphorylation, and force the Tau protein to aggregate and become hp-Tau mimicking the AD pathology [74, 75].

3.1.3 Disease propagation studies by using microfluidic and microfluidic-MEA devices

Based on this concept of integrating microfluidic and MEA devices, this integrated microfluidic-MEA device was designed, fabricated and tested. The added MEA device provided an electrophysiological observation platform to analyze the functional interactions in the neuronal network. Using these two platforms, a co-pathological model was built to study AD propagation between diseased (OA-exposed) and healthy (without OA exposure) neuronal populations and test the concentration-dependent effect on the neuronal network. The experiment process is presented in Figure 40. Primary cortical neurons are first loaded in the two lateral chambers in the device. Then the culture was maintained for 21 days and the mature neural network is built during this time. The neuronal population in the left chamber region was induced with OA, while the morphological and electrophysiological alterations were tracked during the disease propagation in the whole neuronal network, including cytoskeleton alteration, hp-Tau transportation and neuronal activity variation.

3.2 Materials and Methods

3.2.1 Design and fabrication process of microfluidic and microfluidic-MEA devices

For building a diseased and healthy neuronal network with axon isolation in between, the pattern of our microfluidic device was designed with three regions (Figure 41): Region 1. OA-exposed neuronal population; Region 3. Neuronal population without OA exposure (OA-unexposed); Region 2. Central channel for axon growth. Between each two neighboring regions, there are 50 junction channels for physical separation of axon from the OA-exposed and the OA-unexposed neuronal populations (Figure 41 B). The primary neuronal culture was performed in Regions 1 and 3 microchannels with dimension of 1.5 mm in width, 4.5 mm in length and 100 μm in height. The axon connection was formed in Region 2 microchannel with dimension of 1 mm in width, 4.5 mm in length and 100 μm in height. The junction channels are 20 μm in width and 10 μm in height and 500 μm in length, and it serves as physical barriers for neuronal bodies. They stop the soma from entering the junction channel and let the neurite to pass through. As described in the introduction chapter, the 500 μm length of junction channels are able to create an axon-connected region (Region 2) without dendrites

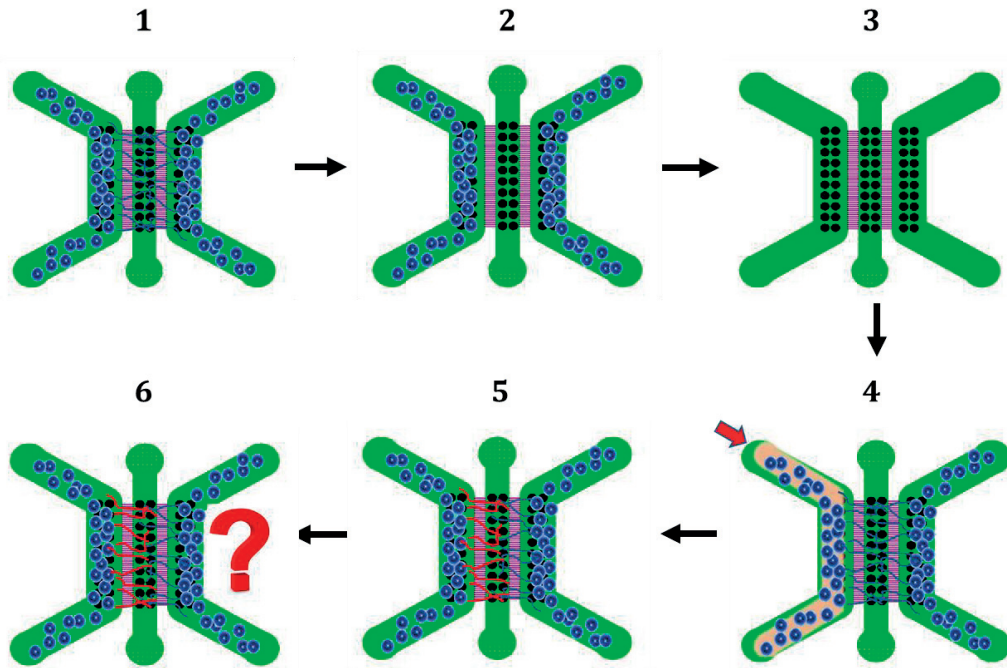


Figure 40: Schematic picture of the experiment process. It includes device (1) (black round spots represent electrodes), cell loading (2), neurons growth and network building (3), OA-exposure (4), cells become diseased (5), and further observation (6)

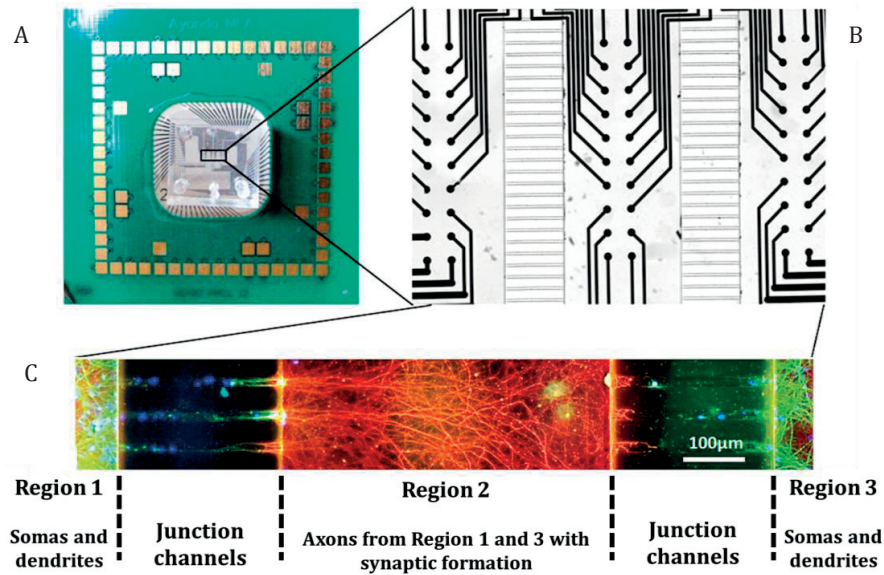


Figure 41: Image of the microfluidic-MEA device and its internal structures. Top view picture of the integrated microfluidic-MEA device (A). It consists of the compartmentalized microfluidic device and the MEA device. (B) Image of the interface between the microfluidic and MEA devices. The MEA device has 60 microelectrodes with 2 by 10 arrangements in the culture regions, and the junction channels from the microfluidic device. (C) Immunofluorescent image of neuronal culture stained with the neuron-specific protein MAP2 (green), axon-specific neurofilaments (red)

growing into the adjacent Region 2 according to previous study [144, 145]. From our result in Figure 41 C, the stained axon in Region 2 proves that the axons are very efficiently separated from the dendrite. For the microfluidic-MEA device (Figure 41 A), the microfluidic device is bonded with the MEA device and the pattern of the electrodes from the MEA device are adapted to the design of the three regions (Figure 41 B). The detailed fabrication processes are presented in Section 2.2.1 and 2.2.2. The bonding method of microfluidic and MEA devices is detailed in Section 2.4.

3.2.2 Preparation and plating procedure for the devices

The microfluidic and microfluidic-MEA devices have the same process for preparation and cell plating. However, the microfluidic devices are used for the immunocytochemistry staining for morphological studies and the microfluidic-MEA devices are used for electrophysiological studies, so that the morphological and the electrophysiological data are not from the same culture sample. The device was coated with 0.05 % PEI solution overnight at 4 °C the day before plating. On the cell placing day, the devices were coated with laminin (20 µg/mL) for 20 min at 37 °C. Between each coating step, the device was washed with sterile DI water three times to remove any residuals from the surface coating step. Before cell suspension injection, the device was washed with fresh neurobasal neuronal culture medium in order to wet the surfaces and avoid air bubbles. All the materials used for cell culture were purchased from Invitrogen (Carlsbad, CA).

All the experimental procedures were carried out according to the Swiss federation rules for animal experiments. Mouse primary cortical neurons were obtained from embryonic day 17 (E17) fetal mouse. Cortices were digested in culture medium added with papain (20 U/mL) and dissociated by mechanical trituration. The cortical neurons were uniformly distributed inside the neurobasal medium supplemented with 2 % B27 and 2×10^{-3} M GlutaMAX as cell suspension. The cell suspension was loaded into a 1.6 mm diameter PTFE tube that can provide sufficient pressure to flow the neurons into the neuronal culture region in a relatively homogeneous distribution. There were 4×10^5 cells injected into the microchannel culture areas in each device. The devices were kept inside 10 mm petri dishes with an additional water container to slow down medium evaporation. All devices were then maintained in normal culture condition (37 °C, 5 % CO₂) and the medium was refilled repeatedly depending on the experiment schedule.

3.2.3 Induce Tau hyperphosphorylation via OA exposure

After 21 days *in vitro* (DIV), these two neuronal populations were mature with neuronal connections built up in the axon-connected region. The drug exposure time point was chosen based on previous studies, which show that mature neuronal networks with stable spontaneous activity patterns have been observed after 21 DIV [23]. For the disease induced cell population, local OA exposures with high and low concentrations (600 nM and 60 nM inside neurobasal medium, respectively) were used in Region 1. This drug exposure procedure lasted for 75 min that can potentially induce hp-Tau. The drug from Region 1 was then washed

away, and replaced by fresh culture medium. In order to observe the propagation from exposed to unexposed neuronal populations, the measurement time points have been set at 0 h (immediately after the 75 min of OA exposure), 6 h, 24 h, and 48 h. The 48 hours observation after the drug exposure is named as a “recovery period” for the neuronal network.

Concerning the liquid isolation requirement for OA exposure in this experiment, it is critical to keep the drug isolated from all the other unexposed channels to exclude the possibility that the drug has effect on the unexposed cell population by diffusion. To fulfil this goal, several aspects were taken into consideration when we designed the device and the experiment manipulation procedure, to ensure the separation of OA exposure. The junction channels are long enough to exclude the dendrite from the axon and the cross-section is small enough to stop the soma to pass through the junction channel. The channels were washed several times by culture medium to clean up the drug that possibly existed in the channels.

Each two neighbor compartments are not absolutely isolated because they are connected by junction channels. In order to demonstrate there is no drug effect on the un-exposed neuronal population during the 75 min drug exposure procedure because of the drug diffusion through the junction channels, a control experiment was designed. The neurons were placed only in the right lateral channels, not in the both sides, and grew for 21 days. On 21 DIV, the drug was injected into the left lateral compartment, kept in the compartment for 75 min and was removed afterwards. The cell population in the right side lateral compartment was imaged by confocal microscope for cytoskeleton analysis.

3.2.4 Immunocytochemistry staining for morphological studies

The samples from the microfluidic devices were used for immunocytochemistry staining. At each selected time point for observation, the neuronal culture in the microfluidic device were fixed with 4 % paraformaldehyde (PFA) in 0.1 M phosphate buffered saline (PBS) buffer for 20 min and rinsed with PBS three times after the fixation. The neurons were permeabilized with 0.25 % Triton and 1 % BSA for 20 min. Then the fixed sample reacted with the primary antibodies overnight at 4 °C, and after that, the solution was removed and washed with PBS buffer. The fixed culture was incubated with secondary antibodies in the dark for 2 h at room temperature. In the end, the secondary antibody solution was removed and washed with PBS buffer, and all the fixed samples were preserved at 4 °C for confocal microscopy imaging.

In this study, neuronal cytoskeleton, axon and hp-Tau at Ser262 site were visualized. The primary antibodies included the rabbit polyclonal antibody which stains for the MAP2 (neuronal marker, 1:150 dilution, Acris antibodies, Germany), rabbit polyclonal antibody which stains for the endogenous level of Tau when it is phosphorylated at Serine 262 (Tau Phospho-Ser262 marker, 1:150 in dilution, Signalway Antibody, Switzerland) and mouse monoclonal antibody which stains for the pan-axonal neurofilament (neuronal axon marker, 1:500 in dilution, COVANCE, USA). The second antibodies were the Alexa488-conjugated antibody for rabbit IgG (1:500 in dilution, Dionova, Switzerland) and the Rhodamine-conjugated antibody for

mouse IgG (1:200 in dilution, Dionova, Switzerland). DAPI was used as well to visualize the nuclear morphology.

For this experiment with microfluidic device, we used 21 DIV neuronal cultures and the experiment was repeated three times with three rounds of neuronal culture respectively. There were 60 devices used in total and 20 devices were used for each round. For each round, 4 samples were fixed before the OA exposure as a control group. There were 8 samples were exposed under the high concentration of OA exposure (600 nM). Among the 8 exposed samples, 2 samples were fixed for each time point, at 0 h, 6 h, 24 h, 48 h, separately. One out of the two samples was stained for the cytoskeleton and the other one was stained for the hp-Tau. Another 8 devices were exposed under the low concentration of OA exposure (60 nM), fixed at the same time points and repetition as the high concentration group.

3.2.5 Extracellular recording method and parameters settings

In order to study this compartmentalized neuronal network in a comprehensive way, not only structural connectivity was studied, but also the functional connectivity between the two neuronal populations has been investigated. In this experiment, the microfluidic-MEA devices were used for recording the neuronal activity in the compartmentalized neuronal culture. In this recording experiment, the extracellular recording was performed on the 21 DIV, using a MEA 1060 recording system (Multichannel Systems, Germany). This MEA 1060 system is equipped with 60 recording channels at 10 or 20 kHz sampling frequency with a hardware bandpass filter of 10-3000 Hz. Mc_Rack software was used for data recording and the recorded data was filtered at 200 Hz (high-pass Butterworth). The analysis of detecting and extracting spikes and bursts was performed with MC_Rack software following the manual provided by Multichannel Systems. For recording reliability reasons, the recording was started 10 min after the MEA was transferred out from the incubator, in order to avoid the effects of mechanical perturbation and environmental transit [153]. Because the environment of the recording room was not under controlled temperature and CO₂ the recording duration for each device was fixed 10 min to avoid prolonged exposure outside an ambient environment. When the recording was done, the sample was transferred back to the incubator until the next experimental time point for recording. After spike sorting, the spikes were stored as series of time stamps for further functional connectivity analysis. There are two quantitative parameters that are defined for analyzing the extracellular recording data: the spike number that corresponds to the total number of spike during the 10 min of recording, and the burst number that corresponds to the total number of burst events occurred over the 10 min of recording.

The neuronal activity recording experiment with the microfluidic-MEA device was repeated 5 times with 5 rounds of cortical neuronal culture respectively from 21 DIV culture. For each round of experiment, one sample was induced under high concentration of OA (600 nM), another sample was treated under low concentration of OA (60 nM) and one sample as a control.

3.2.6 Recording data analysis and statistical analysis

The neuronal activity data was stored in a digital format for spike sorting. Data were analyzed offline using MATLAB (The MathWorks Inc., USA) based on a typical spike sorting algorithm to estimate the signal-to-noise ratio (SNR) [152]. Sensing noise, instrumentation interference, and small amplitude signals from neighboring neurons were considered as background noise. The spikes from a single electrode were not discriminated and sorted for signals from different neurons, so the individual spike train may contain spikes from one or more neurons [76]. All the statistical data were presented in the way of mean \pm standard deviation (SD). The spikes number ratio and bursts per minute ratio were subjected to two-way analysis of variance (ANOVA) for multiple comparisons. A p value of less than 0.05 was considered for the statistical significance.

3.3 Results

3.3.1 Control experiment

Following the experimental design of the control experiment demonstrated in Section 3.2.3, the control experiment was done, and the result is shown in Figure 42. From the cytoskeleton alteration result in Figure 42 B, no severe cell damage was observed from the morphological result, and in Figure 42 C, no severe decline of neural activity was observed. From this result of control experiment, we can exclude the severe effect on the un-exposed cell population from the drug diffusion during the 75 min drug exposure. In the main experiment, the severe morphological and electrophysiological alterations both should be due to the effect from the connected drug-exposed cell population.

3.3.2 Cytoskeleton alterations after OA exposure

One of the main observations that have been observed during AD progression is the loss of microtubule integrity related to neurodegeneration [68, 69]. In our experimental model, the OA-mediated cytoskeleton destabilization was generated and the cytoskeleton integrity with neuron specific MAP2 protein was visualized. This diseased cell model was physically connected to another no drug exposed cell population through axon network. In this way, it is possible to observe the disease propagation from diseased to healthy neuronal population mimicking the disease progression in natural tissue.

Under high concentration of OA exposure (600 nM), as shown in Figure 43 A, the neuronal cytoskeleton of the diseased neuronal population degenerated continuously with time and lost its connection network eventually. Similar phenomenon was observed as well in the unexposed side with a delay compared to the exposed neuronal population. About this original healthy cell population, it eventually revealed degradation until 48 h. This is due to the effect from the OA-induced cell population, and the disease propagated and caused serious damage on the unexposed population. Under the low concentration OA exposure (60 nM), the OA-exposed neuronal population showed higher neurite survival compared to the high con-

centration group. However, a severe neurite loss was observed after 48 h, shown in the Figure 43 B. About the unexposed side, significant neuritic degeneration (compared to the result from high concentration of OA exposure) was not observed until a slight neurite loss was detected at 48 h.

From those results above, we observed the disease was progressing from the OA-induced diseased neuronal population to the healthy neuronal population through the connected axons. Under high concentration of OA exposure, the neurons exhibited more severe damage to the exposed and unexposed cell populations compared to the low concentration condition. Additionally, more rapid and aggressive progressing pattern was revealed from the unexposed side as well. All these evidences indicate that this drug exposure by OA for building a diseased model is concentration dependent, and different propagation patterns were noticed.

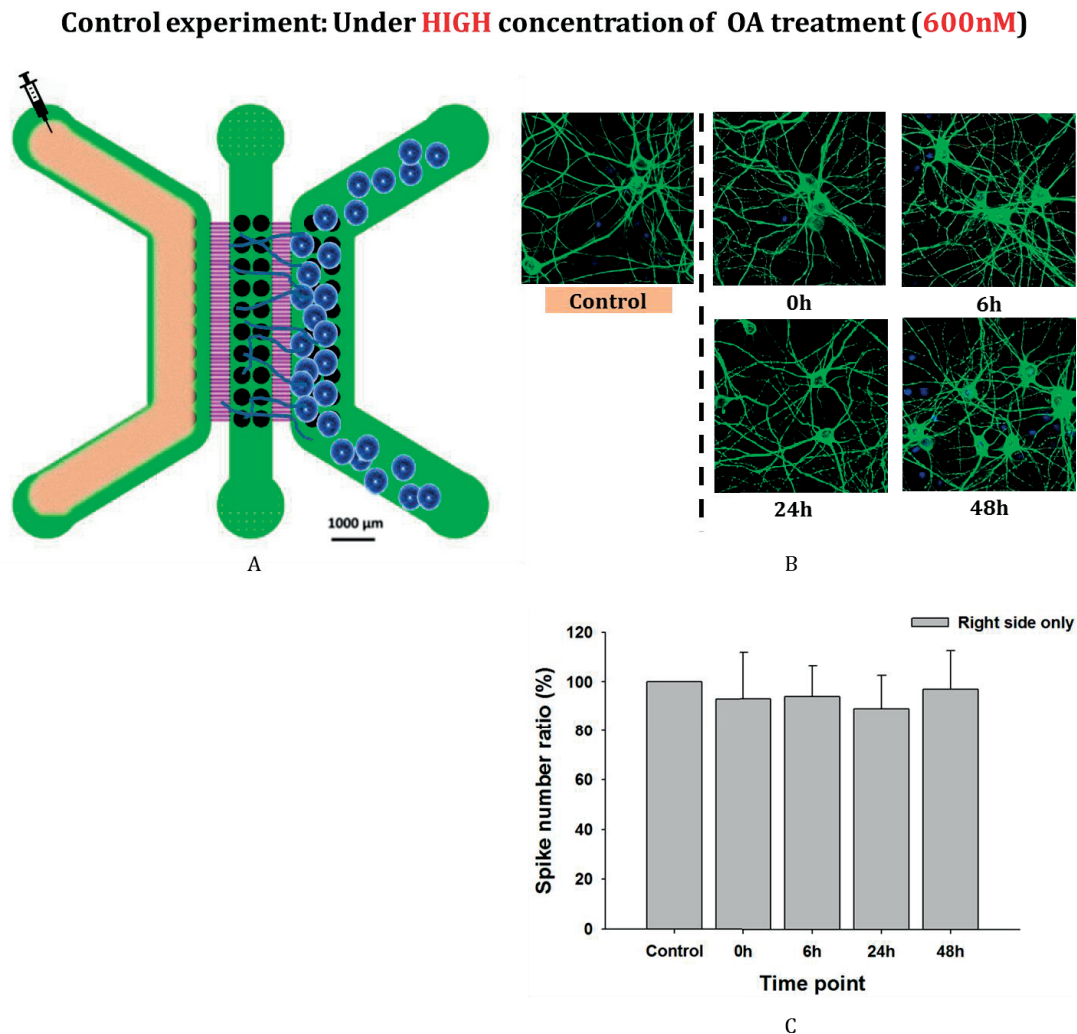


Figure 42: Control experiment for drug diffusion effect test. (A) Schematic of the control experiment design. (B) Cytoskeleton alteration on the cell population in the right lateral compartment. Staining: MAP2, green. (C) Neural activity result on the cell population in the right lateral compartment

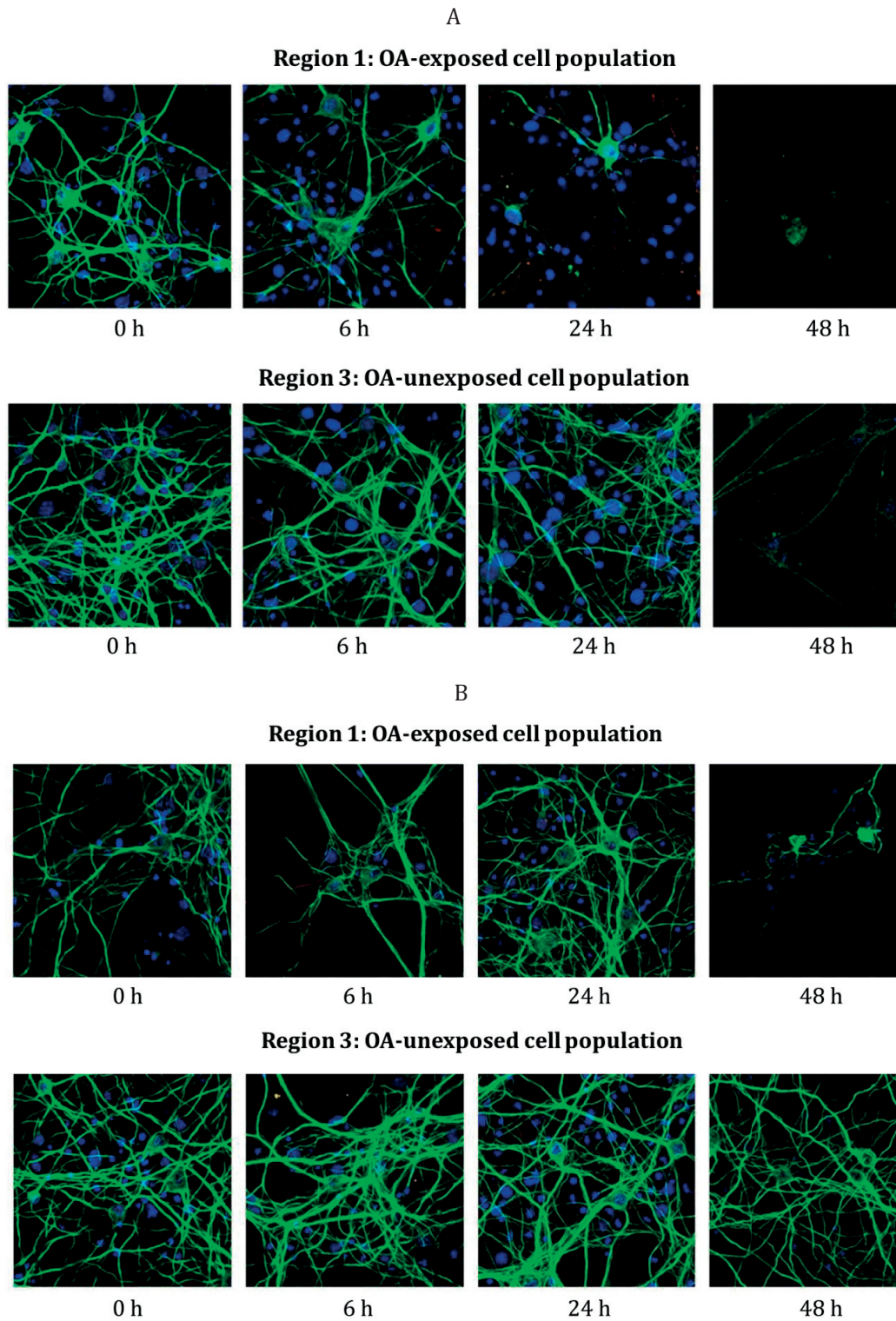


Figure 43: Cytoskeleton alteration visualized by MAP2 immunocytochemistry staining as green color. (A) After high concentration of OA exposure (600 nM). (B) After low concentration of OA exposure (60 nM). Images from Region 1 and 3 were captured from the same device to avoid biological variation. Scale: 100 μ m

3.3.3 Propagation of Tau hyperphosphorylation between diseased and healthy neural populations by axonal connection

Following the fact that the disease propagated between two cell populations through the axonal connections based on the features of cytoskeleton alteration presented above, the next step, the hp-Tau transportation during disease progression and the sequence of its appearance in the neuronal network were investigated. Benefitting from the compartmentalized structure of the microfluidic device, the isolated unobstructed axonal network will permit us to possess a better comprehension on the role of axon during disease propagation.

The experimental procedure on the exposed cell population was as same as the experiment about cytoskeleton alteration presented before: exposed cell population was under OA exposure for 75 min, either at high concentration of OA (600 nM) or at low concentration of OA (60 nM). The samples were fixed at different time points (0 h, 6 h, 24 h and 48 h). For the hp-Tau tracking, the phosphorylation site Tau Ser-262 (pSer262) was marked and tracked as an AD relevant site, which is often found in AD brain [154]. The imaging for Tau Ser-262 staining from the Region 1, 2 and 3 inside the microfluidic device was done with confocal microscope. From the high concentration of OA exposure (600 nM) results in Figure 44, it was firstly observed that immediately after 75 min OA exposure, a significant amount of hp-Tau was distributed in the axon region (Region 2) from diseased towards the OA-unexposed neuronal populations with a gradient pattern. Six hours later, hp-Tau in the axon region suddenly diminished dramatically, possibly dissipated into the culture medium and became residues near the entrance of junction channels. Due to the continuously dissipation, less amount of hp-Tau was observed in the axon region at 24 h and 48 h time points. About the OA-exposed region, uniform hp-Tau protein aggregates were formed directly after the drug exposure, with a significant lower intensity compared to the axon region. Six hours after, hp-Tau aggregated seriously around the neuronal body and in their neurites. More severe hp-Tau aggregates were revealed at 24 h and dissipated into the cell medium between 24 h and 48 h. This phenomenon consists with the observation from the cytoskeleton alteration result at 24 h that the neuronal structure was dramatically damaged (Figure 43). At the unexposed region (Region 3), no hp-Tau protein aggregation was noticed in the unexposed population immediately after the drug exposure. Until 6 hours later, hp-Tau started to aggregate slightly around the neuronal bodies and accumulated in the neurites. More significant hp-Tau aggregation inside neuronal soma appeared at 48 h of recovery.

Based on the result above on the hp-Tau propagation under high concentration OA exposure, the result was compared with the condition of under low concentration of OA exposure (60 nM) in Figure 45. A similar phenomenon was shown that the hp-Tau was firstly accumulated severely at the axon region, instead of the OA-exposed cell population region. However, under low concentration of OA exposure, the speed of hp-Tau aggregation was slower because of the observed delayed of hp-Tau accumulation in the axon region during the first 6 hours. The propagation pattern was less aggressive depending on the intensity of the accumulated hp-Tau in the cell bodies and neurites from both of the exposed and unexposed cell population

regions. There was no distinct hp-Tau aggregation found in the unexposed cell population at 48 h under low concentration of OA exposure while the neurons still had their cytoskeleton with a slight damage (Figure 45 B 48 h).

3.3.4 Spontaneous firing rate and burst rate during the disease propagation

Spontaneous spike activities recorded from the cortical neuronal network *in vitro* were considered as a functional indicator for network behavior [103]. With our integrated microfluidic-MEA device, neuronal activities were recorded from the compartmentalized neuronal network. The results about the spike number variation during disease propagation under high (600 nM) and low (60 nM) concentrations of OA exposure were shown in Fig. 4-6. The spike rate was normalized to the control sample before OA exposure (by definition of 100%). The average values and standard deviations were obtained from five independent cultures.

Under high concentration of OA exposure (600 nM), the spike activities from the exposed neuronal population was significantly inhibited immediately after the OA exposure and remained low at the following 6 h, 24 h and 48 h recording time points. The axon presented a similar neuronal activity decreasing pattern with a slightly delay at the beginning compared to the OA-exposed cell population (Fig. 4-7). Different phenomenon has been shown at the unexposed cell population. The spike number gradually increased with time until 6 h and then started to decrease, like a pattern of temporary excitement. This pattern was also observed in the low concentration of OA exposure situation, but in all the three regions. Decreased spiking activity was first observed in all regions. However, after 24 hours recovery, the excitement pattern started and the activities were increased in all three regions with different ranges. The neuronal activity changing ranges under low concentration exposure were all in a lower level compared to the high concentration exposure.

Besides the spike number, the burst was also analyzed as another characteristic to illustrate the activity of the neuronal network. The bursts are defined as repeated spikes occurring during a short time interval and they are supposed to be synchronized with the spiking activity. The functional importance of generating bursts is to increase the reliability of communication between neurons and to avoid synaptic transmission failure. Compared to spike, burst might afford more precise information and effective mechanisms for selective communication between neurons and produce long-term synaptic plasticity and information processing [22]. In our experiment, the bursts number was normalized to the burst number from the control sample before OA exposure (by definition of 100%). The result about the spike number alteration during disease propagation under high (600 nM) and low (60 nM) concentrations of OA exposure is shown in Fig. 4-6. The average values and standard deviations were obtained from five independent cultures. Under high and low concentration of OA exposure (600 nM and 60 nM), the inhibited and excitement patterns are very similar to the spike number result respectively.

3.4 Discussion

3.4.1 Structural characteristics alterations during disease propagation

Benefitting from this disease propagation model built in the microfluidic device, the structural alterations on the neuronal cytoskeleton were identified in the diseased and healthy cell populations and their axonal network. It provides us the evidence of the disease propagation from the diseased neuronal population to the healthy neuronal population through the neuronal connection. High (600 nM) and low (60 nM) concentrations of OA were used to induce AD. From both situations, the hp-Tau was first accumulated in the axon part. Hp-Tau was then rapidly accumulated at the OA-exposed cell population. As disease propagated, the hp-Tau then became punctuated spots in the axon part and axonal degeneration happened. This observation is consisted with the assumption of Tau toxicity for AD disease from [68] indicating that the hp-Tau should first be accumulated in the axon and then spread into the cell soma. This is due to the main function of Tau protein is to stabilize the microtubules and regulate the motor-driven axonal transport [48]. During the disease propagation, the aggregated hp-Tau started to be dissipated into the medium. The neurons also started to have cytoskeletal damage and lost their structure in the end.

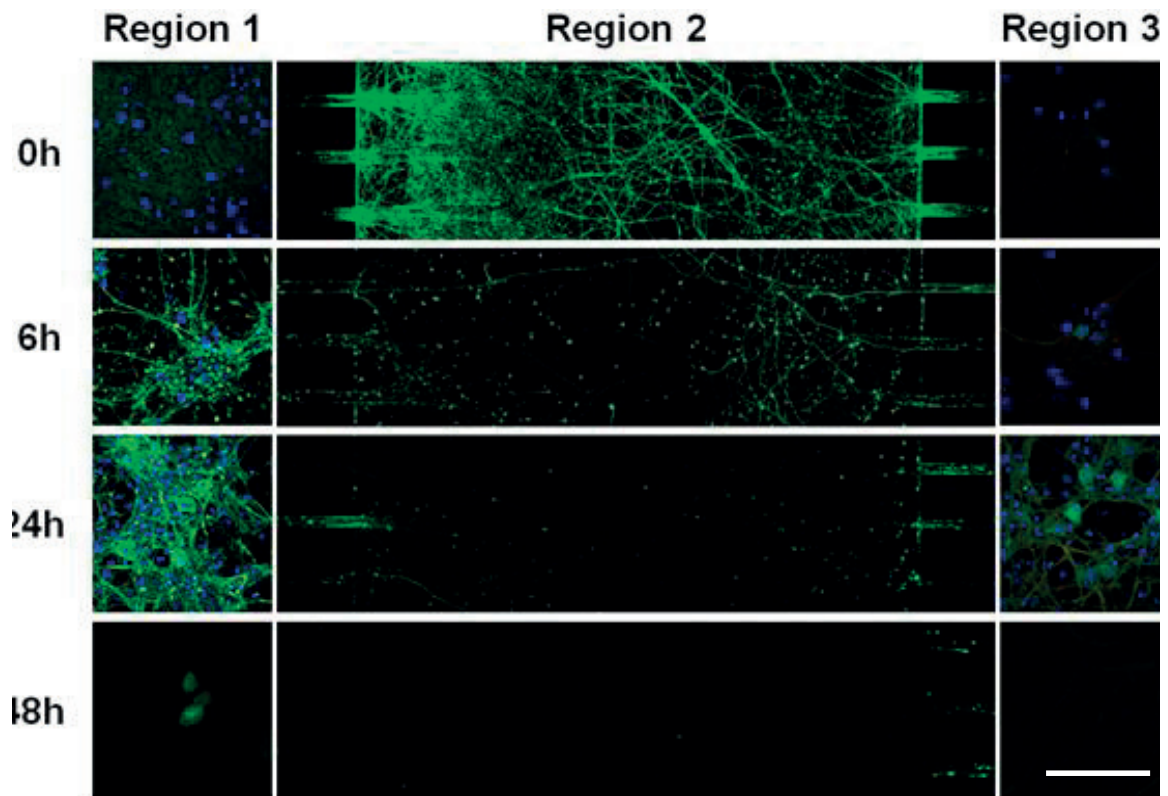


Figure 44: Disease propagation patterns during recovery period (0 h, 6 h, 24 h, 48 h) under high concentration of OA exposure (600 nM). Hp-Tau was visualized by pSer262 immunocytochemistry staining (green). Images from Region 1, 2 and 3 at each time point were captured from the same device. Scale in Region 1 and 3, 50 μm . Scale in Region 2, 100 μm

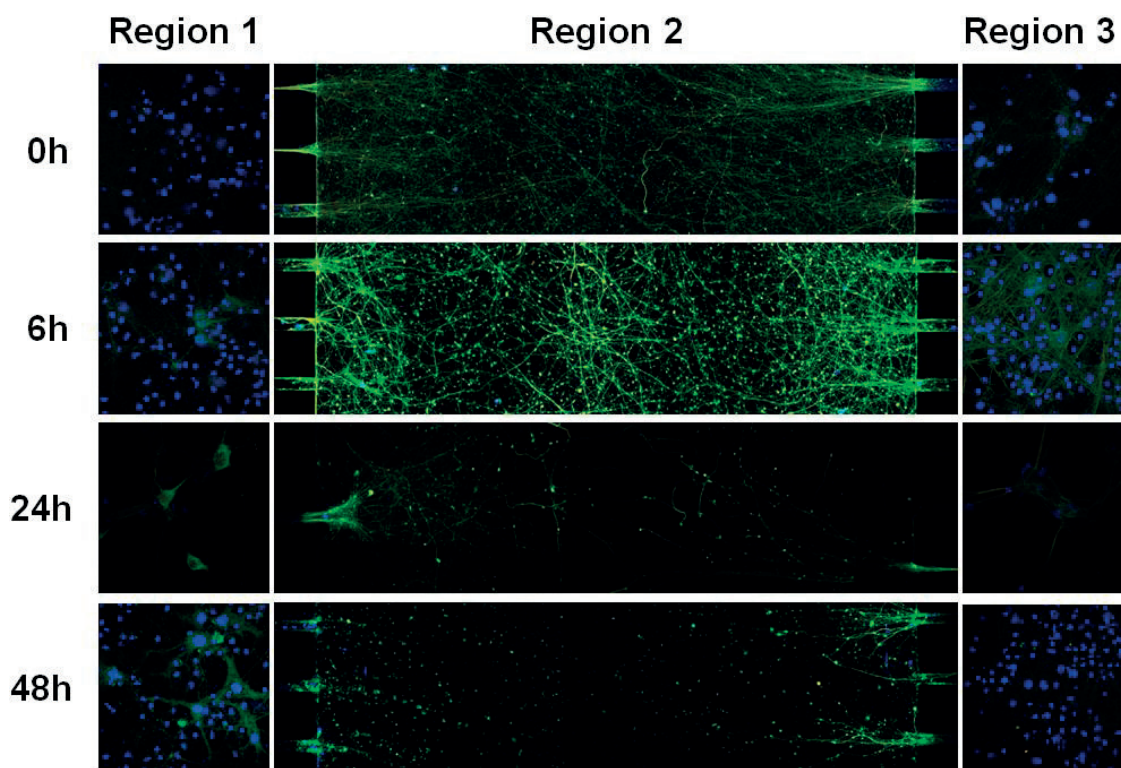


Figure 45: Disease propagation patterns during recovery period (0 h, 6 h, 24 h, 48 h) under low concentration of OA exposure (60 nM). Hp-Tau was visualized as green color by pSer262 immunocytochemistry staining. Images from Region 1, 2 and 3 were captured from the same device. Scales are as same as in Figure 44

Comparing this result of hp-Tau propagation in Figure 44 and Figure 45 with the cytoskeleton alteration in Figure 43, under high concentration of OA exposure, the cytoskeleton was gradually damaged on both the exposed cell populations while the hp-Tau was accumulated in the OA-exposed cell population. This had an effect on the OA-unexposed cell population as well on the level of hp-Tau and the cytoskeleton. Under low concentration of OA exposure, the OA-exposed population showed increasing intensity of hp-Tau and damage on the cytoskeleton, however, the OA-unexposed cell population did not show increasing accumulation of hp-Tau and severe damage on the cytoskeleton. This proves that different concentrations of drug exposure caused different effects on the unexposed cell population and presented different patterns of disease propagation.

3.4.2 Different functional patterns under different concentrations of OA exposure

The integration of compartmentalized microfluidic device and the MEA device provides additional electrophysiological characterization of the neuronal network compare to a normal MEA device without compartmentalized pattern. With this device, the recorded spontaneous

activity data was characterized by the spike rate (Figure 46) and burst rate (Figure 47). During the observation of disease propagation, two distinct electrophysiological patterns were observed: depression and temporary-excitement electrophysiological patterns. Depression pattern was only observed under the high concentration of OA exposure (600 nM), from the OA exposed neuronal population and the axonal network recording result. Significant decrease on the spike rate (Figure 46 A) was observed and the burst activity (Figure 47 A) immediately after the high concentration exposure and without obvious sign of excitement. Unlike the significant rapid decline of the neural activity under high concentration drug exposure, different patterns of temporary-excitement were observed under low concentration of OA exposure (60 nM). The OA exposed neuronal population had reduced around half spiking rate immediately at 0 h (Figure 46 B), with slight disturbance on the burst activity at the beginning (Figure 47 B). With time progressing, dramatically increasing of spike numbers was observed during the first 24 h recovery and then an obvious decrease happened at 48 h, it is named "temporary-excitement pattern" by us. Similar activity pattern was also observed on the OA-unexposed neuronal population in both concentration conditions, which is under the effect from the OA-exposed neuronal population through the axonal connection. This might be related to the functional adaption of neuronal network exposed from pathological challenge. Similar phenomenon was observed and published in the previous studies on the AD-related animal [28, 27, 128], where the neurons from cortical slices of transgenic mice (rTg4510) displayed more excitable behavior after surviving a Tau-induced degenerative disease. From the different patterns above, it was speculated that both the low concentration exposure and indirect drug exposure effect potentiated the synaptic transmission and caused the "temporary-excitement electrophysiological pattern" observed and named, whereas the direct high concentration exposure caused the synaptic depression that we called "depression electrophysiological pattern". These findings verify the previous similar studies focusing on the electrophysiological effect of A β with varied concentrations [131] or different types of A β species mixtures [86].

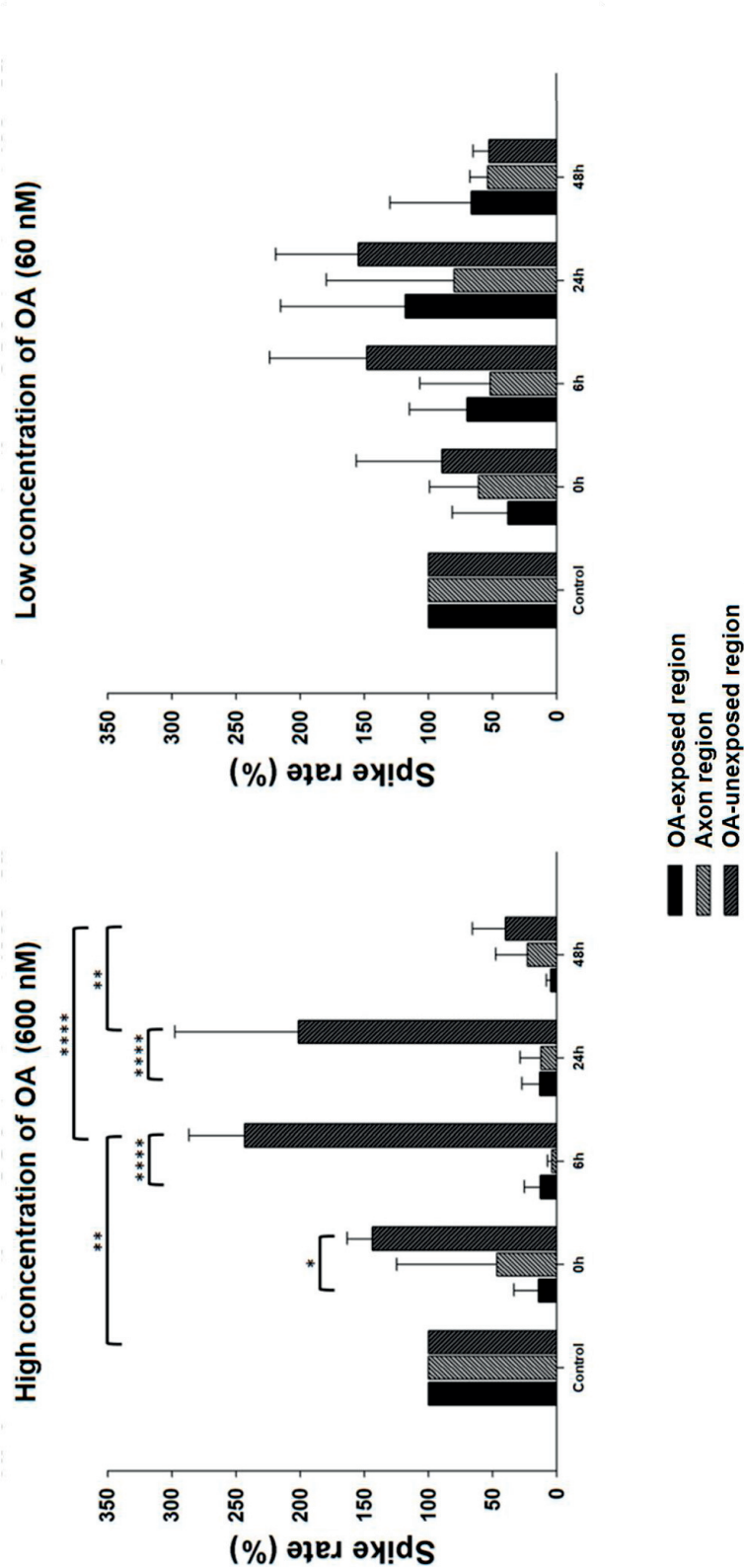


Figure 46: Spike rate acquired by extracellular recording under two concentration of OA treatment (600 nM, 60 nM) which represented the functional patterns during the disease propagation, (N = 5, * p < 0.05, ** p < 0.01, *** p < 0.005, **** p < 0.001)

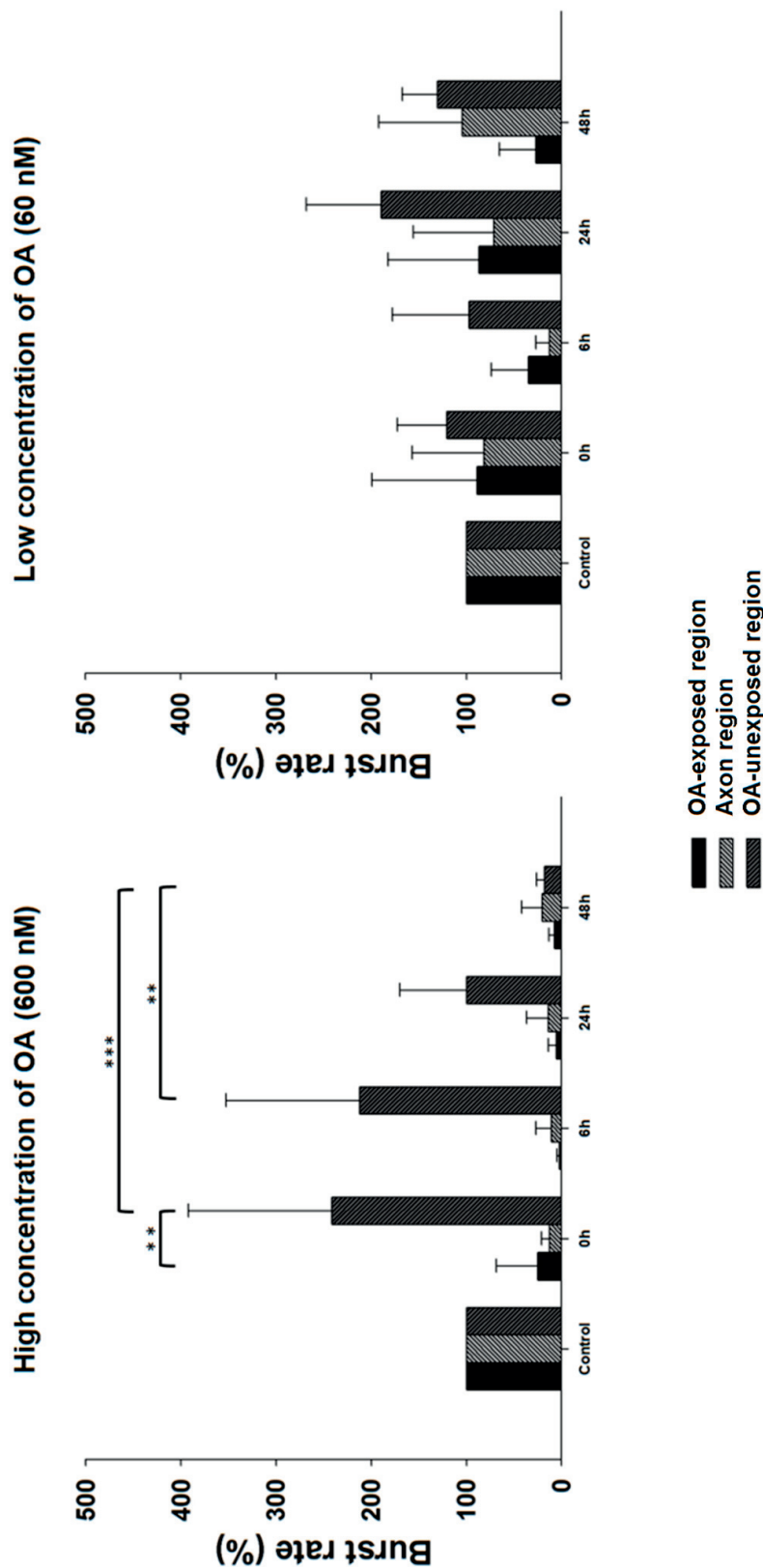


Figure 47: Burst rate acquired by extracellular recording during two concentration of OA treatment (600 nM, 60 nM) which represented the network synchronous pattern changed during disease propagation, (N = 5, * $p < 0.05$, ** $p < 0.01$, *** $p < 0.005$, **** $p < 0.001$). The burst rate was calculated as the value of each recovery period (0 h, 6 h, 24 h, 48 h) and expressed as a percentage of control (before 75 min. OA exposure)

3.4.3 Order of occurrence of structural and functional alterations during disease propagation

Both of our morphological and electrophysiological results confirmed that pathological event was happening during the disease propagation in the neuronal culture from the devices. However, as far as we know, the order in which the structural and functional alterations occur during AD propagation is still not clear. Benefit from microtechnology, we attempted to fill this gap with our microfluidic device for morphological studies and integrated microfluidic-MEA device for electrophysiological studies. Morphological and electrophysiological data are brought together for a more comprehensive analysis. About functional observation on the spike and burst rate, it was observed a 6 h delay of immediate decrease in the burst rate (Figure 47) compare to the spike rate (Figure 46 B) after the OA exposure at low concentration exposure, and both followed with the temporary-excitement pattern activity changes. After comparing the time points of morphological and electrophysiological changes with the OA-exposed neuronal population, the recorded functional changes (declined spike rate) happened much earlier before the observed structural changes (increased hp-Tau accumulation) under the effect from the OA-induced neurotoxicity. For instance, about the unexposed cell population under low concentration of exposure, there was no ph-Tau aggregation existed at 48 h and the cytoskeleton was only with slight damage. But from the neuronal activity data recorded from MEA device, the neurons were still already at an inhibited mode based on the decreasing on the spike rate and burst rate. All this results coincide with the previous studies about the functional electrophysiological changes occur prior to the substantial deposition of NFTs and neuron loss [27] and also the results from the brain imaging technique lately published [4] which indicates that the functional changes/cognitive declines in the AD patients' brains are altered prior to the structural changes/disconnection in AD as well. In this situation, applying biomarkers of neuronal function is able to detect AD even before the structural brain changes happened [39]. This will bring predictive value in early diagnosis for AD which is another issue so far.

3.5 Conclusions and future prospects

In this study, compartmentalized microfluidic device and an integrated microfluidic-MEA device were used to simulate the propagation of neurodegenerative disease with functional and structural observations synchronously. A co-pathological model was built by diseased and healthy neuronal populations co-culture, and the results showed that the Tau pathology seems to propagate along the two distinct neuronal populations through the axon region. From the structural aspect, specific propagation pattern appeared as following sequences: hp-Tau aggregation was appeared in the OA-exposed neuronal population and distributed along the axons. With time progressing, the OA-unexposed neuronal population began to accumulate hp-Tau inside the neuronal soma. Those results proved that the hp-Tau generated from diseased neurons could propagate through axon and cause pathological damage to the cytoskeleton of

healthy neuronal population. This is consisted with our hypotheses on the neuron-to-neuron transmission and proved the importance of axonal network during disease propagation. From the functional aspect, two different functional activity patterns were observed during the disease propagation under two different concentrations of OA exposure, depression and temporary-excitement electrophysiological patterns. The hyperactive property of neuronal network is probably related to the regulation of functional networks [28]. What is more, it was proved that the functional changes occur prior to the visible structural changes as well. This brings us more knowledge that can potentially helpful for AD early detection studies. Under different concentrations of OA, both of the morphological and electrophysiological alterations showed different propagation patterns during AD propagation and this is consisted with our hypothesis on the concentration-dependence on drug effect. This indicates that the different concentrations of drug used to induce disease cell model should be considered to cause different effects on morphology and electrophysiology when we build a diseased model *in vitro* for neurodegenerative disease studies. Above all, all these morphological and electrophysiological evidences obtained from the microfluidic device and microfluidic-MEA device prove that these devices are promising tools for neuroscientists to understand neurodegenerative diseases. The quantitative data obtained from the spontaneous spike activities provided us the status of the neurons. However, for the future study, it is consequential to penetrate deeper to explore how the different neuronal populations communicated. With this microfluidic-MEA device, the functional connectivity maps can be derived by cross-correlation analysis to understand the dynamic and spontaneous neuronal network at different stages of development during disease propagation. In addition, as there are two major hallmarks of AD including NFTs and A β plaques, for our future research on the pathological mechanisms for AD, Tau protein is not the only factor that we should consider. It is necessary to extend our focus on the link between A β and hp-Tau toxicity and this could play a fundamental role in developing potential targeted therapies.

3D beads-based neuronal culture in microfluidic device

4

**“Try not to become a man of success, but rather try to become a man of
value”**

by Albert Einstein

4.1 Introduction

Previous presented studies on AD in this thesis are all based on 2D neuronal culture. However, the neuron, as the most basic element in our nervous system, is very sensitive to the surrounding cultural environment [121]. 2D cell culture is limited to the low cell density and the integrated neural network comparing to the 3D cell culture. There is not only difference on morphological aspect, but also the electrophysiological recording *in vitro* showing different spike patterns between 2D and 3D environments [25, 162]. Many 3D neuron cell cultures have been established until now. The most commonly used method is by using hydrogel as a scaffold to make homogenous 3D cell culture [92]. In this chapter, two different types of beads are presented to build 3D neuronal culture, including silica beads and agarose-alginate beads. Beads are microspheres that can provide flexibility as carriers. For example, they were used as solid-phase carriers for chemical reactions within sealed micromachined device and to capture target analytes such as proteins and nucleic acids [149]. In this experiment, the beads are used as neuron carriers and they bring the neurons into the microfluidic device with layer pattern to create an artificial multi-layer 3D neural cell culture platform. This typical cortical cell layer-pattern model will assist us to study neuron-to-neuron interactions in 3D environment, and will potentially help to overcome the disadvantages of 2D culture for AD studies such as the A β plaques formation.

4.2 Methods

4.2.1 Design of layer pattern in microfluidic device

First, we first injected silica beads from different inlets trying to load the beads into the device. The preliminary test showed that it would help to put the device at a sufficiently large angle as an inclined device to let the beads flow through the channels by gravity and add slightly vibration to make the beads flow. We observed that firstly most of the beads were accumulated at the bottom of the injection reservoir (Figure 48 A). A pump system was added to create a slight flow in the channel. Furthermore, it was impossible to arrange the silica beads into well-organized layers by loading from different channels. All the silica beads ended up being mixed in a random order (Figure 48 B). This indicated that using one main channel is not enough to pattern the beads, it was also necessary to add physical barriers in the main channel to maintain the layer structure and a layer-pattern was designed for the microfluidic device. Three rows of pillars were added into the main channel to guide the beads to flow and be patterned in four layers (Figure 49). Some PDMS pillars were set at the end of the main channel to block the beads.

Different designs had been proposed based on bead size and the fabrication constraints. After some tests, we decided to add rows of pillars (diameter in 40 μm) into the main channel to separate the silica beads. The distance between the centres of two pillars is 70 μm , with the edge-to-edge distance being 30 μm . Therefore, the beads (diameter in 45 μm) will not be able to move to the other layers. The end of each channel is defined by thicker pillars (diameter in

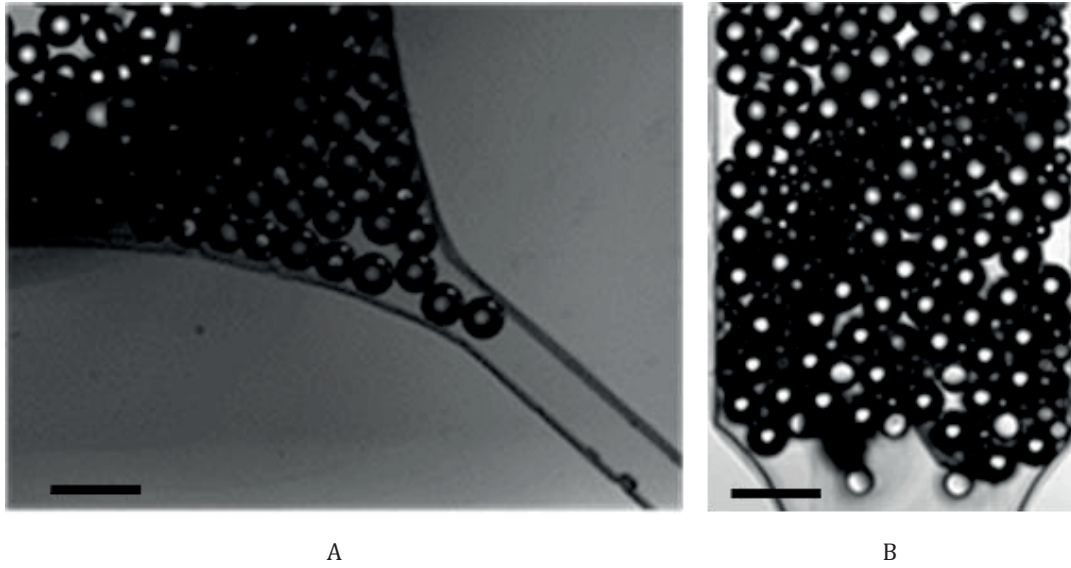


Figure 48: Preliminary results from loading beads into the microfluidic device without pillars pattern in the middle channels. (A) Micro-beads accumulated and blocked at the bottom of the injection reservoir. (B) Micro-beads randomly patterned in the PDMS chip. (Scale: 100 μm). Images were taken by wide field microscope

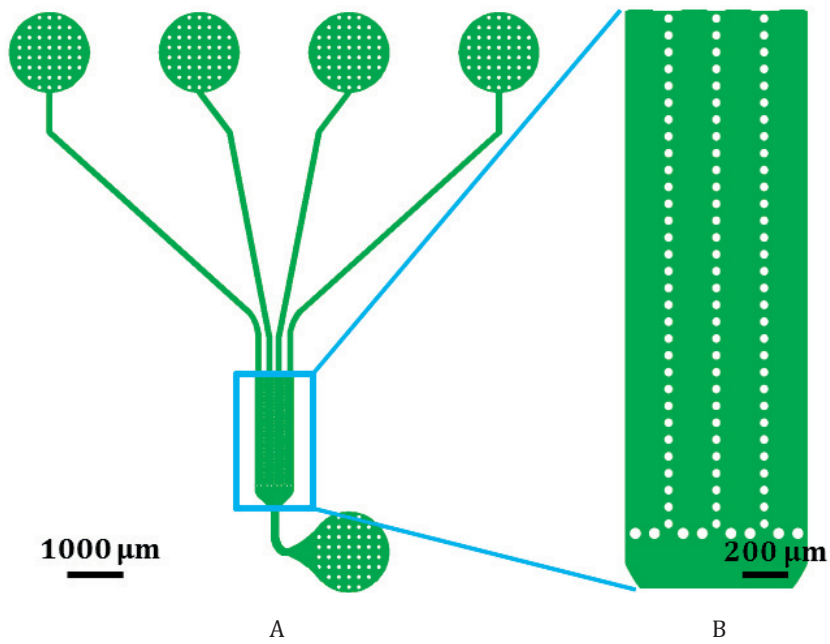


Figure 49: Four-layer pattern design of microfluidic device. (A) Mask design in Clewin for the microfluidic device. (B) Four layers pattern with three rows of pillars and the pillars at the bottom to block the beads and keep them in the channels

50 μm), which constrain the beads to stay within the channel (Figure 49 B). The fabrication of the microfluidic device was followed with the method illustrated in Section 2.2.1.

4.2.2 Experimental set-up

To load cells into the channels of the microfluidic device, sometimes micro-syringes and pumps can be used. Especially, for example, different contents can be brought into the microfluidic system from different channels and then generate a special layer-pattern through the laminar flow regime [83]. Controlling the flow rate during cell loading through micro-syringes and pumps allows us to automate this process. In this experiment, the beads loading setup is shown in Figure 50. This micro-syringe setup was used to load beads and perfuse cell culture medium to refresh the medium.

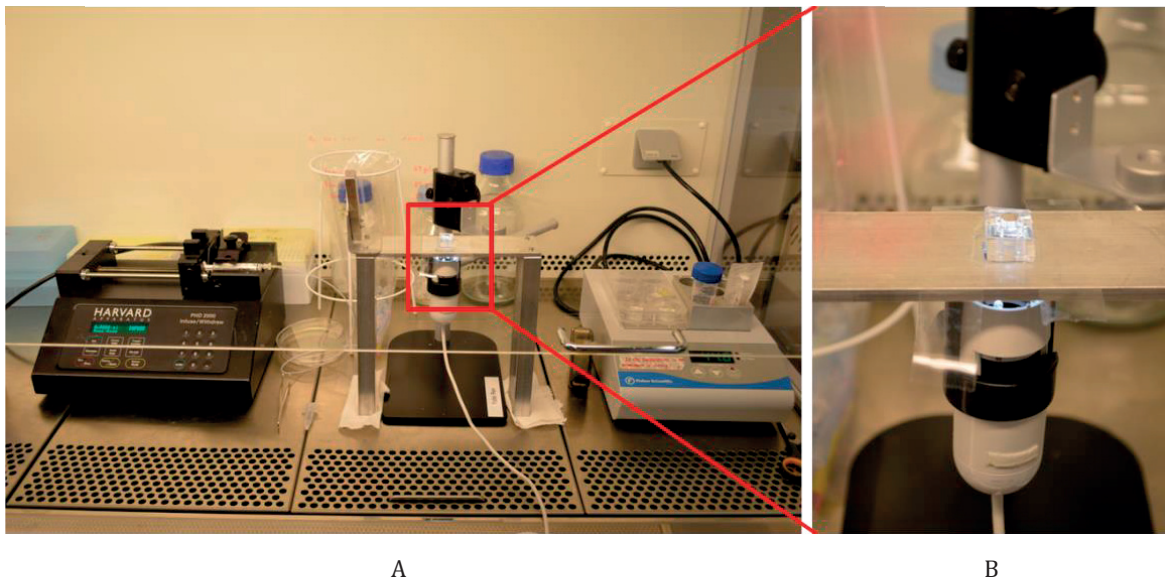


Figure 50: The cell seeding setups for cell culture in a microfluidic device in a sterile environment. The setup consisted of a flow controlling syringe pump, a digital microscope and a heating system. (A) A syringe was attached on the top of a syringe pump and should be connected to a reservoir from the PDMS device. PDMS device was fixed by scotch tape on a holder. A digital microscope, which was connected to a laptop, was placed under the device. Medium was always kept in the heater. (B) Detailed image showing the PDMS microfluidic device and the digital microscope

4.3 3D Silica beads culture in microfluidic device

4.3.1. SHSY-5Y cell line culture on silica beads

The 45 μm silica beads were chosen for our experiment, because the axons can bridge to neighbour beads quicker compare to bigger sizes beads. At the same time, there is no obvious difference on the rate of growth between different sizes of beads [125]. The silica beads were ordered from MO-SCI Specialty Products.

When the microfluidic devices were fabricated, the first question was the technique of culturing cells on the beads surface at a good cell density. The SHSY-5Y cell line was chosen to

run the test. First, the beads needed to be sterilized. 70 % ethanol was used to sterilize the beads overnight on the roller to have a better sterilization. On the second day, we dried the beads in centrifuge machine at 17000 g for 3 min and then incubate the beads in borate buffer solution for 1 h. Then we dried the beads again in centrifuge machine at 17000 g for 3 min. For the coating of the beads surface like surface coating in a normal cell culture dish, PLL coating solution was added into the eppendorf to coat the beads overnight on the roller to make sure all the beads were coated with PLL. In the end, the beads were washed with phosphate-buffered saline (PBS) buffer and dried again in centrifuge machine at 17000 g for 3 min for the experiment. For cell seeding, 200 μ l tip was dipped into the prepare beads sample twice to transfer the prepared beads into the 24 well plate. Then 450 μ l of cell culture medium was added into the 24 well plate. The culture medium for the SHSY-5Y cell line was 1 % penicillin/streptomycin (p/s), 10 % fetal bovine serum (FBS) in Dulbecco's Modified Eagle's medium (DMEM) /F-12 1:1 mixture with GlutaMAX supplement. The beads and the cell medium were shaken in the well plate by hand until the beads were uniform on the surface and a single layer of silica beads were formed under microscope. After that, the cells (8×10^4 cells per well) were injected into each well and air bubbles were avoided during the injection. The cell density was chosen at 8×10^4 cells per well, so that we can better mimic the cell density in the cortex from mouse at around 91,000 cells/mm³, while we can reach the density at approximately 75,000 cells/mm³ in our beads culture environment [1, 125]. After 4 h, the cells were attached on the beads surface under microscope. The DMEM/F-12 GlutaMAX and the p/s solutions were ordered from Invitrogen (Carlsbad, CA) and the PLL and FBS were ordered from Sigma-Aldrich.

As seen from Figure 51 A, the cells were growing on the silica beads by the top focus plane with the microscope, and also the beads surfaces were covered with cells relatively uniformly (Figure 51 B and C). This gave us the evidence that the cells can be cultured on the coated silica beads and protocol of manipulating cells on the coated beads can be applied for primary cortical culture.

4.3.2 Primary neural cell culture on silica beads and patterned in microfluidic device

For the primary neural cell culture, the dissection process was followed with the method present in Section 2.2.3. The protocol of culturing the primary cortical neurons onto the silica beads culture was as same as for the SHSY-5Y cell line present in Section 4.3.1. Under the microscope, we see the cells were on the surface between the beads and move the well plate into incubator. After 4 hours, we see the cells have already started to grow on the beads surface and keep the well plate in the incubator until the next day to transfer the beads into microfluidic device

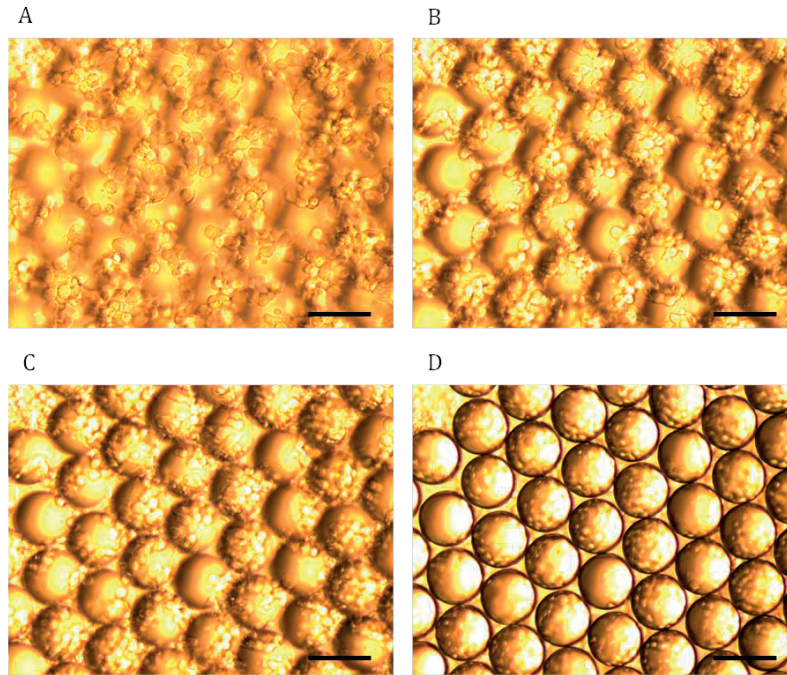


Figure 51: Images of the silica beads with neural culture on the surface, from the top surface focus plane towards the bottom direction. Images were taken by phase contrast microscope. Scale: 50 μm

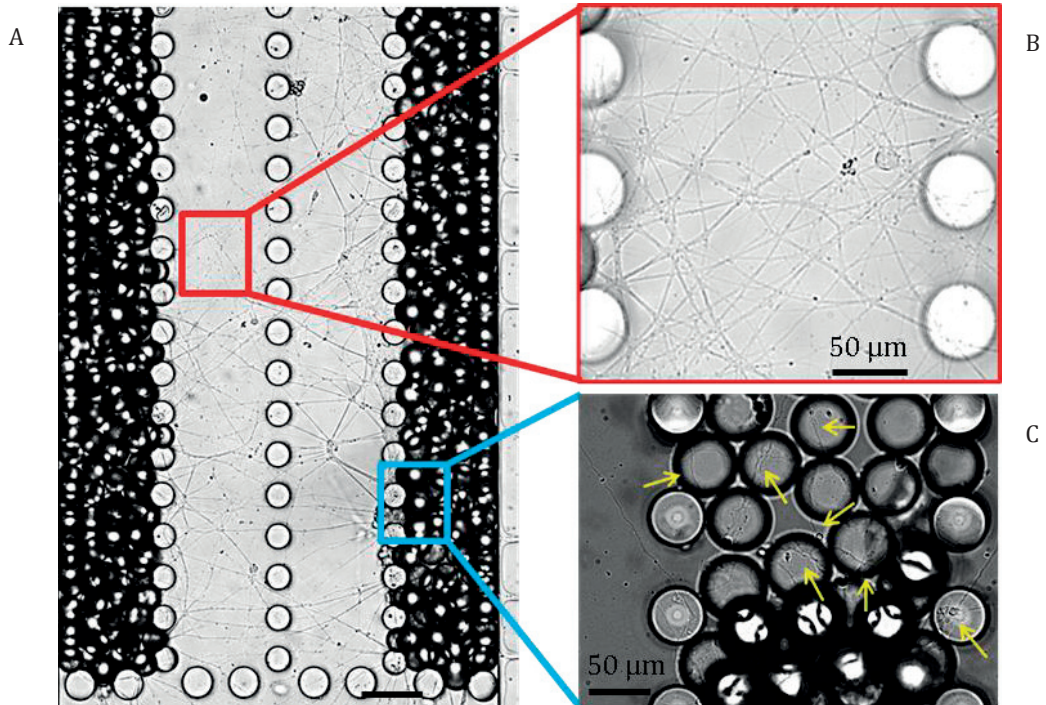


Figure 52: Neurons growing on the surface of silica beads inside the layer-pattern microfluidic device. (B) Neurites are growing in the channel without silica beads. (C) Neurons growing on the silica beads are indicated by yellow arrows. Scale in Fig. A is 100 μm . Images were taken by phase contrast microscope

First, we tried to inject the beads with cells into the two lateral channels while the two middle channels were empty, so that the neurite from the cells could grow through the middle channels and we were able to observe the neural network under the microscope without staining the cells. Neurites were observed in the middle channels without beads. These neurites were from the neurons growing on the two lateral layers of beads (Figure 52). The neurites were growing relatively equally distributed and the neurons were observed on the silica beads. This result proves that the primary cortical neurons were successfully cultured on the PLL-coated silica beads and the neurites were able to grow through the neighbored bead and grow longer and longer. In this way, one cell population could extend to other area in the channels and communicate with other neuronal population.

After the trial of observing the neural growth in a 4-layer pattern microfluidic device while leaving two middle channels empty, we injected beads with cells into all the 4 layers in the microfluidic device. The neural network was built after 21 DIV (Figure 53) and was stained with MAP2 to show the neurites growing between the beads layers. An image of a culture on DIV 6 was taken to analyze the cell distribution and cell density. The distribution of the neurons growing inside the beads in the microfluidic device was analyzed based the 3D image we obtained from confocal microscope. The beads were loaded into a single layer inside the microfluidic device. It is observed that the neurons were uniformly distributed in the layer-pattern microfluidic device (Figure 53 A). The position of the cells in vertical direction was analyzed as well to evaluate the cell sedimentation by gravity in the channel, which could be a problem for 3D gel culture because of the slow gel solidification. As we observed from Figure 54, the neurons were equally distributed in the vertical direction within the imaged specimen. In the end, the cell density for this beads culture was calculated based on the 3D image. There are around 4.6 cells per bead on average which is consist with the previous study [125], and the cell density in this cell culture was around 55 million cells/ml. This result proved that this method of culturing neural cells on silica beads to build a 3D neural network was feasible and the next step was to use the beads with different coating for different guidance and observe the cell-cell interactions between different cell populations.

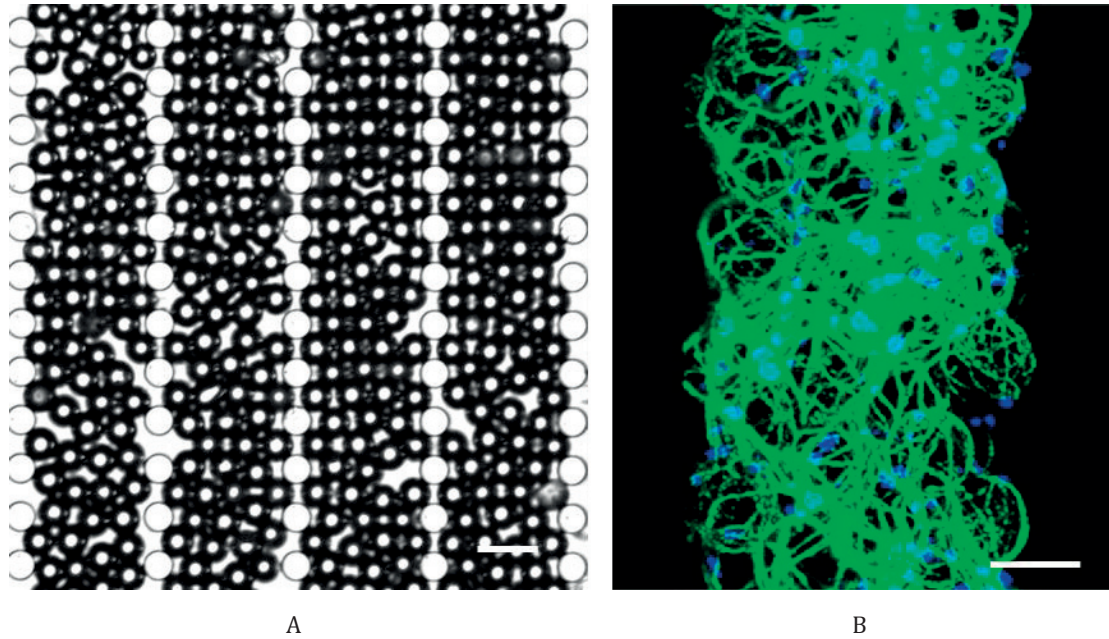


Figure 53: A microfluidic device with 4 layers pattern and fully filled with silica beads (Fig. A) and a 3D neural cell culture on silica beads captured from a 3D imaging result of one channel (Staining: MAP2, neurite) (Fig. B). Scales are 100 μm and 50 μm in Fig. 5-6 A and B respectively. . Images A was taken by phase contrast microscope and image B was taken by confocal microscope

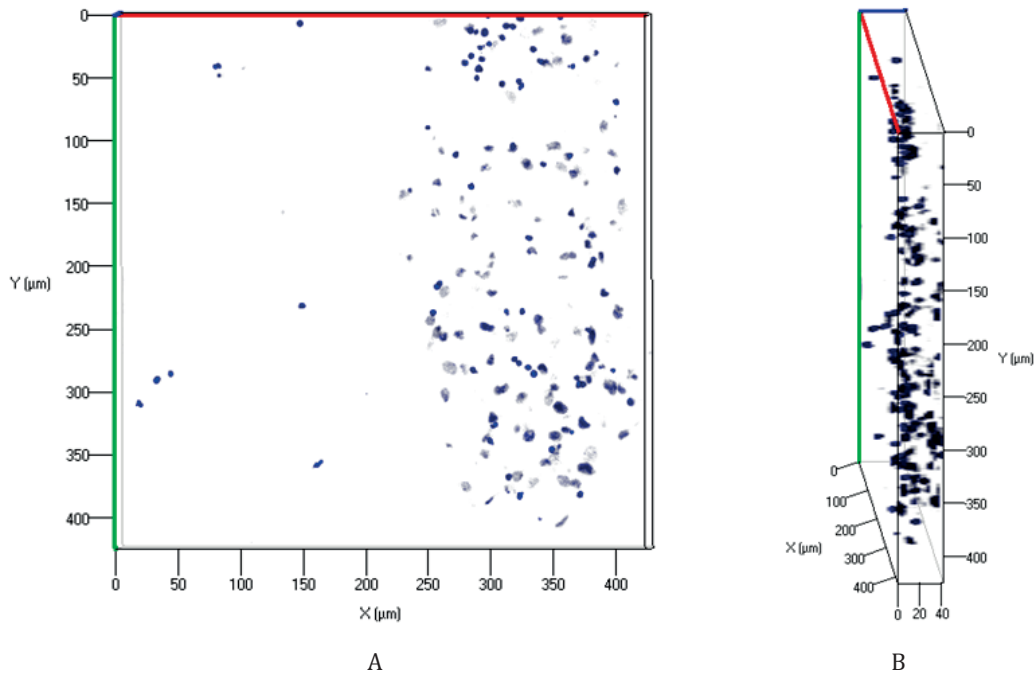


Figure 54: Cell density analysis and cell position in gel analysis based on a 3D image of the beads with cells in a microfluidic device (DIV 6) (one layer of beads). Cell density analysis and cell position in gel analysis based on a 3D image of the beads with cells in a microfluidic device (DIV 12). (A) Analysis for the cell density. (B) Analysis for cell settlement

4.3.3 cAMP and cGMP guidance experiment using 3D silica beads culture

4.3.3.1 Experiment design

Benefiting from the assembly properties of the silica beads with neurons, we pattern the beads carrying neurons in different layers in microfluidic device. By patterning beads with cells on the surface and the coated the beads with chemical attractant as guiding cues for the neurons, we try to build selectively interacted neuronal network that can be useful to answer specific questions from neuroscience. More specifically in our experiment, the design of the 4 layer-patterned arrangement of the beads layers is show in Figure 55. There were 4 layers of beads, A, B, C and D. The 45 μm silica beads were either with PLL coating for cell adhesion or PLL coating and also the guidance coating solution like cGMP and cAMP). The lentivirus transfected neurons are loaded into layer A (tdTomato expression in red) and D (GFP expression in green). The environmental cues for the guidance of the neurons are in layer B (cGMP coated beads to attract dendrites) and C (cAMP coated beads to attract axon). Based on this cell culture model, we intend to observe the structure of the layer-pattern neural network and also investigate the effects on the cell populations under different environmental guidance cues and the interactions between different cell populations. Furthermore, as a fundamental property in neurons, neural activity is also studied by applying fluorescent calcium indicator imaging.

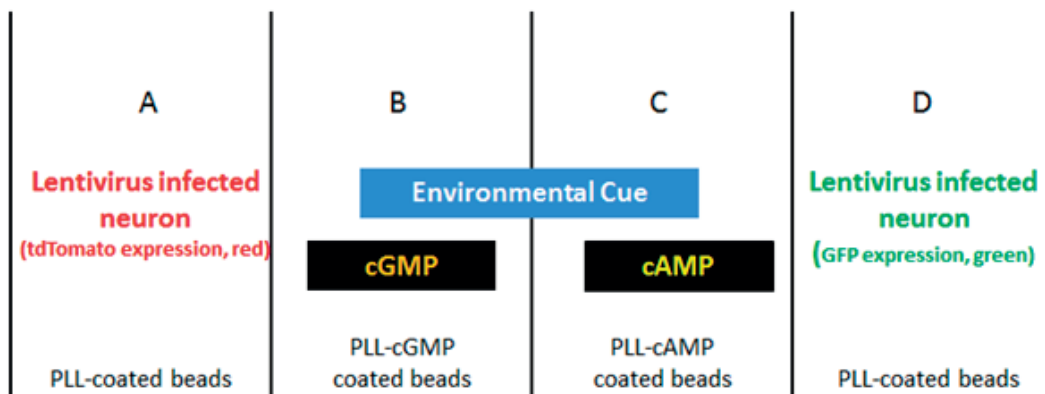


Figure 55: The experiment design of the arrangement of the beads layers

4.3.3.2 Beads coating and neuronal culture maintenance

The beads sterilization protocol and PLL coating protocol for the neuronal culture were as same as presented in Section 4.3.1. For the guidance beads coatings for cAMP and cGMP guidance, 20 mM of cAMP and cGMP were used for the beads coating, and the washing steps for the coating were as same as presented in Section 4.3.1. The lentivirus infections for the GFP and tdTomato neurons were from Dr. Sophie Pautot's lab in Dresden.

4.3.3.3 Beads loading manipulation in microfluidic device

For our beads loading, we first took the 24 well plate out of the incubator and kept in at 45° to let the beads to deposit and accumulated to one corner. Then we used a 200 μ l gel loading tip which has an extremely long thin tip at the end to suck the beads out from the well-plate and injected them slowly into the microfluidic device.

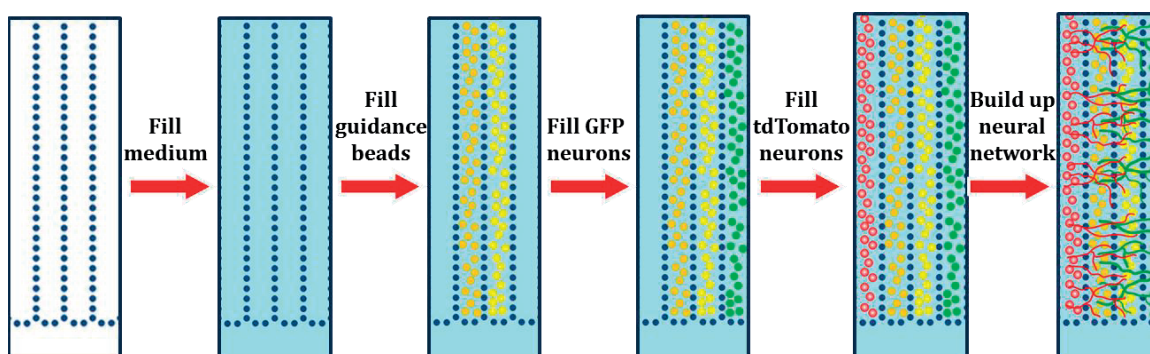


Figure 56: Systematic diagram of loading different layers of beads into microfluidic device

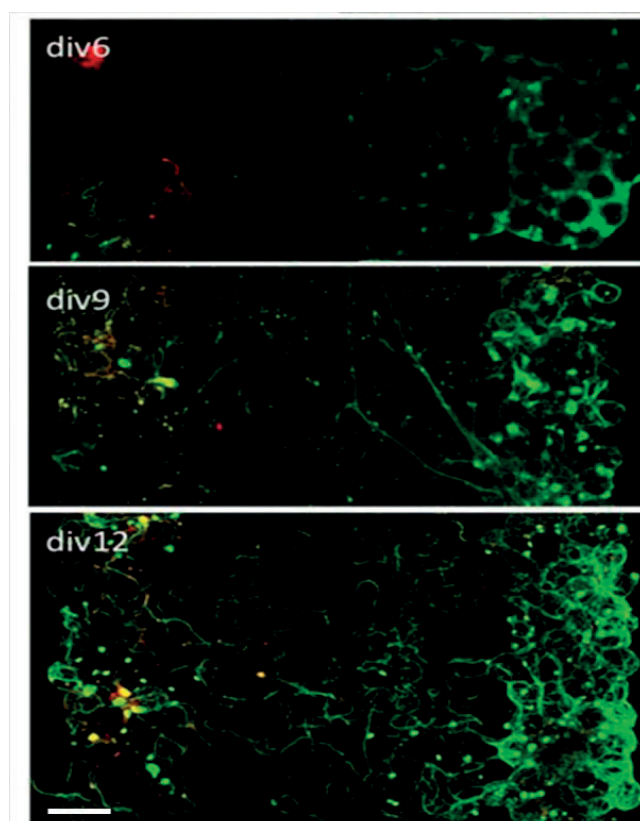


Figure 57: Cell culture on silica beads in microfluidic device on day 6, 9 and 12. Staining: GFP neuron, green; tdTomato neuron: red. Images were taken by confocal microscope. Scale: 100 μ m

The sequence of loading beads into different layers is very strongly linked to the cell culture quality since the vibration inside the device will potentially damage the cells. The procedure we used for beads loading is shown in Figure 56. First, the device was filled with medium to avoid air bubbles for further beads loading. Then the guidance layers B and C were loaded with beads without cells but with different guidance coatings. In the end, the layer D and layer A were loaded with beads with virus transfected neurons. This neural culture was kept in incubator for 12 days and the neural network development was presented in Figure 57. Compared to the GFP neurons, the tdTomato neurons were relatively weak and this was probably due to the infection step.

4.3.3.4 cAMP and cGMP guidance effect

From the guidance result we obtained in Figure 58 A, the cell bodies stayed at their original beads layer, and only a few cells either migrated to other beads layers or transported by the shaking during the beads loading. The neurite included the dendrite and axon were stained with Tuj-1 in green (Figure 58 C), and the axon was stained with SMI312 (Figure 58 D). From the merged image (Figure 58 E), we observed most of the neurite in the guiding layer is axon because of the lack of green color observed in the merged image and mostly dendrite was located at the cell culture layer. The guidance effects from the cAMP and cGMP coated beads were not well observed probably due to the short function period of the coated beads (the first 2 days have the best selection function [125]). Unfortunately, the left lateral cell layer with lentivirus infected neurons with tdTomato expression (red color) was not clearly observed from Figure 58. No result was obtained from the tdTomato neuronal population for the guidance experiment.

In this first part of this chapter, we focused on 3D neural cell culture on silica beads and we transferred the silica beads with neurons into a microfluidic device with layer pattern. The neurons were successfully cultured on the silica beads, and they built layer pattern neural network on the silica beads. These results proved the possibility of culturing neurons on silica beads and using silica bead as a carrier for the neurons in order to build layer pattern to mimic the neuron-to-neuron interaction model for neuroscience studies. This method is more convenient than in the normal microfluidic chips that build the different layers by running laminar flow. It does not require temperature control as well which could be a problem for the manipulation with 3D gel scaffold. This 3D silica beads culture technology is promising for neural cell culture patterning in a 3D environment.

4.4 3D agarose-alginate beads culture in microfluidic device

4.4.1 Agarose-alginate beads

Recent studies highlight the shortcomings of commercial glass particles and stress the benefit of using soft microgel particles (MGPs) instead [127]. We started to investigate on the Inspired from the 3D silica beads neuronal culture concept for patterning neuronal network

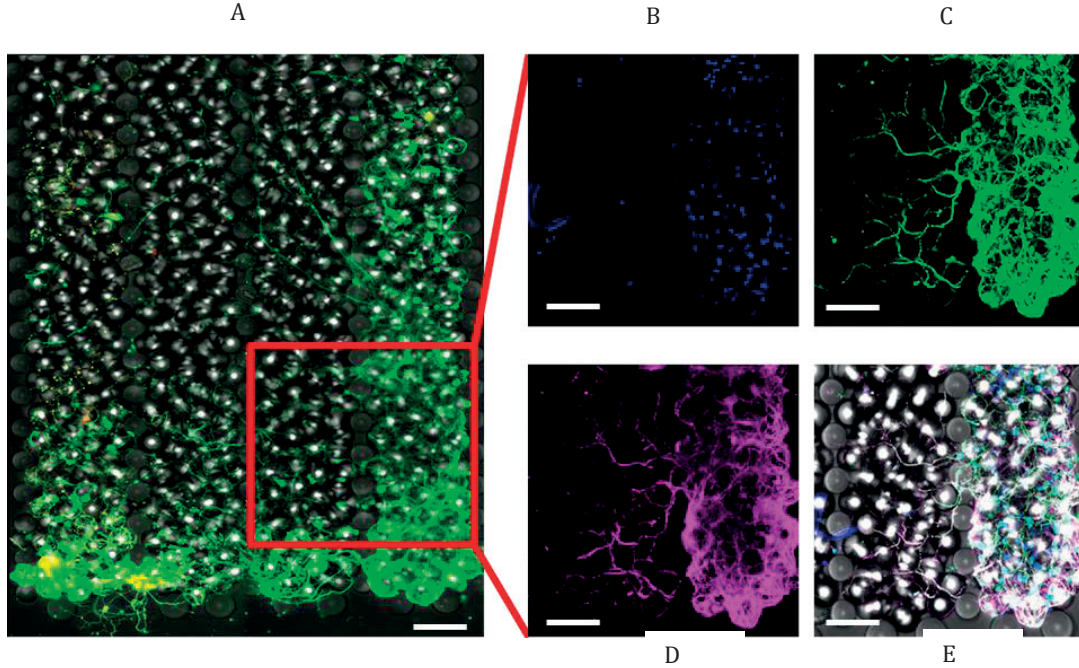


Figure 58: Layer pattern 3D silica beads culture I microfluidic device on 12 DIV. (B) Nucleus, DAPI, blue. (C) Neurite, Tuj-1, green. (D) Axon, SMI312, pink. (E) Merged by staining of Fig. B, C and D. Scale in Fig. A is 100 μm , Scales in Fig. B, C, D and E are 50 μm . Images were taken by confocal microscope

illustrated above and the Hanging Drop Array technique described in Section 1.4.3, agarose-alginate gel was chosen to build a 3D gel based neuronal culture in microfluidic device with layer pattern. Agarose is a widely used naturally derived hydrogel with neutral polymer chains. It has good mechanical properties, large pore size for diffusion and growth, and specific thermosetting behaviour and hysteresis. Agarose is chosen as the scaffold backbone is because it lacks of cell surface receptor binding domains and the established procedures for the controlled coupling of bioactive ligands [29] which are essential properties to open new perspectives for neural tissue engineering applications which may lead to drug development. The concentration of the agarose for fabricating 3D beads was at 0.5 % (w/v) which has the stiffness between 2 kPa and 5 kPa. Alginate, one of the most used hydrogels for cell encapsulation today, was used as free alginate chains at the concentration of 0.3 % (w/v) to improve the neural attachment and survival rate. B27 was added as well to reach a final concentration at 2 % to improve the cell culture growth.

4.4.2 Agarose-alginate beads fabrication

For the fabrication of agarose-alginate gel beads, we applied a gel vortexing method to use the shear force from vortex to separate the gel into small sizes beads [14]. For more precisely control for the fabrication of beads, droplets microfluidic device can be used as well. In this experiment, the size of the beads is not critical, that is the reason that vortex approach is achieved instead of applying droplets microfluidic device. Agarose type VII at 1 % w/v (e.g.,

0.05 g in 5 ml PBS) and alginate at 0.6 % w/v (e.g., 0.03 g in 5 ml) were the main components for the scaffold. The powder of agarose and alginate were weighed and transferred into a 50 ml falcon tube under the cell culture hood. Then the 0.05 g agarose and 0.03 g alginate were mixed with 5 ml deionized (DI) water, heated up in the microwave to dissolve the mixture. When the gel cooled down, 620 μ l of gel mixture was mixed with 580 μ l of cell culture medium, 30 μ l of pluronic acid and 13 μ l of B27, and then mixed by vortex machine for approximately 1 min. Pluronic F-68 helps to protect fragile cell membranes from disruption during agitation of suspension cultures. In the end, the agarose-alginate mixture reached at the final concentration at 0.5 % w/v agarose, 0.3 % w/v alginate and 1 % B27, and mixed with 10^7 cells in neurobasal medium. For the beads fabrication, we injected the gel and cell mixture drop by drop and slowly into 15 ml silicon oil (Dimethylpolysiloxane, viscosity at 50 centistokes) carried by 50 ml falcon tube, under continuously mixing by vortex machine. During the vortexing, the gel was separated into much smaller spherical shape beads and became froze when the falcon tube was transferred on the crushed ice container for 10 min. Then the mixture of silicon oil with frozen beads was centrifuged at 2000 rpm for 5 min. After the centrifugation, an interface appeared between the oil and water phases. Then the silicon oil was carefully removed and the water phase solution with frozen beads inside was transferred into another 15 ml falcon tube. To further wash away the silicon oil, we added 10 ml of PBS into the 15 ml falcon tube with frozen beads and centrifuge the mixture at 2000 rpm for 5 min. The remaining oil was carefully pipetted out after the centrifuge. In the end, we passed the gel beads in the cell culture medium through the filters of 40 μ m and 70 μ m and collected the beads between 40 μ m and 70 μ m (Figure 59). The beads were kept cell culture medium and maintained in the incubator waiting for the loading process to transfer beads into the microfluidic device.

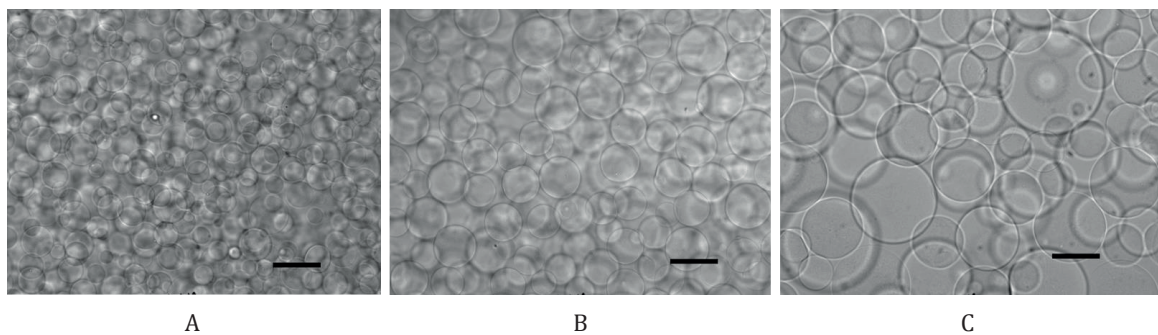


Figure 59: Collected gel-beads without cells inside. (A) Beads under 40 μ m in diameter. (B) Beads between 40 μ m to 70 μ m in diameter. (C) Beads bigger than 70 μ m in diameter. Scale: 50 μ m

4.4.3 3D agarose-alginate beads culture in layered-pattern in microfluidic device

The agarose-alginate beads with neurons inside were loaded into the layer-pattern microfluidic device. It was observed that the primary neurons were growing inside the beads and some of their neurites were growing out of beads and trying to bridge to another beads (Figure 60). The distribution of the neurons growing inside the beads in the microfluidic device was analyzed based on the 3D image we obtained from confocal microscope. The beads were loaded into a single layer inside the microfluidic device. It is observed that the neurons were relatively uniformly distributed in the layer pattern microfluidic device (Figure 61 A). The position of the cells in vertical direction was analyzed as well to evaluate the distribution of the cells in the device horizontally and vertically because the cell sedimentation caused by gravity in the gel could be a problem for 3D gel culture because of the slow gel solidification. As we observed from Figure 61 B, the neurons were equally distributed in the vertical direction within the imaged specimen. In the end, the cell density for this beads culture was calculated based on the 3D image. There were around 4.19 cells per bead on average, and the cell density in this cell culture was around 50 million cells/ml, which is a high density as a 3D cell culture and it is 50 times more than a standard 2D cell culture [83].

Compared to the silica beads, the biggest advantage of agarose-alginate beads is the neurons grow inside the agarose-alginate beads, while for silica beads neurons grow on the surface. This is an important factor for loading beads into the microfluidic device because the collision between the beads during the flowing procedure may damage the neurons on the surface. For the agarose-alginate beads, they behave like cushioning for the neurons that can maximum protect the neurons. That is another reason that the agarose-alginate beads with cells should be loaded into the microfluidic device immediately after the fabrication of the beads, before the development of the neurons start. However, for the silica beads, we have to wait for the neurons to attach well on the silica surface to avoid neurons fall from the carrying beads during the loading, but the developing neurons can have severe damage during the beads loading. Another advantage of the agarose-alginate beads is they have soft tissue which more closer to the tissue from native brain. They have high elasticity, which means higher deformability, and this allows the gel scaffold to easily adapt to the neurons deformation during neural development. From the quantity result, as a cell carrier, the silica beads and the agarose-alginate beads reached similar amount of cells per bead and similar density for cell culture. Further investigation is necessary to perform in the future, e.g., the cell viability assays, increase the density of cells in the gel and try long duration agarose-alginate neuronal culture, in order to move forward on applying this method for neuroscience research.

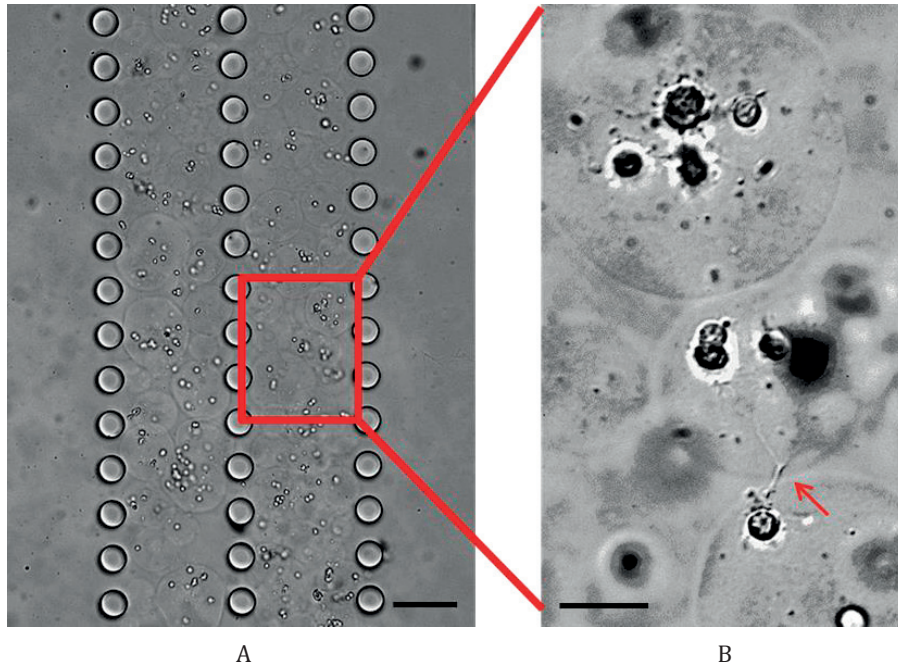


Figure 60: Agarose-alginate beads with cells inside were patterned into two layers inside a microfluidic device that has pillars for layer pattern (DIV 12). (B) Detail of neuron cells growing inside the beads. The red arrow indicated that a neuron was trying to bridge between two beads by its neurites. Scale in Fig. A: 100 μm . Scale in Fig. B: 50 μm

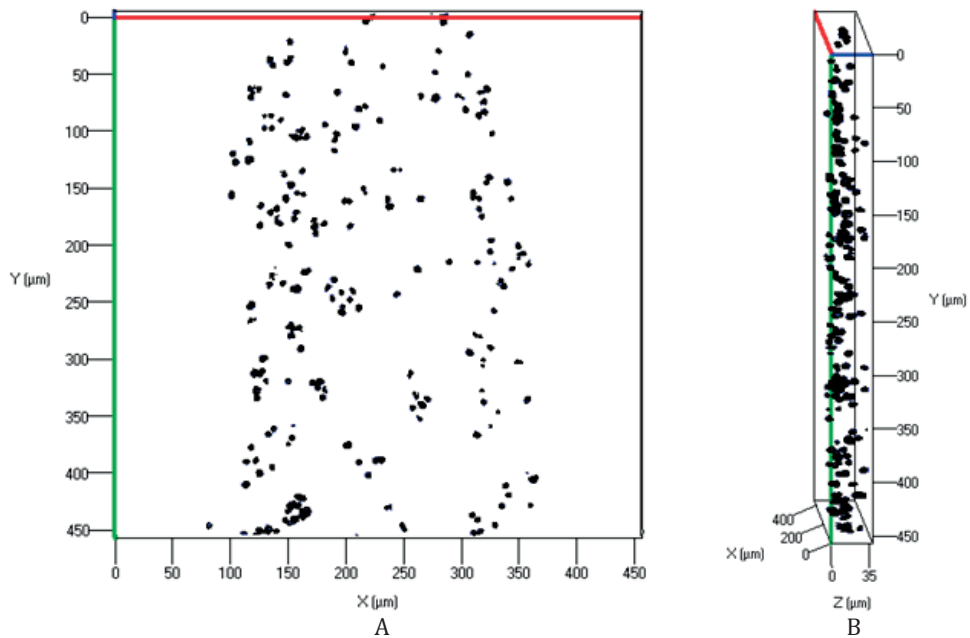


Figure 61: Cell density analysis and cell position in gel analysis based on a 3D image of the beads with cells in a microfluidic device (DIV 12) (one layer of beads). (A) Analysis for the cell density. (B) Analysis for cell settlement

4.5 Conclusion

In this chapter, we explore the 3D neuronal culture on two different types of beads, silica beads and agarose-alginate beads, and the neurons were successfully cultured on both beads environments. Benefitting from the microfluidic device with layer pattern, we transferred the two types of beads with neurons into the microfluidic device. Neural network was built between different layers of silica beads. It proved the possibility of culturing neurons on silica beads and using silica bead as a carrier for the neurons in order to build layer pattern models for brain studies. The agarose-alginate beads have more advantages concerning the properties of the material itself. It reached similar cell density of 3D neuronal culture as the silica beads. Both two methods for culturing neurons in/on beads are adaptable for microfluidic device with layer pattern. They are promising techniques for neural cell culture patterning in a 3D environment to mimic the neuron-to-neuron interaction model in microfluidic device and study AD in a 3D environment. These patternable beads-based methods fit with the MEA device as well to build up 3D cell culture for recording. However, the challenge is to obtain high quality signal from the MEA recording device as the distance between neurons and electrodes are increased in 3D cell culture comparing to 2D cell culture.

Conclusions and perspectives

5

**“I have discovered the secret that after climbing a great hill, one only finds
that there are many more hills to climb.”**

by Nelson Mandela

5.1 Conclusions

5.1.1 PDMS and SU-8 bonding method for microfluidic-MEA device integration

The compartmentalized microfluidic device and the MEA device with 60 recording electrodes are fabricated in this thesis. These two devices are also integrated to build a microfluidic-MEA device. However, a bonding method was required to bond the microfluidic device made of PDMS and the MEA device with a SU-8 insulation layer on its top. It was an issue to bond the PDMS and SU-8 materials because of the chemical bonds on each surface. After theory studies, a surface silanization method using APTES molecule was found and a series of tests had been undertaken to investigate different bonding methods, including the XPS surface analysis and tensile strength tests. In the end, we found that there was strong evidence coming from the XPS analysis of APTES molecule presence on the PDMS surface after the liquid-phase silanization method instead of the vapor-phase silanization methods. Meanwhile, the SU-8 material without hard bake step during fabrication provided better performance on the bonding quality during the tensile strength tests. Based on this APTES silanization method, we were able to perform the integration and therefore build our microfluidic-MEA device.

5.1.2 Applications of using microfluidic and microfluidic-MEA devices for AD propagation studies

These neuronal morphological results from the compartmentalized microfluidic device confirmed the feasibility of using microfluidic devices in neural cell culture for morphological studies. The axonal network isolation design proved its advantages for neurodegenerative disease research. Furthermore, the integrated microfluidic-MEA device that has a co-pathological neuronal culture model was built to mimic the AD spreading model by neuron-to-neuron connections and to investigate the electrophysiological alternations during disease propagation. The morphological result from the microfluidic device proves our hypotheses on the neuron-to-neuron transmission. Tau pathology propagated between the two distinct neuronal populations through the isolated axonal connections and this confirmed our hypothesis about the axonal transportation plays an important role during disease progression. The pattern of hp-Tau's first appearance in the axonal network confirmed the hypothesis proposed in previous publications.

Based on the result from the MEA device recording, the electrophysiological alteration was observed. Depends on the results from the low and high concentrations of drug exposure, the two neural activity patterns were observed: depression and temporary-revive electrophysiological patterns during AD propagation. This confirmed our hypothesis on the concentration-dependent effect of drug during AD propagation. After the comparison with the morphological and electrophysiological result, an innovative result was found that the functional changes occur prior to the structural changes as well. This microfluidic-MEA device is able to give us more knowledge about AD propagation *in vitro*, which indicates that this device will have a promising future in neurodegenerative disease studies and pharmaceutical studies for

drug effect tests, while potentially helping to diagnose AD early. The drug effects on the activity of the neuronal network and the sequential occurrence between the morphological and electrophysiological alterations both demonstrate that this microfluidic-MEA device fulfilled the functions that we originally wanted and required to obtain from this device.

5.1.3 Building a layer-pattern neuronal culture model in a microfluidic device

In this thesis, two microfluidic devices with different designs were fabricated, including a 3-compartment device and a layer-pattern device. The 3-compartment microfluidic device, which provides compartmentalized neuronal culture, is used for morphological observation and integrated with the MEA recording device to build microfluidic-MEA device. With the layer-pattern microfluidic device, we explored 3D neuronal culture on silica and agarose-alginate gel beads cultures in a layer-pattern microfluidic device, in order to mimic the cortex structure, which contains layers of cells in native brain tissues. Inspired from Sophie Pautot's previous work [125] on culturing neurons on silica beads and building a 3D neuronal culture network in the vertical direction, we intended to bring silica beads with neuronal culture on their surfaces into a microfluidic device with layer-pattern. The neural cell culture was successfully brought onto the silica beads and neurites were observed around the silica beads' surfaces. By leaving the middle layers empty, the neurites grew out from the silica beads and extended into the empty layers. This preliminary result proves the success of culturing neurons on silica beads and this beads-based culture technique and further experiments were done on building a neuronal network with guidance. With cGMP and cAMP coating on the silica beads, we expected to observe a selective guidance pattern from the layer-pattern silica beads culture. Unfortunately, the guiding function was not clearly observed in the neuronal network based on the observation with confocal imaging. This is probably due to the short functional period of the molecule coating.

Besides the silica beads, we explored the culture of the neurons in agarose-alginate beads. The beads were fabricated without using microfabrication technologies. Through a strong but enough vortex process, the gel was separated into spheroids and could be distinguished and extracted from the oil environment for collection. The neurons were encapsulated into the agarose and agarose gel mixture, while being distributed uniformly inside the beads when the gel was vortexed. Compared to the laminar flow of gel to build layer pattern in a microfluidic device, this method gives us the convenience of patterning different types of cells into layers without gel mixing and avoiding diffusion during transportation and it can further prevent the settlement of cells by gravity during the long gel freezing period.

Some preliminary results about 3D neuronal culture models with the silica and agarose-alginate beads were obtained in our layer pattern microfluidic device. Based on all these structural characteristics, we think our microfluidic device with layer-pattern has its strengths in building an artificial neural cell layer mimicking typical cortical cell layers patterns and for neuron-to-neuron studies in 3D neuronal culture as well. Further experiments can be undertaken to increase cell survival in the gel culture as well as to find better solution

to flow the beads into the patterned channel inside the microfluidic devices. Because of the large dimensions of the culture niche and the gel mixture, good staining quality and imaging methods are required in the future for obtaining better observations on the neuronal culture network.

5.2 Perspectives

5.2.1 Axonal transmission mechanisms

Based on the morphological results from the microfluidic device, we observed the hp-Tau first accumulated in the axon region and then appeared in the OA-exposed and OA-unexposed cell populations. For the two neuronal populations, axons provide the possibilities to communicate with each other. There are two ways that can explain how the hp-Tau propagates, either by direct physical contact between the axons from the two cell populations for information exchange or the hp-Tau is released into the culture medium by the axons from the diseased cell population. It is possible that at the late stage of AD propagation, the diseased neuronal cell population released hp-Tau into its surrounding environment and it diffuses through the long junction channels to the other regions and has an effect on the unexposed cell population. To understand the mechanisms at the axonal network during disease propagation, microfluidic device with more controls are required to distinguish the functions of the axonal network and other markers can be used to distinguish the synaptic function. For the future experiment, instead of using OA to induce the neurons to build the diseased model which could possibly involve other pathologies, it will bring great value to use different forms of Tau and A β to induce the cells directly such as synthetic Tau or A β aggregates to exclude other possibilities during disease transmission. Further experiment can investigate more in detail during disease progression, such as focusing on synapse level to study synaptic transmission in spreading.

5.2.2 Relation between Tau and A β

As Ittner LM and Gotz J proposed in 2011, it is possible that Tau protein and A β have some interactions in AD[68]. They provided three possible models of this interaction. First, A β drives Tau pathology by causing hyperphosphorylation of Tau protein, which in turn mediates toxicity in neurons (Figure 62 A). Secondly, Tau mediates A β toxicity and hence, A β toxicity is critically dependent on the presence of Tau for example, in the dendrite (Figure 62 B). The last case is that A β and Tau target cellular processes or organelles synergistically, thereby possibly amplifying the toxic effects from each other (Figure 62 C). This is one of the works in the literature that have disclosed the possible relations between Tau and A β during AD propagation [24]. Some other cells in the brain could also participate during AD propagation, for example, the glia cells such as astrocytes and microglia. Glia cells may perceive A β oligomers and fibrils as foreign bodies and could as a result play a role in the pathogenesis of AD [140]. The application of microfluidics to the study of the interaction between Tau protein, amyloid

β and other possible cell types shows great promise in better understanding AD, and may potentially help in fulfilling the urgent need of finding a cure for AD.

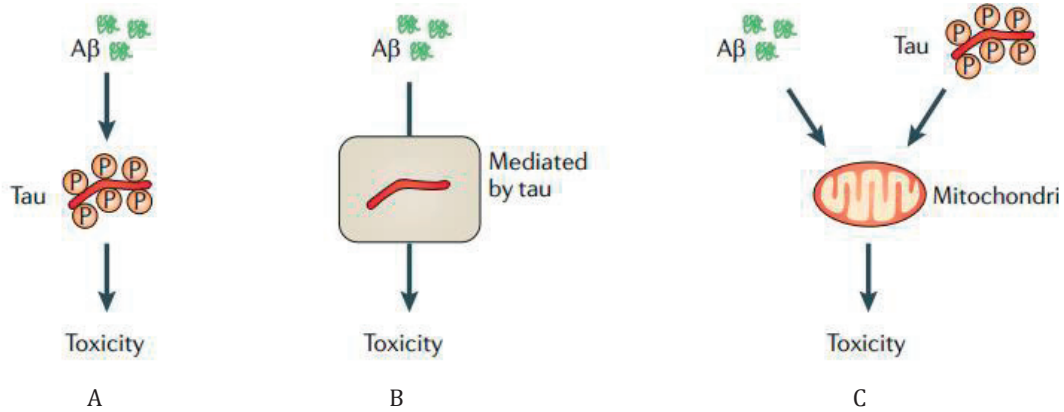


Figure 62: Three possible models of interesting interaction between A β and Tau. Reprinted from[68] with permission

5.2.3 3D cell culture model for AD studies

Most of the culture models used for AD studies are still focusing on *in vitro* 2D culture and *in vivo* experiments. The *in vivo* models provides the complexity of the brain function, however, it is difficult to distinguish the different functions and relations between each component in a native brain. From this point of view, the *in vitro* culture models provide some advantages. Compared to 2D neuronal culture, the 3D models can better present the key events of AD pathology, especially for observations on NFTs and A β plaques. For example, secreted A β first diffuses into the external environment, then A β deposits accumulate, finally forming A β plaques [24]. It is difficult to mimic this situation in a 2D neural cell culture environment, because the secreted A β diffuses into a large volume of culture medium and may even be washed away when the culture medium is refilled with fresh medium, which is necessary for neuronal culture. Although the 3D neuronal culture provides promising results on mimicking the brain, some challenges still exist. AD is a long term neurodegenerative disease and the degeneration of the brain takes years to develop. However, for *in vitro* cell culture, normally it takes around a month between building a mature neuronal network to observing the disease propagation and finally causing neuronal death in the end. As a result the reconstitution of AD conditions and the observation of the late stages of neurodegeneration *in vitro* becomes a problem [30]. Another issue that 3D culture brings is the low imaging quality arising from the increased thickness of the 3D tissue. Therefore, researchers are in great need of new microscopy technologies that can solve these problems.

5.2.4 Towards building a brain-on-a-chip

With the development of microtechnology, numbers of researchers are focusing on building artificial organs mimicking a native organ (usually called “organ-on-a-chip”), such as the “liver-on-a-chip” which is created by mimic the liver sinusoid and acinus structure to accelerate drug testing and toxicology studies[91]. The brain, regarded as the most complex organ in the body by the vast majority of scientists, is also being built *in vitro* to create brain-like tissue which can mimic the structural and functional features of the native brain. For example, we tried to use a layer-patterned microfluidic device to mimic the layer structure of the cortex. In previous work, people use microfluidic devices to provide a constant flow of fluid in order to mimic the brain's interstitial fluid, which provides functions such as providing nutrients, oxygen, cytokine transport and waste removal in native tissue [120]. Towards building a brain-on-a-chip, we selectively mimic some typical characteristics of the brain and focus on some specific issues where microdevices can provide similar structures and/or functions. Microdevices have great potential for building *in vitro* brain models for disease mechanism studies and drug effect tests.

5.2.5 Benefits from using miniaturized devices

Overall, there are many benefits for using miniaturized device for *in vitro* experiments. They provide better control over experiments in order to achieve more stable and accurate results at the microscale. Furthermore, the miniaturized devices, with their micron-sized channels, require much less cell quantities than normal culture dishes, such as petri dishes and well-plates, which means less animals like mice or rats need to be sacrificed for one experiment. At the same time, the biological experiment cost can be reduced significantly, because of the lower quantities of proteins, antibodies and other expensive solutions necessary for experimentation. The devices can also be designed to be reusable. For instance, our microfluidic-MEA device can be used around 20 times before disposal, under proper maintenance. Finally, the compartmentalized microfluidic device and the microfluidic-MEA devices we developed in this thesis are very promising tools for neurodegenerative disease studies and can potentially be used for pharmaceutical tests for drug development.

Bibliography

1. Abeles, M.: Corticonics: neural circuits of the cerebral cortex. *Trends in Neurosciences* 1991, 15(4).
2. Abgrall, P., Conedera, V., Camon, H., Gue, A.M., Nguyen, N.T.: SU-8 as a structural material for labs-on-chips and microelectromechanical systems. *Electrophoresis* 2007, 28(24):4539-4551.
3. Association, A.s.: 2013 Alzheimer's Disease Facts and Figures. 2013.
4. Balachandar, R., John, J.P., Saini, J., Kumar, K.J., Joshi, H., Sadanand, S., Aiyappan, S., Sivakumar, P.T., Loganathan, S., Varghese, M. *et al*: A study of structural and functional connectivity in early Alzheimer's disease using rest fMRI and diffusion tensor imaging. *International journal of geriatric psychiatry* 2015, 30(5):497-504.
5. Ballatore, C., Lee, V.M.-Y., Trojanowski, J.Q.: Tau-mediated neurodegeneration in Alzheimer's disease and related disorders. *Nature Reviews Neuroscience* 2007, 8(9):663-672.
6. Bennett, P.B., Guthrie, H.R.: Trends in ion channel drug discovery: advances in screening technologies. *Trends in biotechnology* 2003, 21(12):563-569.
7. Billingsley ML, K.R.: Regulated phosphorylation and dephosphorylation of tau protein: effects on microtubule interaction, intracellular trafficking and neurodegeneration. *Biochemical Journal* 1997, 323(3):577-591.
8. Black, M.M., Slaughter, T., Moshiah, S., Obrocka, M., Fischer, I.: Tau is enriched on dynamic microtubules in the distal region of growing axons. *Journal of Neuroscience* 1996, 16(11):3601-3619.
9. Blennow, K., de Leon, M.J., Zetterberg, H.: Alzheimer's disease. *Lancet* 2006, 368(9533):387-403.
10. Bozza, A., Coates, E.E., Incitti, T., Ferlin, K.M., Messina, A., Menna, E., Bozzi, Y., Fisher, J.P., Casarosa, S.: Neural differentiation of pluripotent cells in 3D alginate-based cultures. *Biomaterials* 2014, 35(16):4636-4645.
11. Brandt, R., Hundelt, M., Neelam, S.: Tau alteration and neuronal degeneration in tauopathies: mechanisms and models. *Biochimica et biophysica acta* 2005, 1739(2-3):331-354.
12. Bruggemann, D., Wolfrum, B., Maybeck, V., Mourzina, Y., Jansen, M., Offenhausser, A.: Nanostructured gold microelectrodes for extracellular recording from electrogenic cells. *Nanotechnology* 2011, 22(26):265104.
13. Buckley, C.T., Thorpe, S.D., O'Brien, F.J., Robinson, A.J., Kelly, D.J.: The effect of concentration, thermal history and cell seeding density on the initial mechanical properties of agarose hydrogels. *Journal of the mechanical behavior of biomedical materials* 2009, 2(5):512-521.
14. Buffi, N., Merulla, D., Beutier, J., Barbaud, F., Beggah, S., van Lintel, H., Renaud, P., van der Meer, J.R.: Development of a microfluidics biosensor for agarose-bead immobilized Escherichia coli bioreporter cells for arsenite detection in aqueous samples. *Lab on a chip* 2011, 11(14):2369-2377.
15. Butner, K.A., Kirschner, M.W.: Tau protein binds to microtubules through a flexible array of distributed weak sites. *The Journal of Cell Biology*, 1991, 115(3):717-730.
16. Calafate, S., Buist, A., Miskiewicz, K., Vijayan, V., Daneels, G., de Strooper, B., de Wit, J., Verstreken, P., Moechars, D.: Synaptic Contacts Enhance Cell-to-Cell Tau Pathology Propagation. *Cell reports* 2015, 11(8):1176-1183.
17. Calignon, A.d., Polydoro, M., Suárez-Calvet, M., William, C., Adamowicz, D.H., Kopeikina, K.J., Pitstick, R., Sahara, N., Ashe, K.H., Carlson, G.A. *et al*: Propagation of tau pathology in a model of early Alzheimer's disease. *Neuron* 2012, 73(4):685-697.

18. Campenot, R.B.: Local control of neurites development by nerve growth factor. . *Proceedings of the National Academy of Sciences of the United States of America* 1977, 74(10):4516-4519.
19. Campo, A.d., Greiner, C.: SU-8: a photoresist for high-aspect-ratio and 3D submicron lithography. *Journal of Micromechanics and Microengineering* 2007, 17(6):R81-R95.
20. Carlier, J., Chuda, K., Arscott, S., Thomy, V., Verbeke, B., Coqueret, X., Camart, J.C., Druon, C., Tabourier, P.: High pressure-resistant SU-8 microchannels for monolithic porous structure integration. *Journal of Micromechanics and Microengineering* 2006, 16(10):2211-2219.
21. Chamberlain, G., Fox, J., Ashton, B., Middleton, J.: Concise review: Mesenchymal stem cells: their phenotype, differentiation capacity, immunological features, and potential for homing. *Stem Cells* 2007, 25:2739–2749.
22. Chen, L., Deng, Y., Luo, W., Wang, Z., Zeng, S.: Detection of bursts in neuronal spike trains by the mean inter-spike interval method. *Progress in Natural Science* 2009, 19(2):229-235.
23. Chiappalone, M., Bove, M., Vato, A., Tedesco, M., Martinoia, S.: Dissociated cortical networks show spontaneously correlated activity patterns during in vitro development. *Brain research* 2006, 1093(1):41-53.
24. Choi, S.H., Kim, Y.H., Heisch, M., Sliwinski, C., Lee, S., D'Avanzo, C., Chen, H., Hooli, B., Asselin, C., Muffat, J. *et al*: A three-dimensional human neural cell culture model of Alzheimer's disease. *Nature* 2014, 515(7526):274-278.
25. Corner, M.A.: Spontaneous neuronal burst discharges as dependent and independent variables in the maturation of cerebral cortex tissue cultured in vitro: a review of activity-dependent studies in live 'model' systems for the development of intrinsically generated bioelectric slow-wave sleep patterns. *Brain research reviews* 2008, 59(1):221-244.
26. Cowan, C.M., Mudher, A.: Are tau aggregates toxic or protective in tauopathies? *Frontiers in neurology* 2013, 4:114.
27. Crimins, J.L., Rocher, A.B., Luebke, J.I.: Electrophysiological changes precede morphological changes to frontal cortical pyramidal neurons in the rTg4510 mouse model of progressive tauopathy. *Acta neuropathologica* 2012, 124(6):777-795.
28. Crimins, J.L., Rocher, A.B., Peters, A., Shultz, P., Lewis, J., Luebke, J.I.: Homeostatic responses by surviving cortical pyramidal cells in neurodegenerative tauopathy. *Acta neuropathologica* 2011, 122(5):551-564.
29. Cullen, D.K., Lessing, M.C., LaPlaca, M.C.: Collagen-dependent neurite outgrowth and response to dynamic deformation in three-dimensional neuronal cultures. *Annals of biomedical engineering* 2007, 35(5):835-846.
30. D'Avanzo, C., Aronson, J., Kim, Y.H., Choi, S.H., Tanzi, R.E., Kim, D.Y.: Alzheimer's in 3D culture: Challenges and perspectives. *BioEssays : news and reviews in molecular, cellular and developmental biology* 2015, 37(10):1139-1148.
31. Dillon, G.P., Xiaojun, Y., Sridharan, A., Ranieri, J.P., Bellamkonda, R.V.: The influence of physical structure and charge on neurite extension in a 3D hydrogel scaffold. *Journal of Biomaterials Science, Polymer Edition* 1998, 9(10):1049-1069.
32. Dinh, N.D., Chiang, Y.Y., Hardelauf, H., Baumann, J., Jackson, E., Waide, S., Sisnaiske, J., Frimat, J.P., van Thriel, C., Janasek, D. *et al*: Microfluidic construction of minimalistic neuronal co-cultures. *Lab on a chip* 2013, 13(7):1402-1412.
33. Doody, R.S., Raman, R., Farlow, M., Iwatsubo, T., Vellas, B., Joffe, S., Kieburtz, K., He, F., Sun, X., Thomas, R.G. *et al*: A phase 3 trial of semagacestat for treatment of Alzheimer's disease. *The New England journal of medicine* 2013, 369(4):341-350.

34. Dotti, C.G., Sullivan, C.A., Banker, G.A.: The establishment of polarity by hippocampal neurons in culture *The Journal of Neuroscience* 1988, 8(4):1454-1468.
35. Duce, J.A., Tsatsanis, A., Cater, M.A., James, S.A., Robb, E., Wikhe, K., Leong, S.L., Perez, K., Johanssen, T., Greenough, M.A. *et al*: Iron-export ferroxidase activity of beta-amyloid precursor protein is inhibited by zinc in Alzheimer's disease. *Cell* 2010, 142(6):857-867.
36. Dujardin, S., Lécolle, K., Caillierez, R., Bégard, S., Zommer, N., Lachaud, C., Carrier, S., Dufour, N., Aurégan, G., Winderickx, J. *et al*: Neuron-to-neuron wild-type Tau protein transfer through a trans-synaptic mechanism: relevance to sporadic tauopathies. *Acta Neuropathologica Communications* 2014, 2(14).
37. Dworak, B.J., Wheeler, B.C.: Novel MEA platform with PDMS microtunnels enables the detection of action potential propagation from isolated axons in culture. *Lab on a chip* 2009, 9(3):404-410.
38. Eversmann, B., Jenkner, M., Hofmann, F., Paulus, C., Brederlow, R., Holzapfl, B., Fromherz, P., Merz, M., Brenner, M., Schreiter, M. *et al*: A 128 × 128 CMOS biosensor array for extracellular recording of neural activity. *IEEE JOURNAL OF SOLID-STATE CIRCUITS* 2003, 38(12):2306-2317.
39. Ewers, M., Sperling, R.A., Klunk, W.E., Weiner, M.W., Hampel, H.: Neuroimaging markers for the prediction and early diagnosis of Alzheimer's disease dementia. *Trends Neurosci* 2011, 34(8):430-442.
40. Fan, R., Yue, M., Karnik, R., Majumdar, A., Yang, P.: Polarity switching and transient responses in single nanotube nanofluidic transistors. *Physical Review Letters* 2005, 95(8).
41. Franke, F., Jackel, D., Dragas, J., Muller, J., Radivojevic, M., Bakkum, D., Hierlemann, A.: High-density microelectrode array recordings and real-time spike sorting for closed-loop experiments: an emerging technology to study neural plasticity. *Frontiers in neural circuits* 2012, 6:105.
42. Fujii, T.: PDMS-based microfluidic devices for biomedical applications. *Microelectronic Engineering* 2002, 61-62:907-914.
43. Garofalo, M., Nieus, T., Massobrio, P., Martinoia, S.: Evaluation of the performance of information theory-based methods and cross-correlation to estimate the functional connectivity in cortical networks. *PloS one* 2009, 4(8):1-14.
44. Goedert, M., Spillantini, M.G., Jakes, R., Rutherford, D., Crowther, R.A.: Multiple isoforms of human microtubule-associated protein Tau: sequences and localization in neurofibrillary tangles of Alzheimer's disease. *Neuron* 1989, 3:519-526.
45. Goldman, Y.E., FranziniArmstrong, C., Armstrong, C.M.: Andrew Fielding Huxley (1917-2012). *Nature* 2012, 486(7404):474.
46. Gorazd B. Stokin, C.n.L., Toma's L. Falzone, Richard G. Brusch, Edward Rockenstein, Stephanie L. Mount, Rema Raman, Peter Davies, Eliezer Masliah, David S. Williams, Lawrence S. B. Goldstein: Axonopathy and transport deficits early in the pathogenesis of Alzheimer's disease. *Science* 2005, 307:1282-1288.
47. Gortz, P., Siebler, M., Ihl, R., Henning, U., Luckhaus, C., Supprian, T., Lange-Asschenfeldt, C.: Multielectrode array analysis of cerebrospinal fluid in Alzheimer's disease versus mild cognitive impairment: a potential diagnostic and treatment biomarker. *Biochemical and biophysical research communications* 2013, 434(2):293-297.
48. Gotz, J., Ittner, L.M., Kins, S.: Do axonal defects in tau and amyloid precursor protein transgenic animals model axonopathy in Alzheimer's disease? *Journal of neurochemistry* 2006, 98(4):993-1006.

49. Gregory J. Brewer, M.D.B., Stathis Leondopoulos, Liangbin Pan, Sankaraleengam Alagapan, Thomas B. DeMarse, and Bruce Wheeler: Toward a self-wired active reconstruction of the hippocampal trisynaptic loop: DG-CA3. *Frontiers in neural circuits* 2013, 7:165.
50. Greig, R.E.B.a.N.H.: Alzheimer's disease drug development in 2008 and beyond: problems and opportunities. *Current Alzheimer Research* 2008, 5:346-357.
51. Greig, R.E.B.a.N.H.: Why so few drugs for Alzheimer's disease? Are methods failing drugs? *Current Alzheimer Research* 2010, 7(7):642-651.
52. Griffith, L.G., Swartz, M.A.: Capturing complex 3D tissue physiology in vitro. *Nature reviews Molecular cell biology* 2006, 7(3):211-224.
53. Guzman-Martinez, L., Farias, G.A., Maccioni, R.B.: Tau oligomers as potential targets for Alzheimer's diagnosis and novel drugs. *Frontiers in neurology* 2013, 4:167.
54. Hai, A., Dormann, A., Shappir, J., Yitzchaik, S., Bartic, C., Borghs, G., Langedijk, J.P., Spira, M.E.: Spine-shaped gold protrusions improve the adherence and electrical coupling of neurons with the surface of micro-electronic devices. *Journal of the Royal Society, Interface / the Royal Society* 2009, 6(41):1153-1165.
55. Hardy, J.: The amyloid hypothesis for Alzheimer's disease: a critical reappraisal. *Journal of neurochemistry* 2009, 110(4):1129-1134.
56. Hardy, J., Selkoe, D.J.: The amyloid hypothesis of Alzheimer's disease: progress and problems on the road to therapeutics. *Science* 2002, 297:353-356.
57. Harris, J.A., Devidze, N., Verret, L., Ho, K., Halabisky, B., Thwin, M.T., Kim, D., Hamto, P., Lo, I., Yu, G.Q. *et al*: Transsynaptic progression of amyloid-beta-induced neuronal dysfunction within the entorhinal-hippocampal network. *Neuron* 2010, 68(3):428-441.
58. Haycock, J.W.: 3D cell culture: a review of current approaches and techniques. *Methods in molecular biology* 2011, 695:1-15.
59. Haycock, J.W.: 3D cell culture: Methods and protocols. *Methods in Molecular Biology* 695 published by Springer 2011.
60. Heuschkel, M.O.: Fabrication of multi-electrode array devices for electrophysiological monitoring of in-vitro cell/tissue cultures. *PhD thesis No 2370 from École Polytechnique Fédérale de Lausanne* 2001.
61. Higgins, J.A.H.a.G.A.: Alzheimer's disease: the amyloid cascade hypothesis. *Science* 1992, 256:184-185.
62. Hodgkin, A.L., Huxley, A.F.: A quantitative description of membrane current and its application to conduction and excitation in nerve. *The Journal of physiology* 1952, 117(4):500-544.
63. Hodgkin, A.L., Huxley, A.F.: Resting and action potentials in single nerve fibres. *Journal of Physiology* 1945, 104:176-195.
64. Holly J. Martin, K.H.S., Joel D. Bumgardner, and Keisha B. Walters: XPS Study on the Use of 3-Aminopropyltriethoxysilane to Bond Chitosan to a Titanium Surface. *Langmuir: the ACS journal of surfaces and colloids* 2007, 23:6645-6651.
65. Huxley, A.: KENNETH STEWART COLE 1900-1984, A biographical Memoir by SIR ANDREW HUXLEY. *National Academy of Sciences* 1996.
66. Isik, S., Berdondini, L., Oni, J., Blochl, A., Koudelka-Hep, M., Schuhmann, W.: Cell-compatible array of three-dimensional tip electrodes for the detection of nitric oxide release. *Biosensors & bioelectronics* 2005, 20(8):1566-1572.
67. Israel, M.A., Yuan, S.H., Bardy, C., Reyna, S.M., Mu, Y., Herrera, C., Hefferan, M.P., Van Gorp, S., Nazor, K.L., Boscolo, F.S. *et al*: Probing sporadic and familial Alzheimer's disease using induced pluripotent stem cells. *Nature* 2012, 482(7384):216-220.
68. Ittner, L.M., Gotz, J.: Amyloid-beta and tau--a toxic pas de deux in Alzheimer's disease. *Nature reviews Neuroscience* 2011, 12(2):65-72.

69. Jean, D.C., Baas, P.W.: It cuts two ways: microtubule loss during Alzheimer disease. *The EMBO journal* 2013, 32(22):2900-2902.
70. Jeong, C.G., Hollister, S.J.: Mechanical, permeability, and degradation properties of 3D designed poly(1,8 octanediol-co-citrate) scaffolds for soft tissue engineering. *Journal of biomedical materials research Part B, Applied biomaterials* 2010, 93(1):141-149.
71. Jiguet, S., Bertsch, A., Judelewicz, M., Hofmann, H., Renaud, P.: SU-8 nanocomposite photoresist with low stress properties for microfabrication applications. *Microelectronic Engineering* 2006, 83(10):1966-1970.
72. Johnson, G.V.W., Stoothoff, W.H.: Tau phosphorylation in neuronal cell function and dysfunction. *Journal of Cell Science* 2004, 117(24):5721-5729.
73. Johnston, I.D., McCluskey, D.K., Tan, C.K.L., Tracey, M.C.: Mechanical characterization of bulk Sylgard 184 for microfluidics and microengineering. *Journal of Micromechanics and Microengineering* 2014, 24(3):035017.
74. Kamat, P.K., Rai, S., Nath, C.: Okadaic acid induced neurotoxicity: an emerging tool to study Alzheimer's disease pathology. *Neurotoxicology* 2013, 37:163-172.
75. Kamat, P.K., Rai, S., Swarnkar, S., Shukla, R., Nath, C.: Molecular and cellular mechanism of okadaic acid (OKA)-induced neurotoxicity: a novel tool for Alzheimer's disease therapeutic application. *Molecular neurobiology* 2014, 50(3):852-865.
76. Kanagasabapathi, T.T., Ciliberti, D., Martinoia, S., Wadman, W.J., Decre, M.M.: Dual-compartment neurofluidic system for electrophysiological measurements in physically segregated and functionally connected neuronal cell culture. *Frontiers in neuroengineering* 2011, 4:13.
77. Kanagasabapathi, T.T., Franco, M., Barone, R.A., Martinoia, S., Wadman, W.J., Decre, M.M.: Selective pharmacological manipulation of cortical-thalamic co-cultures in a dual-compartment device. *Journal of neuroscience methods* 2013, 214(1):1-8.
78. Kanagasabapathi, T.T., Massobrio, P., Barone, R.A., Tedesco, M., Martinoia, S., Wadman, W.J., Decre, M.M.: Functional connectivity and dynamics of cortical-thalamic networks co-cultured in a dual compartment device. *Journal of neural engineering* 2012, 9(3):036010.
79. Kempf, M., Clement, A., Faissner, A., Lee, G., Brandt, R.: Tau binds to the distal axon early in development of polarity in a microtubule- and microfilament- dependent manner. *The Journal of Neuroscience* 1996, 16(18):5583-5592.
80. Kenessey, A., Yen, S.H.: The extent of phosphorylation of fetal tau is comparable to that of PHF-tau from Alzheimer paired helical filaments. *Brain research* 1993, 629(1):40-46.
81. Kim, K., Park, S.W., Yang, S.S.: The optimization of PDMS-PMMA bonding process using silane primer. *BioChip Journal* 2010, 4(2):148-154.
82. Kiss, L., Bennett, P.B., Uebele, V.N., Koblan, K.S., Kane, S.A., Neagle, B., Schroede, K.: High throughput ion-channel pharmacology: Planar-array-based voltage clamp. *ASSAY and Drug Development Technologies* 2003, 1(1-2):127-135.
83. Kunze, A., Giugliano, M., Valero, A., Renaud, P.: Micropatterning neural cell cultures in 3D with a multi-layered scaffold. *Biomaterials* 2011, 32(8):2088-2098.
84. Kunze, A., Lengacher, S., Dirren, E., Aebischer, P., Magistretti, P.J., Renaud, P.: Astrocyte-neuron co-culture on microchips based on the model of SOD mutation to mimic ALS. *Integrative biology : quantitative biosciences from nano to macro* 2013, 5(7):964-975.
85. Kunze, A., Meissner, R., Brando, S., Renaud, P.: Co-pathological connected primary neurons in a microfluidic device for Alzheimer studies. *Biotechnology and bioengineering* 2011, 108(9):2241-2245.
86. Kuperstein, I., Broersen, K., Benilova, I., Rozenski, J., Jonckheere, W., Debulpaep, M., Vandersteen, A., Segers-Nolten, I., Van Der Werf, K., Subramaniam, V. et al: Neurotoxicity

- of Alzheimer's disease Abeta peptides is induced by small changes in the Abeta42 to Abeta40 ratio. *The EMBO journal* 2010, 29(19):3408-3420.
87. Kuret, J., Congdon, E.E., Li, G., Yin, H., Yu, X., Zhong, Q.: Evaluating triggers and enhancers of tau fibrillization. *Microscopy research and technique* 2005, 67(3-4):141-155.
 88. Lambacher, A., Vitzthum, V., Zeitler, R., Eickenscheidt, M., Eversmann, B., Thewes, R., Fromherz, P.: Identifying firing mammalian neurons in networks with high-resolution multi-transistor array (MTA). *Applied Physics A* 2010, 102(1):1-11.
 89. LaPlaca, M.C., Vernekar, V.N., Shoemaker, J.T., Cullen, D.K.: Methods in bioengineering: Three-dimensional neuronal cultures. *Berthiaume F, Morgan J R, Eds; Methods in Bioengineering Artech House Publishers: Norwood, MA, USA* 2010.
 90. Lee, G., Cowan, N., Kirschner, M.: The primary structure and heterogeneity of tau protein from mouse brain. *Science* 1988, 239(4837):285-288.
 91. Lee, J., Kim, S.H., Kim, Y.C., Choi, I., Sung, J.H.: Fabrication and characterization of microfluidic liver-on-a-chip using microsomal enzymes. *Enzyme and microbial technology* 2013, 53(3):159-164.
 92. Lee, K.Y., Mooney, D.J.: Hydrogels for Tissue Engineering. *Chemical Reviews* 2001, 101:1869-1879.
 93. Lei, K.F.: Chapter 1. Materials and Fabrication Techniques for Nano- and Microfluidic Devices. 2014:1-28.
 94. Levental, I., Georges, P.C., Janmey, P.A.: Soft biological materials and their impact on cell function. *Soft Matter* 2007, 3(3):299-306.
 95. Lewicki, M.S.: A review of methods for spike sorting: the detection and classification of neural action potentials. *Network: Comput Neural Syst* 1998, 9:R53-R78.
 96. Lippiat, J.D.: Planar patch clamp: Advances in electrophysiology. 2009, 491.
 97. Liu, L., Drouet, V., Wu, J.W., Witter, M.P., Small, S.A., Clelland, C., Duff, K.: Trans-Synaptic Spread of Tau Pathology In Vivo. *PloS one* 2012, 7(2).
 98. Lorenz, H., Despont, M., Fahrni, N., Brugger, J., Vettiger, P., Renaud, P.: High-aspect-ratio, ultrathick, negative-tone near-UV photoresist and its applications for MEMS. *Sensors and Actuators A: Physical* 1998, 64(1):33-39.
 99. Lu, J., Miao, J., Su, T., Liu, Y., He, R.: Formaldehyde induces hyperphosphorylation and polymerization of Tau protein both in vitro and in vivo. *Biochimica et biophysica acta* 2013, 1830(8):4102-4116.
 100. Mandrekar, S., Landreth, G.E.: Microglia and Inflammation in Alzheimer's Disease. *CNS Neurol Disord Drug Targets* 2010, 9(2):156-167.
 101. Mangialasche, F., Solomon, A., Bengt Winblad, M., Mecocci, P., Kivipelto, M.: Alzheimer's disease: clinical trials and drug development. *THE LANCET Neurology* 2010, 9(7):702-716.
 102. Martin, L., Page, G., Terro, F.: Tau phosphorylation and neuronal apoptosis induced by the blockade of PP2A preferentially involve GSK3beta. *Neurochem Int* 2011, 59(2):235-250.
 103. Martinoia, S., Bonzano, L., Chiappalone, M., Tedesco, M., Marcoli, M., Maura, G.: In vitro cortical neuronal networks as a new high-sensitive system for biosensing applications. *Biosensors & bioelectronics* 2005, 20(10):2071-2078.
 104. Masuda, S., Washizu, M., Nanba, T.: Novel method of cell fusion in field constriction area in fluid integrated circuit. *IEEE TRANSACTIONS ON BIOMEDICAL CIRCUITS AND SYSTEMS* 1989, 25(4):732-737.
 105. Mata, A., Fleischman, A.J., Roy, S.: Characterization of polydimethylsiloxane (PDMS) properties for biomedical micro/nanosystems. *Biomedical Microdevices* 2005, 7(4):281-293.

106. Matyash, M., Despong, F., Mandal, R., Fiore, D., Gelinsky, M., Ikonomidou, C.: Novel soft alginate hydrogel strongly supports neurite growth and protects neurons against oxidative stress. *Tissue engineering Part A* 2012, 18(1-2):55-66.
107. McDonald, J.C., Duffy, D., Anderson, J.R., T.Chiu, D., Wu, H., Schueller, O.A., Whitesides, G.M.: Fabrication of microfluidic systems in poly(dimethylsiloxane). *Electrophoresis* 2000, 21(1):27-40.
108. Miller, K., Chinzei, K., Orssengo, G., Bednarz, P.: Mechanical properties of brain tissue in-vivo: experiment and computer simulation. *Journal of Biomechanics* 2000, 33:1369-1376.
109. Mohamed, N.V., Herrou, T., Plouffe, V., Piperno, N., Leclerc, N.: Spreading of tau pathology in Alzheimer's disease by cell-to-cell transmission. *The European journal of neuroscience* 2013, 37(12):1939-1948.
110. Mollenhauer, H.H., Morre, D.J., Pikaard, D., Clark, D.E.: An ultrastructural evaluation of toluene toxicity using cultured mammalian cells. *J Submicrosc Cytol Pathol* 1990, 22(4):523-527.
111. Möller, H.J., Graeber, M.B.: The case described by Alois Alzheimer in 1911. Historical and conceptual perspectives based on the clinical record and neurohistological sections. *European archives of psychiatry and clinical neuroscience* 1998, 248(3):111-122.
112. Morfini, G.A., Burns, M., Binder, L.I., Kanaan, N.M., LaPointe, N., Bosco, D.A., Brown, R.H., Jr., Brown, H., Tiwari, A., Hayward, L. *et al*: Axonal transport defects in neurodegenerative diseases. *The Journal of neuroscience : the official journal of the Society for Neuroscience* 2009, 29(41):12776-12786.
113. Nath, S., Agholme, L., Kurudenkandy, F.R., Granseth, B., Marcusson, J., Hallbeck, M.: Spreading of neurodegenerative pathology via neuron-to-neuron transmission of beta-amyloid. *The Journal of neuroscience : the official journal of the Society for Neuroscience* 2012, 32(26):8767-8777.
114. Novellino, A., Scelfo, B., Palosaari, T., Price, A., Sobanski, T., Shafer, T.J., Johnstone, A.F., Gross, G.W., Gramowski, A., Schroeder, O. *et al*: Development of micro-electrode array based tests for neurotoxicity: assessment of interlaboratory reproducibility with neuroactive chemicals. *Frontiers in neuroengineering* 2011, 4:4.
115. O'Connor, S.M., Stenger, D.A., Shaffer, K.M., Ma, W.: Survival and neurite outgrowth of rat cortical neurons in three-dimensional agarose and collagen gel matrices. *Neuroscience Letters* 2001, 304:189-193.
116. Ojovan, S.M., Rabieh, N., Shmoel, N., Erez, H., Maydan, E., Cohen, A., Spira, M.E.: A feasibility study of multi-site, intracellular recordings from mammalian neurons by extracellular gold mushroom-shaped microelectrodes. *Scientific reports* 2015, 5:14100.
117. Ou, J., Glawdel, T., Ren, C.L., Pawliszyn, J.: Fabrication of a hybrid PDMS/SU-8/quartz microfluidic chip for enhancing UV absorption whole-channel imaging detection sensitivity and application for isoelectric focusing of proteins. *Lab on a chip* 2009, 9(13):1926-1932.
118. Pan, L., Alagapan, S., Franca, E., Brewer, G.J., Wheeler, B.C.: Propagation of action potential activity in a predefined microtunnel neural network. *Journal of neural engineering* 2011, 8(4):046031.
119. Park, J., Koito, H., Li, J., Han, A.: Microfluidic compartmentalized co-culture platform for CNS axon myelination research. *Biomed Microdevices* 2009, 11(6):1145-1153.
120. Park, J., Lee, B.K., Jeong, G.S., Hyun, J.K., Lee, C.J., Lee, S.H.: Three-dimensional brain-on-a-chip with an interstitial level of flow and its application as an in vitro model of Alzheimer's disease. *Lab on a chip* 2015, 15(1):141-150.

121. Park, J.W., Kim, H.J., Kang, M.W., Jeon, N.L.: Advances in microfluidics-based experimental methods for neuroscience research. *Lab on a chip* 2013, 13(4):509-521.
122. Patel, J.N., Gray, B.L., Kaminska, B., Wu, N.-C., Gates, B.D.: SU-8- and PDMS-based hybrid fabrication technology for combination of permanently bonded flexible and rigid features on a single device. *Journal of Micromechanics and Microengineering* 2013, 23(6):065029.
123. Patel, J.N., Kaminska, B., Gray, B.L., Gates, B.D.: PDMS as a sacrificial substrate for SU-8-based biomedical and microfluidic applications. *Journal of Micromechanics and Microengineering* 2008, 18(9):095028.
124. Paulson, J.B., Ramsden, M., Forster, C., Sherman, M.A., McGowan, E., Ashe, K.H.: Amyloid plaque and neurofibrillary tangle pathology in a regulatable mouse model of Alzheimer's disease. *The American journal of pathology* 2008, 173(3):762-772.
125. Pautot, S., Wyart, C., Isacoff, E.Y.: Colloid-guided assembly of oriented 3D neuronal networks. *Nature methods* 2008, 5(8):735-740.
126. Place, E.S., George, J.H., Williams, C.K., Stevens, M.M.: Synthetic polymer scaffolds for tissue engineering. *Chemical Society reviews* 2009, 38(4):1139-1151.
127. Platen, M., Mathieu, E., Luck, S., Schubel, R., Jordan, R., Pautot, S.: Poly(2-oxazoline)-Based Microgel Particles for Neuronal Cell Culture. *Biomacromolecules* 2015, 16(5):1516-1524.
128. Pooler, A.M., Phillips, E.C., Lau, D.H., Noble, W., Hanger, D.P.: Physiological release of endogenous tau is stimulated by neuronal activity. *EMBO reports* 2013, 14(4):389-394.
129. Potter, S.M.: Distributed processing in cultured neuronal networks. *Progress in Brain Research* 2001, 130.
130. Priller, C., Bauer, T., Mitteregger, G., Krebs, B., Kretzschmar, H.A., Herms, J.: Synapse formation and function is modulated by the amyloid precursor protein. *The Journal of neuroscience : the official journal of the Society for Neuroscience* 2006, 26(27):7212-7221.
131. Puzzo, D., Privitera, L., Leznik, E., Fa, M., Staniszewski, A., Palmeri, A., Arancio, O.: Picomolar amyloid-beta positively modulates synaptic plasticity and memory in hippocampus. *The Journal of neuroscience : the official journal of the Society for Neuroscience* 2008, 28(53):14537-14545.
132. Ravi, M., Paramesh, V., Kaviya, S.R., Anuradha, E., Solomon, F.D.: 3D cell culture systems: advantages and applications. *Journal of cellular physiology* 2015, 230(1):16-26.
133. Rutten, W.L.: Selective electrical interfaces with the nervous system. *Annual review of biomedical engineering* 2002, 4:407-452.
134. Sakman, B., Neher, E.: Patch clamp techniques for studying ionic channels in excitable membranes. *Annual Review of Physiology* 1984, 46:455-472.
135. Sigworth, F.J.: Opportunities for microtechnology in ion channel research. *Proceedings of the 3rd Annual International IEEE EMBS Special Topic* 2005.
136. Siskova, Z., Justus, D., Kaneko, H., Friedrichs, D., Henneberg, N., Beutel, T., Pitsch, J., Schoch, S., Becker, A., von der Kammer, H. *et al*: Dendritic structural degeneration is functionally linked to cellular hyperexcitability in a mouse model of Alzheimer's disease. *Neuron* 2014, 84(5):1023-1033.
137. Smith, E.A., Chen, W.: How to prevent the loss of surface functionality derived from aminosilanes. *Langmuir : the ACS journal of surfaces and colloids* 2008, 24(21):12405-12409.
138. Song, H.-j., Ming, G.-l., Poo, M.-m.: cAMP-induced switching in turning direction of nerve growth cones. *Nature* 1997, 388:275-279.
139. Spira, M.E., Hai, A.: Multi-electrode array technologies for neuroscience and cardiology. *nature nanotechnology* 2013, 8:83-94.

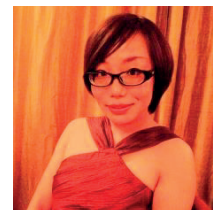
140. Suh, Y.-h., Checler, F.: Amyloid precursor protein, presenilins, and alpha-synuclein: molecular pathogenesis and pharmacological applications in Alzheimer's disease. *Pharmacological Reviews* 2002, 54(3).
141. Sunkara, V., Cho, Y.K.: Investigation on the mechanism of aminosilane-mediated bonding of thermoplastics and poly(dimethylsiloxane). *ACS applied materials & interfaces* 2012, 4(12):6537-6544.
142. Sunkara, V., Park, D.K., Hwang, H., Chantiwas, R., Soper, S.A., Cho, Y.K.: Simple room temperature bonding of thermoplastics and poly(dimethylsiloxane). *Lab on a chip* 2011, 11(5):962-965.
143. Tang, L., Lee, N.Y.: A facile route for irreversible bonding of plastic-PDMS hybrid microdevices at room temperature. *Lab on a chip* 2010, 10(10):1274-1280.
144. Taylor, A.M., Blurton-Jones, M., Rhee, S.W., Cribbs, D.H., Cotman, C.W., Jeon, N.L.: A microfluidic culture platform for CNS axonal injury, regeneration and transport. *Nature methods* 2005, 2(8):599-605.
145. Taylor, A.M., Dieterich, D.C., Ito, H.T., Kim, S.A., Schuman, E.M.: Microfluidic local perfusion chambers for the visualization and manipulation of synapses. *Neuron* 2010, 66(1):57-68.
146. Taylor, A.M., Rhee, S.W., Tu, C.H., Cribbs, D.H., Cotman, C.W., Jeon, N.L.: Microfluidic Multicompartment Device for Neuroscience Research. *Langmuir : the ACS journal of surfaces and colloids* 2003, 19(5):1551-1556.
147. Thies, W., Bleiler, L., Alzheimer's, A.: 2013 Alzheimer's disease facts and figures. *Alzheimer's & dementia : the journal of the Alzheimer's Association* 2013, 9(2):208-245.
148. Thomas, C.A., Springer, P.A., Loeb, G.E., Berwald-Netter, Y., Okun, L.M.: A miniature microelectrode array to monitor the bioelectric activity of cultured cells. *Experimental Cell Research* 1972, 74(1):61-66.
149. Thompson, J.A.: Microbead-based biosensing in microfluidic devices. *Penn Dissertations* 2011:Paper 331.
150. Tung, Y.C., Hsiao, A.Y., Allen, S.G., Torisawa, Y.S., Ho, M., Takayama, S.: High-throughput 3D spheroid culture and drug testing using a 384 hanging drop array. *The Analyst* 2011, 136(3):473-478.
151. Turner, P.R., O'Connor, K., Tate, W.P., Abraham, W.C.: Roles of amyloid precursor protein and its fragments in regulating neural activity, plasticity and memory. *Progress in neurobiology* 2003, 70(1):1-32.
152. Vetter, R.J., Williams, J.C., Hetke, J.F., Nunamaker, E.A., Kipke, D.R.: Chronic neural recording using silicon-substrate microelectrode arrays implanted in cerebral cortex. *IEEE TRANSACTIONS ON BIOMEDICAL ENGINEERING* 2004, 51(6).
153. Wagenaar, D.A., Pine, J., Potter, S.M.: An extremely rich repertoire of bursting patterns during the development of cortical cultures. *BMC neuroscience* 2006, 7:11.
154. Wang, Y., Zhang, G., Zhou, H., Barakat, A., Querfurth, H.: Opposite effects of low and high doses of Ab42 on electrical network and neuronal excitability in the rat prefrontal cortex. *PloS one* 2009, 4(12): e8366.
155. Ward, S.M., Himmelstein, D.S., Lancia, J.K., Binder, L.I.: Tau oligomers and tau toxicity in neurodegenerative disease. *Biochemical Society transactions* 2012, 40(4):667-671.
156. Wolfe, P.S., Sell, S.A., Bowlin, G.L.: Natural and Synthetic Scaffolds. 2011:41-67.
157. Yang, Y.L., Motte, S., Kaufman, L.J.: Pore size variable type I collagen gels and their interaction with glioma cells. *Biomaterials* 2010, 31(21):5678-5688.
158. Zhang, Z., Simpkins, J.W.: An okadaic acid-induced model of tauopathy and cognitive deficiency. *Brain research* 2010, 1359:233-246.

159. Zhang, Z., Zhao, P., Xiao, G.: The fabrication of polymer microfluidic devices using a solid-to-solid interfacial polyaddition. *Polymer* 2009, 50(23):5358-5361.
160. Zhang, Z., Zhao, P., Xiao, G., Watts, B.R., Xu, C.: Sealing SU-8 microfluidic channels using PDMS. *Biomicrofluidics* 2011, 5(4):46503-465038.
161. Zhu, M., Lerum, M.Z., Chen, W.: How to prepare reproducible, homogeneous, and hydrolytically stable aminosilane-derived layers on silica. *Langmuir : the ACS journal of surfaces and colloids* 2012, 28(1):416-423.
162. Zilberter, Y., Zilberter, T., Bregestovski, P.: Neuronal activity in vitro and the in vivo reality: the role of energy homeostasis. *Trends in pharmacological sciences* 2010, 31(9):394-401.

Yufei Ren

General information

Nationality: Chinese (B permit) Tel.: +41 78 912 62 58
Date of birth: 14.07.1987 Email: yufei.ren.faye@gmail.com
Languages: Chinese - native Address: Chemin du Croset 8
English - fluent CH-1024 Ecublens
French - basic Switzerland



I. Education background

- ◆ **Microsystems Laboratory 4, École Polytechnique Fédérale de Lausanne EPFL, Switzerland**
Ph.D. Student of Doctoral Program in Bioengineering and Biotechnology (EDBB) Nov. 2011- Present
Thesis: Towards brain-on-a-chip: microfluidic and microelectrode array platforms for morphological and electrophysiological observations on the propagation of Alzheimer's disease
- ◆ **École Polytechnique Fédérale de Lausanne EPFL, Switzerland**
Master of Bioengineering and Biotechnology Sept. 2010 - Jun. 2011
- ◆ **Tianjin University, China**
Bachelor of Chemical Engineering and Technology Sept. 2006 - Jul. 2010
Thesis: Sugar-assisted precipitation method for improving CLEAs activity and its application in biosynthesis of amoxicillin

II. Selected awards

- ◆ Bioalps Best Poster Prize at NanoBioTech Conference, Montreux, Switzerland Nov. 2014
- ◆ Best Presentation Award at 7th International NAMIS "Bio-inspired MEMS/NEMS" hosted by Seoul National University, Seoul, South Korea Sept. 2013
- ◆ Silver Medal at international Genetically Engineered Machine competition (iGEM) hosted by Massachusetts Institute of Technology (MIT), Cambridge, USA Nov. 2009

III. Publications

- ◆ Invited book chapter "Compartmentalized microfluidics for *in vitro* Alzheimer's disease studies", in the book entitled "Microfluidic and Compartmentalized Platforms for Neurobiological Research", **Y. Ren**, A. Kunze, Ph. Renaud; Ed. E. Biffi, Springer Neuromethods series 2015, 103, 197-215.
- ◆ "A simple and reliable PDMS and SU-8 irreversible bonding method and its application on a microfluidic-MEA device for neuroscience research", **Y. Ren**, S.-H. Huang, S. Mosser, M. Heuschkel, A. Bertsch, P. Fraering, J.-J. Chen, Ph. Renaud. *Micromachines* 2015, 6, 1923-1934.
- ◆ "Functional and structural patterns of neurodegenerative disease propagation simulated by okadaic acid induced tauopathy model", **Y. Ren** et al., in preparation.
- ◆ "Morphological observations on hyperphosphorylated-Tau propagation in an Alzheimer's disease model using 5-compartment microfluidic device", **Y. Ren** et al., in preparation.
- ◆ "Enhancement of activity of cross-linked enzyme aggregates by a novel sugar-assisted precipitation strategy: technical development and molecular mechanism", M. Wang, W. Qi, C. Jia, **Y. Ren**, R. Su, Z. He, *Journal of Biotechnology*, Elsevier, 2011

IV. Conference proceedings

- ◆ "Mimicking Alzheimer's disease spreading via an integrated microfluidics-MEA device *in vitro*", the 12th International Conference on Alzheimer's & Parkinson's Diseases, Nice, France.
- ◆ "A reliable PDMS-SU8 irreversible bonding method and its application on an integrated PDMS-MEA system", NanoBioTech Conference 2014, Montreux, Switzerland
- ◆ "Establishment of a 3D *in vitro* cortical cell layers model for neuroscience application", 7th International NAMIS "Bio-inspired MEMS/NEMS", Seoul, South Korea

V. Seminars

- ◆ “Morphological and electrophysiological observations for Alzheimer’s disease propagation *in vitro* via microfluidic devices”, AC Immune SA, Lausanne, Switzerland. *Feb. 2015*
- ◆ “Morphological and electrophysiological observations for Alzheimer’s disease propagation *in vitro* via biomedical microdevices”, Novartis-EPFL-UNIL Science Day, Basel, Switzerland. *Dec. 2014*

VI. Teaching and Master project co-supervision

- ◆ Teaching assistant (EPFL):
Practical work for Master students: Wafer design, cleanroom fabrication and characterization of silicon oxide micro-cantilevers *Jun. 2011 - Jul. 2014*
- ◆ Master project co-supervision (EPFL):
Building a cortex on a chip: Neurons in agarose-alginate beads, Sebastien Hissette *Feb. 2013 - Dec. 2013*
Building a 3D bead-based neural network in microfluidic device, Francesca Sorba *Feb. 2014 - Jun. 2014*

VII. Current and former main collaborations

- ◆ Qwane Bioscience SA, Switzerland. *May. 2012 – Present*
- ◆ Prof. Patrick Fraering, Fraering-Lab, Brain Mind Institute, EPFL, Switzerland. *Nov. 2011 – Present*
- ◆ Dr. Shun-Ho Huang, from Prof. Jia-Jin Jason Chen’s lab, Department of Biomedical Engineering, Medical Device Innovation Center, National Cheng Kung University, Taiwan. *Feb. 2012 – Sep. 2013*
- ◆ Prof. Hilal Lashuel, Laboratory of Molecular Neurobiology and Neuroproteomics, Brain Mind Institute, EPFL, Switzerland. *Oct. 2013 – Jun. 2014*

VIII. Proficient technical skills

- ◆ Life Science: 2D and 3D cell culture in normal culture dish and in microfluidic device, microscopy, immunocytochemistry, neural cell morphological and electrophysiological experiments and data analysis
- ◆ Microtechnology: microdevice design, microfabrication, microfluidic device manipulation, microelectrode arrays (MEAs) manipulation for neural activity recording
- ◆ Others: communication and presentation skills

IX. Personal interests

- ◆ Technical interests: disease diagnosis, bio-inspired applications
- ◆ Sports: Swimming, fitness and nutrition, yoga, dancing
- ◆ Music: singing, electronic keyboard

